2005-12-09

kp Theory of Semiconductor Nanostructures

Calin Galeriu
Worcester Polytechnic Institute

$k \cdot p$ THEORY OF SEMICONDUCTOR NANOSTRUCTURES

by

CALIN GALERIU, B.S., M.S., M.A.

A Dissertation

Submitted to the Faculty

of the

WORCESTER POLYTECHNIC INSTITUTE

in partial fulfillment of the requirements for the

Degree of Doctor of Philosophy

in

Physics

November 30, 2005

APPROVED:

_____

Professor Lok C. Lew Yan Voon, Dissertation Advisor

_____

Professor Richard S. Quimby, Committee Member

_____

Professor Florin Catrina, Committee Member

Abstract

The objective of this project was to extend fundamentally the current $\mathbf{k} \cdot \mathbf{p}$ theory by applying the Burt-Foreman formalism, rather than the conventional Luttinger-Kohn formalism, to a number of novel nanostructure geometries. The theory itself was extended in two ways. First in the application of the Burt-Foreman theory to computing the momentum matrix elements. Second in the development of a new formulation of the multiband $\mathbf{k} \cdot \mathbf{p}$ Hamiltonian describing cylindrical quantum dots.

A number of new and interesting results have been obtained. The computational implementation using the finite difference method of the Burt-Foreman theory for two dimensional nanostructures has confirmed that a non-uniform grid is much more efficient, as had been obtained by others in one dimensional nanostructures. In addition we have demonstrated that the multiband problem can be very effectively and efficiently solved with commercial software (FEMLAB).

Two of the most important physical results obtained and discussed in the dissertation are the following. One is the first *ab initio* demonstration of possible electron localization in a nanowire superlattice in a barrier material, using a full numerical solution to the one band $\mathbf{k} \cdot \mathbf{p}$ equation. The second is the demonstration of the exactness of the Sercel-Vahala transformation for cylindrical wurtzite nanostructures. Comparison of the subsequent calculations to experimental data on CdSe nanorods revealed the important role of the linear spin splitting term in the wurtzite valence band.

Acknowledgments

I would like to thank my advisor, Professor Lok C. Lew Yan Voon, for his patient guidance and constant encouragement during the course of my research.

I would like to thank all members of our research group, and especially Professor Morten Willatzen, Professor Roderik Melnik, Dr. Smagul Karazhanov, and Benny Lassen.

I would like to thank all faculty members, staff persons, and fellow students at Worcester Polytechnic Institute.

I would like to thank my family, and especially my wife Luminiţa, for her patience and support during my years of graduate studies.

I would like to thank my cat Pisoancă, who has kept me company during many hours of typing and programming.

The research was supported through grants from the National Science Foundation, Grant No. DMR-9984059 and Grant No. DMR-0454849, and by the Department of Physics at Worcester Polytechnic Institute.

Contents

List of Figures

List of Tables

Chapter 1

Introduction

The invention of the solid state transistor in 1947 launched the age of semiconductor based electronics. Over the last decade optical fiber communication has become the choice for the world wide communication network. Semiconductor based light sources and detectors are critically important to this emerging technology. Progress in optoelectronics has occurred not so much by device scaling as by new device physics. For example, the use of quantum wells in the active region of lasers has reduced threshold current density by an order of magnitude [1].

A semiconductor heterostructure can have a quantum confinement in one dimension (quantum well), two dimensions (quantum wire), or three dimensions (quantum dot) [2]. Laser operation in a quantum wells was demonstrated in 1974. AlGaAs/GaAs was the first heterostructure ever made and enjoyed the most success in many areas. Today the InP based laser dominates the optical fiber communications. In the past several years the nitride system [3] has attracted a lot of attentions due to its wide bandgap, which gives blue light sources. Quantum wires offer lateral confinement beyond the confinement in the growth direction, which will further decrease the threshold current and increase the differential gain. Quantum dot structures have discrete density of electronic states and in this regard they behave more like atoms rather than solids.

The current state of research in this field is principally one of applying existing theories to various nanostructures. The most commonly used method, in particular with optoelectronic device modeling in mind, is based upon the conventional Luttinger-Kohn (LK) model [4]. While

a competing first principles approach was already developed in the 80's and 90's by Burt and Foreman (BF) [5, 6, 7, 8, 9, 10, 11, 12], the application of the latter was until recently limited to only demonstrating the differences between the two theories for quantum well structures. Therefore the approach taken for this Ph.D. project was to generalize the application of the BF theory to higher confinement nanostructures and to calculate physical properties beyond just band structures, namely optical momentum matrix elements, since the later are relevant to modeling optoelectronic devices. The other area of focus of this project is related to the current interest in the influence of size and shape on physical properties [13]. Indeed in the last few years there has been tremendous activity in the investigation, both theoretical and experimental, of nanostructures with various shapes, such as nanorods, nanowires of different cross-sectional shapes, and modulated nanowires. This has led us to apply the theory described above to a number of different shapes. Details of the actual work now follow.

In Chapter 2 we discuss the role of symmetry in the calculation of matrix elements. The $\mathbf{k} \cdot \mathbf{p}$ theory [14] relies heavily on the use of momentum matrix elements. Using symmetry arguments [15] we can show that many of these matrix elements are zero, and many of them are equal. This dramatically reduces the number of non-zero matrix elements that show up in the $\mathbf{k} \cdot \mathbf{p}$ equations. The reduced number of these matrix elements also allows us to treat them as fitting parameters, and to get their empirical values [16].

In Chapter 3 we discuss the $\mathbf{k} \cdot \mathbf{p}$ theory in the formulation of Kane [17, 18, 19, 20, 21, 22]. We give a detailed treatment of the 1-band, 4-band, 6-band, and 8-band Hamiltonians for bulk ZB semiconductors. The derivation of the spin-orbit interaction and the folding-down of the Hamiltonian [23] are treated in the greatest detail.

In Chapter 4 we discuss the $\mathbf{k} \cdot \mathbf{p}$ theory in the formulation of Burt [5, 6, 7, 8, 9, 10]. The symmetry properties derived in Chapter 2 are now used extensively, and the 8-band Hamiltonian for ZB heterostructures is obtained. Comparisons between calculations using the symmetrized and the non-symmetrized Hamiltonians have been made for quantum wells [11, 24, 25, 26], wires [27], and dots [28]. The differences between the Burt Hamiltonian and the symmetrized one are pointed out.

In Chapter 5 we discuss the calculation of the momentum matrix elements. This is no easy

task, since the full eigenfunctions are never found, and only the eigenfunctions of the folded down Hamiltonian are available [29, 30]. The formula for calculating the MME is derived in the greatest detail, and the effects of using the Burt Hamiltonian or the symmetrized one are shown.

In Chapter 6 we discuss the $\mathbf{k} \cdot \mathbf{p}$ theory under a change of basis. This happens when we diagonalize the spin-orbit Hamiltonian [17, 31], but also when we rotate the Cartesian axes [18]. The theory developed in this chapter enables us to write very general and efficient computer programs to deal with any possible crystallographic orientation of the heterostructure.

In Chapter 7 we discuss the calculation of strain in cylindrical heterostructures [32]. Although we ignore strain in all calculations presented in this thesis, more detailed calculations will have to include the effects of strain. The introduction of strain in a solid changes the lattice parameters and the symmetry of the material. These in turn change the valence and conduction bands [33].

In Chapter 8 we analyze a conical quantum dot, using a 1-band $\mathbf{k} \cdot \mathbf{p}$ method. The effect of imposing Dirichlet or van Neumann boundary conditions is discussed.

In Chapter 9 we analyze an elliptical quantum dot, using a 1-band $\mathbf{k} \cdot \mathbf{p}$ method [34]. We show that the eigenvalue equation is not separable, contrary to what was asserted in Ref. [35].

In Chapter 10 we analyze a nanowire superlattice (NWSL), using a 1-band $\mathbf{k} \cdot \mathbf{p}$ method [36]. We derive the Hamiltonian in cylindrical coordinates, and we calculate the band structure. Free-standing semiconductor NWSL have been grown experimentally [37, 38]. Extremely polarized photoluminescence is one characteristic that makes NWSL likely candidates for practical applications. In addition, a recent one-dimensional theory predicted the remarkable existence of an inversion regime when the localization of the electron states can be reversed [39].

The calculation of intervalence subband optical transitions in quantum wells goes back to a paper by Chang and James (CJ) in 1989 [40]. It established that these transitions can have both TE and TM polarizations. The calculations were done using the four-band Luttinger-Kohn (LK) Hamiltonian with infinite-barrier quantum-well states. Szmulowicz [29] generalized the CJ equation to allow for position-dependent $k \cdot p$ parameters. In Chapter 11 we present an envelope-function-representation derivation and calculations of the band structure and the momentum

matrix elements between valence subbands in [001] quantum wells using the Luttinger-Kohn-Kane and the Burt-Foreman Hamiltonians. We also discuss the numerical implementation of the 8-band $\mathbf{k} \cdot \mathbf{p}$ method.

The III-V nitride semiconductors, with wurtzite (WZ) crystal structure, have received a great deal of attention in recent years [41]. The detailed band structure of these materials was studied after the discovery (in 1993) of blue light emission of WZ GaN on sapphire [3]. In Chapter 12 we analyze a WZ cylindrical quantum dot, using a 6-band $\mathbf{k} \cdot \mathbf{p}$ method. We derive the Hamiltonian in cylindrical coordinates, and we calculate the band structure, using a formulation of the multiband envelope function theory first derived and applied by Sercel and Vahala to spherical quantum dots and cylindrical quantum wires of zincblende (ZB) materials [42, 43]. We show that the formulation is exact for WZ materials, i.e., *no axial approximation* is needed. The reduction in dimensionality greatly decreases the needed computational resources.

The above described work has resulted in five published papers:

1. L. C. Lew Yan Voon, C. Galeriu, M. Willatzen, Comment on: "Confined states in two-dimensional flat elliptic quantum dots and elliptic quantum wires", *Physica E* **18** (2003), 547-549.

2. M. Willatzen, R. V. N. Melnik, C. Galeriu, L. C. Lew Yan Voon, Finite Element Analysis of Nanowire Superlattice Structures, *Proc. ICCSA 2003* (2003), 755-763.

3. C. Galeriu, L. C. Lew Yan Voon, R. Melnik, M. Willatzen, Modeling a nanowire superlattice using the finite difference method in cylindrical polar coordinates, *Computer Physics Communications* **157** (2004), 147-159.

4. M. Willatzen, R. V. N. Melnik, C. Galeriu, L. C. Lew Yan Voon, Quantum confinement phenomena in nanowire superlattice structures, *Mathematics and Computers in Simulation* **65** (2004), 385-397.

5. L. C. Lew Yan Voon, C. Galeriu, B. Lassen, M. Willatzen, R. Melnik, Electronic structure of wurtzite quantum dots with cylindrical symmetry, *Applied Physics Letters* **87** (2005), 041906-1–041906-3.

Chapter 2

Symmetry and the calculation of matrix elements

2.1 Introduction

An important component of the $\mathbf{k} \cdot \mathbf{p}$ theory is the application of group theory to reduce the number of elements in the Hamiltonian. We provide our discussion of results derived in Ref. [15] and Ref. [14].

2.2 Selection rules for matrix elements

We are concerned with the calculation of matrix elements of the type

$$\langle \psi_i^{(\alpha)} | P_j^{(\beta)} | \psi_k^{(\gamma)} \rangle, \tag{2.1}$$

where $\psi_i^{(\alpha)}$ and $\psi_k^{(\gamma)}$ are functions, and $P_j^{(\beta)}$ is an operator. Under the symmetry operations of the symmetry group of the system, the function $\psi_i^{(\alpha)}$ transforms according to the i-th row of the $\Gamma^{(\alpha)}$ irreducible representation (IRR), the function $\psi_k^{(\gamma)}$ transforms according to the k-th row of the $\Gamma^{(\gamma)}$ IRR, and the operator $P_j^{(\beta)}$ transforms according to the j-th row of the $\Gamma^{(\beta)}$ IRR.

The matrix element (2.1) will be non-zero only if the identity IRR Γ_1 appears in the reduction of the direct product $\Gamma^{(\alpha)} \otimes \Gamma^{(\beta)} \otimes \Gamma^{(\gamma)}$. Or, equivalently, only if the IRR $\Gamma^{(\alpha)}$ appears in

the reduction of the direct product $\Gamma^{(\beta)} \otimes \Gamma^{(\gamma)}$, since the identity IRR Γ_1 appears only in the direct product of two identical IRR [44].

As a practical example we will analyze the momentum matrix elements at the $\mathbf{k} = 0$ point (Γ point) of a semiconductor with the zincblende (ZB) structure. The momentum operators $p_x = -i\hbar\partial/\partial x$, $p_y = -i\hbar\partial/\partial y$, $p_z = -i\hbar\partial/\partial z$, and the valence-band functions $|X\rangle$, $|Y\rangle$, $|Z\rangle$ transform according to the Γ_{15} IRR. The first conduction-band function $|S\rangle$ transforms according to the Γ_1 IRR.

Since [14]

$$\Gamma_{15} \otimes \Gamma_1 = \Gamma_{15}, \tag{2.2}$$

only functions F transforming according to Γ_{15} will produce non-zero matrix elements $\langle F|p_i|S\rangle$.

Since [14]

$$\Gamma_{15} \otimes \Gamma_{15} = \Gamma_1 \oplus \Gamma_{12} \oplus \Gamma_{15} \oplus \Gamma_{25}, \tag{2.3}$$

only functions F transforming according to Γ_1, Γ_{12}, Γ_{15}, or Γ_{25} will produce non-zero matrix elements $\langle F|p_i|X\rangle$,$\langle F|p_i|Y\rangle$,$\langle F|p_i|Z\rangle$.

2.3 Wigner-Eckart theorem

The Wigner-Eckart theorem [45] states that

$$\langle \psi_i^{(\alpha)}|P_j^{(\beta)}|\psi_k^{(\gamma)}\rangle = CG(i,j,k,\alpha,\beta,\gamma)\langle \psi^{(\alpha)}||P^{(\beta)}||\psi^{(\gamma)}\rangle, \tag{2.4}$$

where CG is a Clebsh-Gordan coefficient. This relation dramatically reduces the number of independent matrix elements. Many of the matrix elements are eliminated because the Clebsh-Gordan coefficient is zero.

However, since the Clebsh-Gordan coefficients are hard to find, we use an alternative method to obtain the non-zero matrix elements. We use the fact that, under a symmetry operation $\hat{G}$ of the symmetry group of the system, the functions and the operator transform according to

$$\hat{G}\psi_i^{(\alpha)} = \sum_u \psi_u^{(\alpha)} G_{ui}^{(\alpha)}, \tag{2.5}$$

where $G_{ui}^{(\alpha)}$ is a matrix element. Since point group operations leave inner products invariant, the matrix element becomes [15]

$$\langle\psi_i^{(\alpha)}|P_j^{(\beta)}|\psi_k^{(\gamma)}\rangle = \langle\hat{G}\psi_i^{(\alpha)}|\hat{G}P_j^{(\beta)}|\hat{G}\psi_k^{(\gamma)}\rangle = \sum_u\sum_v\sum_w G_{ui}^{(\alpha)}G_{vj}^{(\beta)}G_{wk}^{(\gamma)}\langle\psi_u^{(\alpha)}|P_v^{(\beta)}|\psi_w^{(\gamma)}\rangle. \quad (2.6)$$

Although the triple sum (2.6) is intimidating, in practice, due to the $G_{ui}^{(\alpha)}G_{vj}^{(\beta)}G_{wk}^{(\gamma)}$ product, only a few matrix elements remain in the sum. We are left with simple relations like

$$\langle\psi_i^{(\alpha)}|P_j^{(\beta)}|\psi_k^{(\gamma)}\rangle = -\langle\psi_i^{(\alpha)}|P_j^{(\beta)}|\psi_k^{(\gamma)}\rangle, \quad (2.7)$$

which indicate that the respective matrix element is zero, or

$$\langle\psi_i^{(\alpha)}|P_j^{(\beta)}|\psi_k^{(\gamma)}\rangle = \langle\psi_u^{(\alpha)}|P_v^{(\beta)}|\psi_w^{(\gamma)}\rangle, \quad (2.8)$$

which indicate the equality of the two matrix elements. In rare occasions we obtain relations between three or more matrix elements. In this case we have to solve the system of linear equations in order to find the non-zero elements and the proportionality relations.

2.4 Momentum matrix elements at the Γ point in ZB structures

Some IRR, their dimensions, and their basis functions [46], for the symmetry group T_d (Γ point of zincblende (ZB) structure) are listed in Table 2.4. By x, y, z we mean a basis transforming like a polar vector. By S_x, S_y, S_z we mean a basis transforming like an axial vector. By R we mean a function going into itself under all proper and improper rotations.

IRR	dim.	basis for T_d
Γ_1	1	R or xyz
Γ_{12}	2	$2z^2-x^2-y^2, \sqrt{3}(x^2-y^2)$
Γ_{15}	3	S_x, S_y, S_z
Γ_{25}	3	x, y, z

Table 2.4. Some IRR, their dimensions, and their basis functions, for the symmetry group T_d.

Knowing the basis functions, and knowing how x, y, z transform under the symmetry operations, allows us to find the matrices $G^{(\alpha)}$ for the IRR α of interest and for all the 24 symmetry operations $\hat{G}$ of the T_d symmetry group. These matrices are listed in [47]. With these matrices, the calculation of (2.6) is straightforward. For a given choice of i, j, k, α, γ ($\beta = \Gamma_{15}$) the calculation is performed for all 24 symmetry operations. The results are summarized below.

2.4.1 $\langle\Gamma_{15}|\Gamma_{15}|\Gamma_1\rangle$ momentum matrix elements

The non-zero elements are

$$\langle X|p_x|S\rangle = \langle Y|p_y|S\rangle = \langle Z|p_z|S\rangle. \tag{2.9}$$

2.4.2 $\langle\Gamma_{15}|\Gamma_{15}|\Gamma_{15}\rangle$ momentum matrix elements

The non-zero elements are

$$\langle X|p_y|Z'\rangle = \langle X|p_z|Y'\rangle = \langle Y|p_x|Z'\rangle = \langle Y|p_z|X'\rangle = \langle Z|p_x|Y'\rangle = \langle Z|p_y|X'\rangle. \tag{2.10}$$

2.4.3 $\langle\Gamma_{15}|\Gamma_{15}|\Gamma_{25}\rangle$ momentum matrix elements

The non-zero elements are

$$\langle X|p_y|Z'\rangle = -\langle X|p_z|Y'\rangle = -\langle Y|p_x|Z'\rangle = \langle Y|p_z|X'\rangle = \langle Z|p_x|Y'\rangle = -\langle Z|p_y|X'\rangle. \tag{2.11}$$

2.4.4 $\langle\Gamma_{15}|\Gamma_{15}|\Gamma_{12}\rangle$ momentum matrix elements

The non-zero elements are

$$\langle X|p_x|A_{12}\rangle = -\langle Y|p_y|A_{12}\rangle = -\sqrt{3}\langle X|p_x|B_{12}\rangle = -\sqrt{3}\langle Y|p_y|B_{12}\rangle = \sqrt{3}/2\langle Z|p_z|B_{12}\rangle, \tag{2.12}$$

where $A_{12} \equiv 2z^2 - x^2 - y^2$ and $B_{12} \equiv \sqrt{3}(x^2 - y^2)$.

2.5 Momentum matrix elements at the Γ point in DM structures

Some IRR, their dimensions, and their basis functions [46], for the symmetry group O (Γ point of diamond (DM) structure) are listed in Table 2.5.

IRR	dim.	basis for O
Γ_1	1	R
Γ_{12}	2	$2z^2 - x^2 - y^2, \sqrt{3}(x^2 - y^2)$
Γ_{15}	3	S_x, S_y, S_z
Γ_{25}	3	yz, xz, xy

Table 2.5. Some IRR, their dimensions, and their basis functions, for the symmetry group O.

The momentum matrix elements for DM satisfy the same relations as the momentum matrix elements for ZB.

2.6 Momentum matrix elements at the Γ point in WZ structures

Some IRR, their dimensions, and their basis functions [46, 25], for the symmetry group C_{6v}^4 (Γ point of wurzite (WZ) structure) are listed in Table 2.6.

IRR	dim.	basis for C_{6v}	$l=0$	$l=1$	$l=2$
Γ_1	1	R or z	1	z	x^2+y^2, z^2
Γ_2	1	S_z			
Γ_3	1	x^3-3xy^2			
Γ_4	1	y^3-3yx^2			
Γ_5	2	$(S_x-iS_y), -(S_x+iS_y)$			$x^2-y^2, 2xy$
Γ_6	2	$\Gamma_3 \times \Gamma_5$		x, y	xz, yz

Table 2.6. Some IRR, their dimensions, and their basis functions, for the symmetry group C_{6v}. l is the angular momentum.

2.6.1 $\langle\Gamma_1|\Gamma_1|\Gamma_1\rangle$ momentum matrix elements

The non-zero element is

$$\langle S|p_z|Z\rangle. \tag{2.13}$$

2.6.2 $\langle\Gamma_1|\Gamma_6|\Gamma_6\rangle$ momentum matrix elements

The non-zero elements are

$$\langle S|p_x|X\rangle = \langle S|p_y|Y\rangle. \tag{2.14}$$

Chapter 3

$\mathbf{k} \cdot \mathbf{p}$ theory - Kane

3.1 Introduction

In this chapter we present a review of the $\mathbf{k} \cdot \mathbf{p}$ method. The $\mathbf{k} \cdot \mathbf{p}$ method was originally an application of the perturbation method to the study of energy bands and wave functions in the vicinity of some important points in $\mathbf{k}$ space. The paper of Dresselhaus, Kip, and Kittel [16] established the importance of the $\mathbf{k} \cdot \mathbf{p}$ approach as a rigorous basis for the empirical determination of band structure. Symmetry arguments are used by the $\mathbf{k} \cdot \mathbf{p}$ method to show that the band structure in a small region of $\mathbf{k}$ space depends only on a few parameters. Extensive derivations and calculations using the $\mathbf{k} \cdot \mathbf{p}$ method, and many review papers by E.O. Kane [17, 18, 19, 20, 21, 22] have transformed this perturbative approach into one of the main methods used in Solid State Physics.

3.2 1-band model

The simplest example for an application of the $\mathbf{k} \cdot \mathbf{p}$ theory is when the electronic state is non-degenerate and only weakly interacting with all other states. In this situation we have to solve the one electron Schrödinger equation

$$H\psi_{n,\mathbf{k}}(\mathbf{r}) = E_{n,\mathbf{k}}\psi_{n,\mathbf{k}}(\mathbf{r}), \tag{3.1}$$

with the Hamiltonian

$$H = \frac{p^2}{2m_o} + V(\mathbf{r}) + \frac{\hbar}{4m_o^2c^2}(\sigma \times \nabla V)\cdot\mathbf{p}, \tag{3.2}$$

and the Bloch wave-function

$$\psi_{n,\mathbf{k}}(\mathbf{r}) = e^{i\mathbf{k}\cdot\mathbf{r}}u_{n,\mathbf{k}}(\mathbf{r}). \tag{3.3}$$

Since

$$(-i\hbar\nabla)e^{i\mathbf{k}\cdot\mathbf{r}}u_{n,\mathbf{k}}(\mathbf{r}) = \hbar\mathbf{k}e^{i\mathbf{k}\cdot\mathbf{r}}u_{n,\mathbf{k}}(\mathbf{r}) + e^{i\mathbf{k}\cdot\mathbf{r}}(-i\hbar\nabla)u_{n,\mathbf{k}}(\mathbf{r}), \tag{3.4}$$

$$(-i\hbar\nabla)^2e^{i\mathbf{k}\cdot\mathbf{r}}u_{n,\mathbf{k}}(\mathbf{r}) = \hbar^2k^2e^{i\mathbf{k}\cdot\mathbf{r}}u_{n,\mathbf{k}}(\mathbf{r}) + 2\hbar\mathbf{k}\cdot e^{i\mathbf{k}\cdot\mathbf{r}}(-i\hbar\nabla)u_{n,\mathbf{k}}(\mathbf{r}) + e^{i\mathbf{k}\cdot\mathbf{r}}(-i\hbar\nabla)^2u_{n,\mathbf{k}}(\mathbf{r}), \tag{3.5}$$

substitution of (3.3) into (3.1) gives

$$\left(\frac{\hbar^2k^2}{2m_o} + \frac{2\hbar\mathbf{k}\cdot\mathbf{p}}{2m_o} + \frac{p^2}{2m_o} + V(\mathbf{r}) + \frac{\hbar}{4m_o^2c^2}(\sigma\times\nabla V)\cdot(\hbar\mathbf{k}+\mathbf{p})\right)u_{n,\mathbf{k}}(\mathbf{r}) = E_{n,\mathbf{k}}u_{n,\mathbf{k}}(\mathbf{r}). \tag{3.6}$$

With the notation

$$\pi = \mathbf{p} + \frac{\hbar}{4m_oc^2}(\sigma\times\nabla V), \tag{3.7}$$

equation (3.6) becomes

$$\left(H + \frac{\hbar^2k^2}{2m_o} + \frac{\hbar}{m_o}\mathbf{k}\cdot\pi\right)u_{n,\mathbf{k}}(\mathbf{r}) = E_{n,\mathbf{k}}u_{n,\mathbf{k}}(\mathbf{r}). \tag{3.8}$$

Equation (3.8) is solved using second order non-degenerate perturbation theory. The perturbation is the $\mathbf{k}$ dependent part of the Hamiltonian. The solution, up to second order, is:

$$E_{n,\mathbf{k}} = E_{n,\mathbf{0}} + \frac{\hbar^2k^2}{2m_o} + \frac{\hbar\mathbf{k}}{m_o}\cdot\langle n,0|\pi|n,0\rangle + \frac{\hbar^2}{m_o^2}\sum_{m\neq n}\frac{|\mathbf{k}\cdot\langle n,0|\pi|m,0\rangle|^2}{E_{n,\mathbf{0}} - E_{m,\mathbf{0}}}. \tag{3.9}$$

Since the energy band has a minimum at $\mathbf{k}=0$, the term linear in $\mathbf{k}$ is zero. We introduce the Cartesian indices $\alpha,\beta = x,y,z$, and assume Einstein's summation convention for these indices. We have

$$E_{n,\mathbf{k}} = E_{n,\mathbf{0}} + \frac{\hbar^2k^2}{2m_o} + \frac{\hbar^2}{m_o^2}k_\alpha k_\beta\sum_{m\neq n}\frac{\langle n,0|\pi_\alpha|m,0\rangle\langle m,0|\pi_\beta|n,0\rangle}{E_{n,\mathbf{0}} - E_{m,\mathbf{0}}}, \tag{3.10}$$

$$E_{n,\mathbf{k}} = E_{n,\mathbf{0}} + \frac{\hbar^2}{2}k_\alpha k_\beta\left(\frac{1}{m_n^*}\right)_{\alpha,\beta}, \tag{3.11}$$

where the tensor of the effective mass is

$$\left(\frac{1}{m_n^*}\right)_{\alpha,\beta} = \left(\frac{1}{m_o}\right)\delta_{\alpha,\beta} + \frac{2}{m_o^2}\sum_{m\neq n}\frac{\langle n,0|\pi_\alpha|m,0\rangle\langle m,0|\pi_\beta|n,0\rangle}{E_{n,\mathbf{0}} - E_{m,\mathbf{0}}}. \tag{3.12}$$

3.3 2-band model, CB-VB coupling only

In this model the spin is not considered. The conduction band consists of one non-degenerate band $|s\rangle$ and the valence band consists of three degenerate bands $|p_x\rangle, |p_y\rangle, |p_z\rangle$. The 2-band model considers the coupling of the conduction band to one of the valence bands. Perturbation theory is applied to the two bands independently.

3.3.1 Electron in GaAs

We consider coupling of the s band only with the three valence bands, which are closest in energy. The calculation of matrix elements gives

$$\langle s|p_\alpha|p_\beta\rangle = P\delta_{\alpha,\beta}, \tag{3.13}$$

$$\langle p_\gamma|p_\alpha|p_\beta\rangle = 0. \tag{3.14}$$

Symmetry requires the three non-zero elements to be equal. Therefore the effective mass is isotropic. Introducing the energy gap $E_g \equiv E_{CB,\mathbf{0}} - E_{VB,\mathbf{0}}$ we get

$$\frac{1}{m^*_{CB}} = \frac{1}{m_o} + \frac{2|P|^2}{m_o^2 E_g}. \tag{3.15}$$

3.3.2 Light hole in GaAs

Along a given $\mathbf{k}$ direction, $[k_x, 0, 0]$ as an example, only one of the three valence bands will couple to the conduction band. This is due to (3.13)-(3.14). Therefore we can treat that band with non-degenerate perturbation theory. The effective mass is again isotropic, and usually negative.

$$\frac{1}{m^*_{VB}} = \frac{1}{m_o} - \frac{2|P|^2}{m_o^2 E_g}. \tag{3.16}$$

3.4 4-band model, CB-VB coupling only

This model allows coupling only between the one CB and the three VB, and ignores completely the influences of the other bands. Spin is not considered. Within this approximation, the

problem is solved exactly. The equations for the 4 bands at $\mathbf{k}=0$ are

$$H_o u_{s,\mathbf{0}} = E_{CB,\mathbf{0}} u_{s,\mathbf{0}}, \tag{3.17}$$

$$H_o u_{p_x,\mathbf{0}} = E_{VB,\mathbf{0}} u_{p_x,\mathbf{0}}, \tag{3.18}$$

$$H_o u_{p_y,\mathbf{0}} = E_{VB,\mathbf{0}} u_{p_y,\mathbf{0}}, \tag{3.19}$$

$$H_o u_{p_z,\mathbf{0}} = E_{VB,\mathbf{0}} u_{p_z,\mathbf{0}}, \tag{3.20}$$

where

$$H_o \equiv \frac{p^2}{2m_o} + V(\mathbf{r}). \tag{3.21}$$

When $\mathbf{k}\neq 0$ we need to solve the equation (3.8). We do this by expanding $u_{s,\mathbf{k}}, u_{p_x,\mathbf{k}}, u_{p_y,\mathbf{k}}, u_{p_z,\mathbf{k}}$ as linear combinations of $u_{s,\mathbf{0}}, u_{p_x,\mathbf{0}}, u_{p_y,\mathbf{0}}, u_{p_z,\mathbf{0}}$.

$$u_{n,\mathbf{k}} = \sum_m C_{n,m} u_{m,\mathbf{0}}, \qquad n\in\{1,..,4\}, m\in\{s,p_x,p_y,p_z\}. \tag{3.22}$$

Next we introduce (3.22) into (3.8)

$$\left(H_o + \frac{\hbar^2k^2}{2m_o} + \frac{\hbar}{m_o}\mathbf{k}\cdot\mathbf{p}\right)\sum_m C_{n,m}u_{m,\mathbf{0}} = E_{n,\mathbf{k}}\sum_m C_{n,m}u_{m,\mathbf{0}}. \tag{3.23}$$

Taking the scalar product of (3.23) with the 4 states $u_{s,\mathbf{0}}$, $u_{p_x,\mathbf{0}}$, $u_{p_y,\mathbf{0}}$, $u_{p_z,\mathbf{0}}$ we obtain

$$\begin{pmatrix} E_{CB,\mathbf{0}}+\frac{\hbar^2k^2}{2m_o} & \frac{\hbar}{m_o}k_xP & \frac{\hbar}{m_o}k_yP & \frac{\hbar}{m_o}k_zP \\ \frac{\hbar}{m_o}k_xP^* & E_{VB,\mathbf{0}}+\frac{\hbar^2k^2}{2m_o} & 0 & 0 \\ \frac{\hbar}{m_o}k_yP^* & 0 & E_{VB,\mathbf{0}}+\frac{\hbar^2k^2}{2m_o} & 0 \\ \frac{\hbar}{m_o}k_zP^* & 0 & 0 & E_{VB,\mathbf{0}}+\frac{\hbar^2k^2}{2m_o} \end{pmatrix} \begin{pmatrix} C_{n,s} \\ C_{n,p_x} \\ C_{n,p_y} \\ C_{n,p_z} \end{pmatrix} = E_{n,\mathbf{k}} \begin{pmatrix} C_{n,s} \\ C_{n,p_x} \\ C_{n,p_y} \\ C_{n,p_z} \end{pmatrix}. \tag{3.24}$$

The determinant of the eigenvalue system (3.24) is

$$\left(E_{n,\mathbf{k}} - \tfrac{\hbar^2k^2}{2m_o} - E_{VB,\mathbf{0}}\right)^2 \times\left[\left(E_{n,\mathbf{k}}-\tfrac{\hbar^2k^2}{2m_o}\right)^2 - \left(E_{n,\mathbf{k}}-\tfrac{\hbar^2k^2}{2m_o}\right)(E_{CB,\mathbf{0}}+E_{VB,\mathbf{0}}) + E_{CB,\mathbf{0}}E_{VB,\mathbf{0}} - \left(\tfrac{\hbar}{m_o}k|P|\right)^2\right]. \tag{3.25}$$

Therefore the energy bands are

$$E_{n,\mathbf{k}} = E_{VB,\mathbf{0}} + \tfrac{\hbar^2k^2}{2m_o}, \text{doubly degenerate}, \tag{3.26}$$

$$E_{n,\mathbf{k}} = \tfrac{E_{CB,\mathbf{0}}+E_{VB,\mathbf{0}}}{2} + \sqrt{\left(\tfrac{E_{CB,\mathbf{0}}-E_{VB,\mathbf{0}}}{2}\right)^2 + \left(\tfrac{\hbar}{m_o}k|P|\right)^2} + \tfrac{\hbar^2k^2}{2m_o}, \tag{3.27}$$

$$E_{n,\mathbf{k}} = \tfrac{E_{CB,\mathbf{0}}+E_{VB,\mathbf{0}}}{2} - \sqrt{\left(\tfrac{E_{CB,\mathbf{0}}-E_{VB,\mathbf{0}}}{2}\right)^2 + \left(\tfrac{\hbar}{m_o}k|P|\right)^2} + \tfrac{\hbar^2k^2}{2m_o}. \tag{3.28}$$

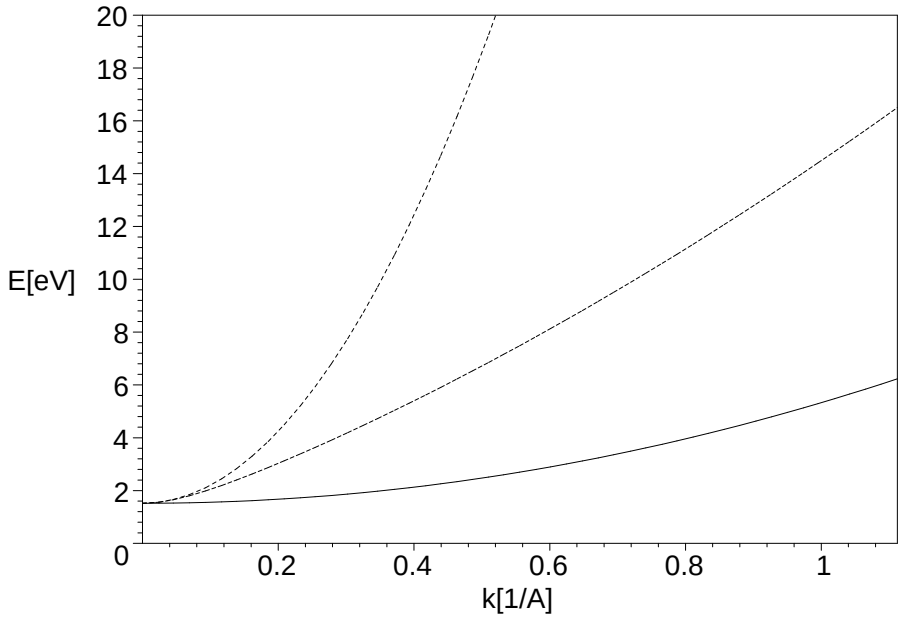

Figure 3.1: Energy band in the FBZ for the conduction electron. Solid = free electron (lower curve), dot = effective mass approximation (upper curve), dash = 2-band model. Calculation for GaAs, with $E_g = 1.52$ eV, $2|P|^2/m_o = 25.7$ eV, $a = 5.65$ Å.

The main result is that now we have non-parabolicity. Up to second order in k the equations (3.27) and (3.28) reduce to

$$E_{n,\mathbf{k}} = E_{CB,\mathbf{0}} + \frac{\hbar^2 k^2 |P|^2}{m_o^2 E_g} + \frac{\hbar^2 k^2}{2m_o}, \tag{3.29}$$

$$E_{n,\mathbf{k}} = E_{VB,\mathbf{0}} - \frac{\hbar^2 k^2 |P|^2}{m_o^2 E_g} + \frac{\hbar^2 k^2}{2m_o}, \tag{3.30}$$

and we recover the effective masses (3.15) and (3.16).

3.5 3-band model

This model calculates the valence bands in Ge or Si [16]. The three degenerate states at $\mathbf{k} = 0$ belong to the Γ_{25}^+ irreducible representation (IRR), and are labeled $\epsilon_1^+ \sim yz$, $\epsilon_2^+ \sim zx$, $\epsilon_3^+ \sim xy$. The momentum operators $p_x \sim x$, $p_y \sim y$, $p_z \sim z$ belong to the Γ_{15}^- IRR.

The first order contributions from degenerate perturbation theory are zero, since the mo-

mentum operator is odd under inversion, while the ϵ^+ functions are even.

$$\langle\epsilon_r^+|p_\alpha|\epsilon_s^+\rangle = 0, \qquad r,s\in\{1,2,3\}, \alpha\in\{x,y,z\}. \tag{3.31}$$

In other words

$$\Gamma_1^+ \notin \Gamma_{25}^+\otimes\Gamma_{15}^-\otimes\Gamma_{25}^+. \tag{3.32}$$

The second order contributions from degenerate perturbation theory are due to the matrix elements

$$H_{rs} = \frac{\hbar^2}{m_o^2}k_\alpha k_\beta \sum_{n\neq\epsilon^+}\frac{\langle\epsilon_r^+|p_\alpha|n\rangle\langle n|p_\beta|\epsilon_s^+\rangle}{E_{VB,\mathbf{0}}-E_n}. \tag{3.33}$$

Because of the symmetry

$$\langle xy|p_z|n\rangle = \langle yz|p_x|n\rangle = \langle zx|p_y|n\rangle, \tag{3.34}$$

$$\langle xy|p_x|n\rangle = \langle yz|p_y|n\rangle = \langle zx|p_z|n\rangle = \langle xy|p_y|n\rangle = \langle yz|p_z|n\rangle = \langle zx|p_x|n\rangle. \tag{3.35}$$

Consider the case $r=s$. In the group of DM there are symmetry operators that invert only one coordinate. The matrix element $\langle\epsilon_r^+|p_\alpha|n\rangle\langle n|p_\beta|\epsilon_r^+\rangle$ would cancel unless $\alpha=\beta$. The matrix elements, with the help of (3.35), can be written as

$$H_{11} = Lk_x^2 + M(k_y^2+k_z^2), \tag{3.36}$$

$$H_{22} = Lk_y^2 + M(k_x^2+k_z^2), \tag{3.37}$$

$$H_{33} = Lk_z^2 + M(k_x^2+k_y^2), \tag{3.38}$$

where

$$L = \frac{\hbar^2}{m_o^2}\sum_{n\neq\epsilon^+}\frac{\langle yz|p_x|n\rangle\langle n|p_x|yz\rangle}{E_{VB,\mathbf{0}}-E_n}, \tag{3.39}$$

$$M = \frac{\hbar^2}{m_o^2}\sum_{n\neq\epsilon^+}\frac{\langle yz|p_y|n\rangle\langle n|p_y|yz\rangle}{E_{VB,\mathbf{0}}-E_n}. \tag{3.40}$$

Consider the case $r\neq s$. In the matrix element $\langle\epsilon_r^+|p_\alpha|n\rangle\langle n|p_\beta|\epsilon_s^+\rangle$ we need to have all Cartesian coordinates paired. Since ϵ_r^+ and ϵ_s^+ share one Cartesian coordinate, the two remaining Cartesian coordinates determine α and β. There will be two contributions to the matrix element, since α and β are not uniquely determined, but up to a permutation. Nonetheless, the product

$k_\alpha k_\beta$ will factor out. The matrix elements, with the help of (3.35), can be written as

$$H_{12} = H_{21} = Nk_xk_y, \tag{3.41}$$

$$H_{13} = H_{31} = Nk_xk_z, \tag{3.42}$$

$$H_{23} = H_{32} = Nk_yk_z, \tag{3.43}$$

where

$$N = \frac{\hbar^2}{m_o^2}\sum_{n\neq\epsilon^+}\frac{\langle xy|p_z|n\rangle\langle n|p_x|yz\rangle + \langle xy|p_x|n\rangle\langle n|p_z|yz\rangle}{E_{VB,\mathbf{0}} - E_n}. \tag{3.44}$$

The energy bands are given by

$$E_{n,\mathbf{k}} = E_{VB,\mathbf{0}} + \frac{\hbar^2k^2}{2m_o} + \lambda, \tag{3.45}$$

where λ is an eigenvalue of the DKK Hamiltonian

$$H_{DKK} = \begin{pmatrix} Lk_x^2 + M(k_y^2+k_z^2) & Nk_xk_y & Nk_xk_z \\ Nk_xk_y & Lk_y^2 + M(k_x^2+k_z^2) & Nk_yk_z \\ Nk_xk_z & Nk_yk_z & Lk_z^2 + M(k_x^2+k_y^2) \end{pmatrix}. \tag{3.46}$$

For $\mathbf{k}$ in a general direction there will be three different eigenvalues.

3.5.1 k in the [1,0,0] direction

When $k_x = k$, $k_y = 0$, $k_z = 0$ the DKK Hamiltonian reduces to

$$H_{DKK} = \begin{pmatrix} Lk^2 & 0 & 0 \\ 0 & Mk^2 & 0 \\ 0 & 0 & Mk^2 \end{pmatrix}, \tag{3.47}$$

with eigenvalues

$$\lambda_1 = Lk^2, \tag{3.48}$$

$$\lambda_2 = Mk^2, \tag{3.49}$$

$$\lambda_3 = Mk^2. \tag{3.50}$$

3.5.2 k in the [1,1,1] direction

When $k_x = k/\sqrt{3}$, $k_y = k/\sqrt{3}$, $k_z = k/\sqrt{3}$ the DKK Hamiltonian reduces to

$$H_{DKK} = \begin{pmatrix} (L+2M)k^2/3 & Nk^2/3 & Nk^2/3 \\ Nk^2/3 & (L+2M)k^2/3 & Nk^2/3 \\ Nk^2/3 & Nk^2/3 & (L+2M)k^2/3 \end{pmatrix}, \tag{3.51}$$

with eigenvalues

$$\lambda_1 = \tfrac{L+2M+2N}{3}k^2, \tag{3.52}$$

$$\lambda_2 = \tfrac{L+2M-N}{3}k^2, \tag{3.53}$$

$$\lambda_3 = \tfrac{L+2M-N}{3}k^2. \tag{3.54}$$

The point here is that we have introduced anisotropy. Only when $L = M + N$ the effective masses in the [1,0,0] and [1,1,1] directions are equal. If this is the case, the DKK Hamiltonian becomes

$$H_{DKK} = \begin{pmatrix} Nk_x^2 + Mk^2 & Nk_xk_y & Nk_xk_z \\ Nk_xk_y & Nk_y^2 + Mk^2 & Nk_yk_z \\ Nk_xk_z & Nk_yk_z & Nk_z^2 + Mk^2 \end{pmatrix}, \tag{3.55}$$

with eigenvalues

$$\lambda_1 = (M+N)k^2, \tag{3.56}$$

$$\lambda_2 = Mk^2, \tag{3.57}$$

$$\lambda_3 = Mk^2. \tag{3.58}$$

Therefore the effective mass is isotropic when $L = M + N$.

Another limiting case is when we restrict the interaction to only the first conduction band, of symmetry $s \sim xyz$. In this case

$$L = N = \tfrac{\hbar^2}{m_o^2}\tfrac{\langle yz|p_x|xyz\rangle\langle xyz|p_x|yz\rangle}{E_{VB,\mathbf{0}} - E_{CB,\mathbf{0}}} = -\tfrac{\hbar^2|P|^2}{m_o^2 E_g}, \tag{3.59}$$

$$M = 0, \tag{3.60}$$

and we recover the energy bands (3.26) and (3.30).

3.6 6-band model

This is a generalization of the 3-band model, when we introduce the spin-orbit interaction. The spin-orbit interactions is most easily treated as a perturbation acting on the cell periodic function $u_{n,\mathbf{k}}$. From eq. (3.6), this perturbation is

$$H_{so} = \frac{\hbar}{4m_o^2c^2}(\sigma \times \nabla V)\cdot(\hbar\mathbf{k}+\mathbf{p}). \tag{3.61}$$

Since the velocity of the electron in its atomic orbit is very much greater than the velocity of a wave packet made up of wave vectors in the neighborhood of k, the first term of H_{so} can be neglected, leading to [17]:

$$H_{so} \approx \frac{\hbar}{4m_o^2c^2}(\sigma \times \nabla V)\cdot\mathbf{p} = \frac{\hbar}{4m_o^2c^2}(\nabla V \times \mathbf{p})\cdot\sigma. \tag{3.62}$$

$\nabla V \times \mathbf{p}$ is an axial vector, which simplifies the matrix elements. We need to calculate the matrix elements of the first order degenerate perturbation for the spin-orbit interaction. The basis consists of $\epsilon_1^+ \uparrow\sim yz$, $\epsilon_2^+ \uparrow\sim zx$, $\epsilon_3^+ \uparrow\sim xy$, $\epsilon_1^+ \downarrow\sim yz$, $\epsilon_2^+ \downarrow\sim zx$, $\epsilon_3^+ \downarrow\sim xy$. Consider the matrix element

$$\langle\epsilon_r^+|\epsilon_{\alpha\beta\gamma}\frac{\partial V}{\partial x_\beta}p_\gamma|\epsilon_s^+\rangle, \qquad r,s\in\{1,2,3\},\alpha,\beta,\gamma\in\{x,y,z\}. \tag{3.63}$$

When $r=s$ the two Cartesian components γ and β are not paired, and the matrix element is zero. When $r\neq s$, ϵ_r^+ and ϵ_s^+ share one Cartesian coordinate, and the two remaining Cartesian coordinates determine β and γ, up to a permutation. The permutation, however, is already included in the cross-product. Because of the symmetry, the non-zero elements will be equal:

$$\langle yz|\frac{\partial V}{\partial x}p_y - \frac{\partial V}{\partial y}p_x|xz\rangle = \langle zx|\frac{\partial V}{\partial y}p_z - \frac{\partial V}{\partial z}p_y|yx\rangle = \langle xy|\frac{\partial V}{\partial z}p_x - \frac{\partial V}{\partial x}p_z|zy\rangle \equiv \Delta\frac{4m_o^2c^2}{3i\hbar}. \tag{3.64}$$

The transposed elements will have opposite sign, since the matrix elements are purely imaginary (due to $\mathbf{p}=i\hbar\nabla$), and complex conjugation reduces to a change of sign. Therefore evaluation

of the spatial part of the matrix elements of H_{so} gives

$$\begin{array}{c} \\ yz \\ xz \\ xy \\ yz \\ xz \\ xy \end{array} \begin{array}{c} \begin{array}{cccccc} yz & xz & xy & yz & xz & xy \end{array} \\ \begin{pmatrix} 0 & \sigma_z & -\sigma_y & 0 & \sigma_z & -\sigma_y \\ -\sigma_z & 0 & \sigma_x & -\sigma_z & 0 & \sigma_x \\ \sigma_y & -\sigma_x & 0 & \sigma_y & -\sigma_x & 0 \\ 0 & \sigma_z & -\sigma_y & 0 & \sigma_z & -\sigma_y \\ -\sigma_z & 0 & \sigma_x & -\sigma_z & 0 & \sigma_x \\ \sigma_y & -\sigma_x & 0 & \sigma_y & -\sigma_x & 0 \end{pmatrix} \end{array} \frac{\Delta}{3i}. \tag{3.65}$$

Now the evaluation of the spin part of the matrix elements of H_{so} is trivial, since the Pauli matrices are [48]

$$\sigma_x = \begin{array}{c} \\ \uparrow \\ \downarrow \end{array} \begin{array}{c} \begin{array}{cc} \uparrow & \downarrow \end{array} \\ \begin{pmatrix} 0 & 1 \\ 1 & 0 \end{pmatrix} \end{array}, \qquad \sigma_y = \begin{array}{c} \\ \uparrow \\ \downarrow \end{array} \begin{array}{c} \begin{array}{cc} \uparrow & \downarrow \end{array} \\ \begin{pmatrix} 0 & -i \\ i & 0 \end{pmatrix} \end{array}, \qquad \sigma_z = \begin{array}{c} \\ \uparrow \\ \downarrow \end{array} \begin{array}{c} \begin{array}{cc} \uparrow & \downarrow \end{array} \\ \begin{pmatrix} 1 & 0 \\ 0 & -1 \end{pmatrix} \end{array}. \tag{3.66}$$

Therefore the matrix elements of H_{so} are given by [17]

$$H_{so} = \begin{array}{c} \\ yz\uparrow \\ xz\uparrow \\ xy\uparrow \\ yz\downarrow \\ xz\downarrow \\ xy\downarrow \end{array} \begin{array}{c} \begin{array}{cccccc} yz\uparrow & xz\uparrow & xy\uparrow & yz\downarrow & xz\downarrow & xy\downarrow \end{array} \\ \begin{pmatrix} 0 & 1 & 0 & 0 & 0 & i \\ -1 & 0 & 0 & 0 & 0 & 1 \\ 0 & 0 & 0 & -i & -1 & 0 \\ 0 & 0 & -i & 0 & -1 & 0 \\ 0 & 0 & 1 & 1 & 0 & 0 \\ i & -1 & 0 & 0 & 0 & 0 \end{pmatrix} \end{array} \frac{\Delta}{3i}. \tag{3.67}$$

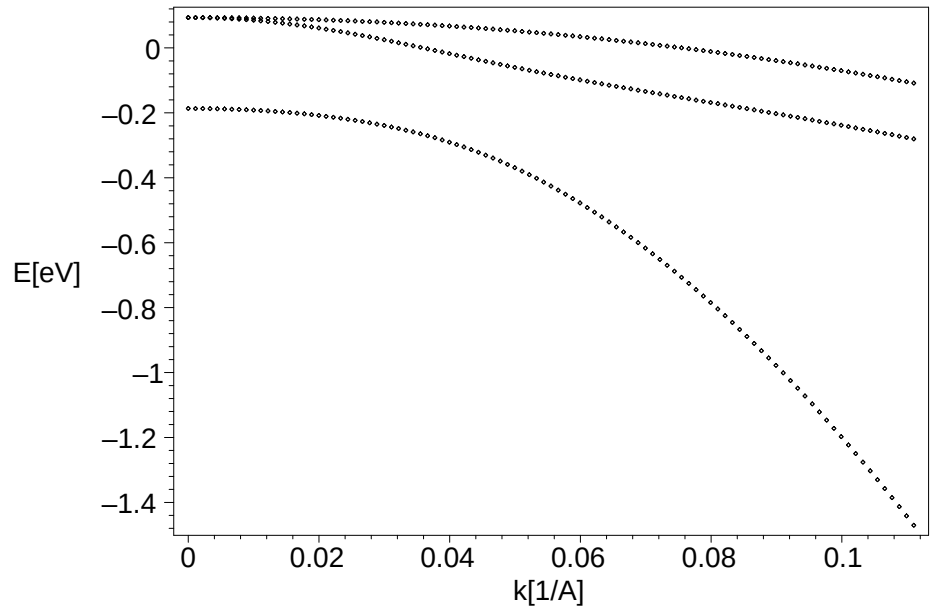

Figure 3.2: Energy bands along the [100] direction in 10% of the FBZ for holes in Ge. Calculation with $L = -32.0[\hbar^2/2m_o]$, $M = -5.30[\hbar^2/2m_o]$, $N = -32.4[\hbar^2/2m_o]$, $\Delta = 0.28$ [eV], $a = 5.66$ [Å].

The spin-orbit Hamiltonian (3.67) ads to the $\mathbf{k}\cdot\mathbf{p}$ Hamiltonian (3.46)

$$H_{kp} = \begin{array}{c} \\ yz\uparrow \\ xz\uparrow \\ xy\uparrow \\ yz\downarrow \\ xz\downarrow \\ xy\downarrow \end{array} \begin{array}{c} \begin{array}{cccccc} yz\uparrow & xz\uparrow & xy\uparrow & yz\downarrow & xz\downarrow & xy\downarrow \end{array} \\ \begin{pmatrix} & & & 0 & 0 & 0 \\ & H_{DKK} & & 0 & 0 & 0 \\ & & & 0 & 0 & 0 \\ 0 & 0 & 0 & & & \\ 0 & 0 & 0 & & H_{DKK} & \\ 0 & 0 & 0 & & & \end{pmatrix} \end{array}. \tag{3.68}$$

Diagonalization of the total Hamiltonian $H = H_{kp} + H_{so} + \hbar^2k^2/(2m_o)I$ gives the energy bands (see Appendix A for degenerate perturbation theory with first and second order mixed contributions). An exact diagonalization cannot be performed. An approximate diagonalization can be performed by diagonalization of H_{so} (in the $|J, m_J\rangle$ basis), followed by neglecting terms of order k^4/Δ in the solutions of the determinantal equation [16]. When Δ is pretty small, this

approach is not justified (but it is necessary if you need to fit the experimental effective mass in order to get the L, M, N parameters).

In Figure 3.2 we see the results of a numerical diagonalization. All three bands are doubly degenerate, as expected from Kramer's theorem. The calculations shown here reproduce the results of Kane [17].

3.7 8-band model, CB-VB coupling only

This model applies to semiconductors with a direct gap, where both the CB and VB have a minimum at $\mathbf{k} = 0$. The 8-band model is an extension of the 4-band model, where we introduce the spin-orbit coupling. The effect of the other bands is not considered. The spin-orbit coupling is introduced as a perturbation, together with the $\mathbf{k}\cdot\mathbf{p}$ term. This is done to minimize the number of parameters in the theory [20]. The spin-orbit coupling, if introduced in the $\mathbf{k} = 0$ basis, will lift some of the degeneracy of the valence band states [49]. Therefore more parameters will be introduced when we add the $\mathbf{k}\cdot\mathbf{p}$ interaction, due to the reduction in symmetry.

We use the same eigenfunctions from (3.17)-(3.20). A special phase convention will be used, with the $u_{s,\mathbf{0}}$ function purely imaginary. This is to make the matrix element $P \equiv i\langle xyz|p_z|xy\rangle$ real. We expand $u_{n,\mathbf{k}}$, (n=1..8), as linear combinations of $u_{s,\mathbf{0}\uparrow}, u_{p_x,\mathbf{0}\uparrow}, u_{p_y,\mathbf{0}\uparrow}, u_{p_z,\mathbf{0}\uparrow}$, $u_{s,\mathbf{0}\downarrow}, u_{p_x,\mathbf{0}\downarrow}, u_{p_y,\mathbf{0}\downarrow}, u_{p_z,\mathbf{0}\downarrow}$.

$$u_{n,\mathbf{k}} = \sum_m C_{n,m\uparrow} u_{m,\mathbf{0}\uparrow} + \sum_m C_{n,m\downarrow} u_{m,\mathbf{0}\downarrow}, \qquad n \in \{1,..,8\}, m \in \{s, p_x, p_y, p_z\}. \tag{3.69}$$

We write (3.6) as

$$\left(H_o + \frac{\hbar^2 k^2}{2m_o} + \frac{\hbar\mathbf{k}\cdot\mathbf{p}}{m_o} + \frac{\hbar}{4m_o^2c^2}(\sigma\times\nabla V)\cdot(\hbar\mathbf{k}+\mathbf{p})\right) u_{n,\mathbf{k}}(\mathbf{r}) = E_{n,\mathbf{k}} u_{n,\mathbf{k}}(\mathbf{r}), \tag{3.70}$$

where

$$H_o = \frac{p^2}{2m_o} + V(\mathbf{r}), \tag{3.71}$$

is the unperturbed Hamiltonian (3.21). Next we introduce (3.69) into (3.70). Again, we neglect the spin-orbit term linear in $\mathbf{k}$.

$$\begin{aligned}\left(H_o + \tfrac{\hbar^2k^2}{2m_o} + \tfrac{\hbar}{m_o}\mathbf{k}\cdot\mathbf{p} + \tfrac{\hbar}{4m_o^2c^2}(\sigma\times\nabla V)\cdot\mathbf{p}\right)\left(\textstyle\sum_m C_{n,m\uparrow}u_{m,\mathbf{0}\uparrow} + \sum_m C_{n,m\downarrow}u_{m,\mathbf{0}\downarrow}\right)\\ = E_{n,\mathbf{k}}\left(\textstyle\sum_m C_{n,m\uparrow}u_{m,\mathbf{0}\uparrow} + \sum_m C_{n,m\downarrow}u_{m,\mathbf{0}\downarrow}\right).\end{aligned} \tag{3.72}$$

Taking the scalar product of (3.72) with the 8 states $u_{s,\mathbf{0}\uparrow}$, $u_{p_x,\mathbf{0}\uparrow}$, $u_{p_y,\mathbf{0}\uparrow}$, $u_{p_z,\mathbf{0}\uparrow}$, $u_{s,\mathbf{0}\downarrow}$, $u_{p_x,\mathbf{0}\downarrow}$, $u_{p_y,\mathbf{0}\downarrow}$, $u_{p_z,\mathbf{0}\downarrow}$ we obtain

$$H_{CB-VB}\begin{pmatrix} C_{n,s\uparrow} \\ C_{n,p_x\uparrow} \\ C_{n,p_y\uparrow} \\ C_{n,p_z\uparrow} \\ C_{n,s\downarrow} \\ C_{n,p_x\downarrow} \\ C_{n,p_y\downarrow} \\ C_{n,p_z\downarrow} \end{pmatrix} = E_{n,\mathbf{k}}\begin{pmatrix} C_{n,s\uparrow} \\ C_{n,p_x\uparrow} \\ C_{n,p_y\uparrow} \\ C_{n,p_z\uparrow} \\ C_{n,s\downarrow} \\ C_{n,p_x\downarrow} \\ C_{n,p_y\downarrow} \\ C_{n,p_z\downarrow} \end{pmatrix}, \tag{3.73}$$

where the Hamiltonian matrix has two parts

$$H_{CB-VB} = \begin{pmatrix} H_4 & 0 \\ 0 & H_4 \end{pmatrix} + \begin{pmatrix} 0 & 0 & 0 & 0 & 0 & 0 & 0 & 0 \\ 0 & 0 & 1 & 0 & 0 & 0 & 0 & i \\ 0 & -1 & 0 & 0 & 0 & 0 & 0 & 1 \\ 0 & 0 & 0 & 0 & 0 & -i & -1 & 0 \\ 0 & 0 & 0 & 0 & 0 & 0 & 0 & 0 \\ 0 & 0 & 0 & -i & 0 & 0 & -1 & 0 \\ 0 & 0 & 0 & 1 & 0 & 1 & 0 & 0 \\ 0 & i & -1 & 0 & 0 & 0 & 0 & 0 \end{pmatrix} \frac{\Delta}{3i}. \tag{3.74}$$

H_4 is the matrix (3.24) calculated for the 4-band model, due to the $\mathbf{k}\cdot\mathbf{p}$ perturbation

$$H_4 = \begin{pmatrix} E_{CB,\mathbf{0}} + \frac{\hbar^2k^2}{2m_o} & \frac{\hbar}{m_o}k_xP & \frac{\hbar}{m_o}k_yP & \frac{\hbar}{m_o}k_zP \\ \frac{\hbar}{m_o}k_xP & E_{VB,\mathbf{0}} + \frac{\hbar^2k^2}{2m_o} & 0 & 0 \\ \frac{\hbar}{m_o}k_yP & 0 & E_{VB,\mathbf{0}} + \frac{\hbar^2k^2}{2m_o} & 0 \\ \frac{\hbar}{m_o}k_zP & 0 & 0 & E_{VB,\mathbf{0}} + \frac{\hbar^2k^2}{2m_o} \end{pmatrix}. \tag{3.75}$$

The spin-orbit part has been calculated in (3.67). Two more rows and columns (first and fifth) are added for the conduction band. All these added matrix elements are zero, due to symmetry ($s \sim xyz$).

The determinant of the eigenvalue problem (3.73) is computed using Maple. All the eigenvalues are doubly degenerate. The energy bands are isotropic, since only $k^2 = k_x^2 + k_y^2 + k_z^2$ appears

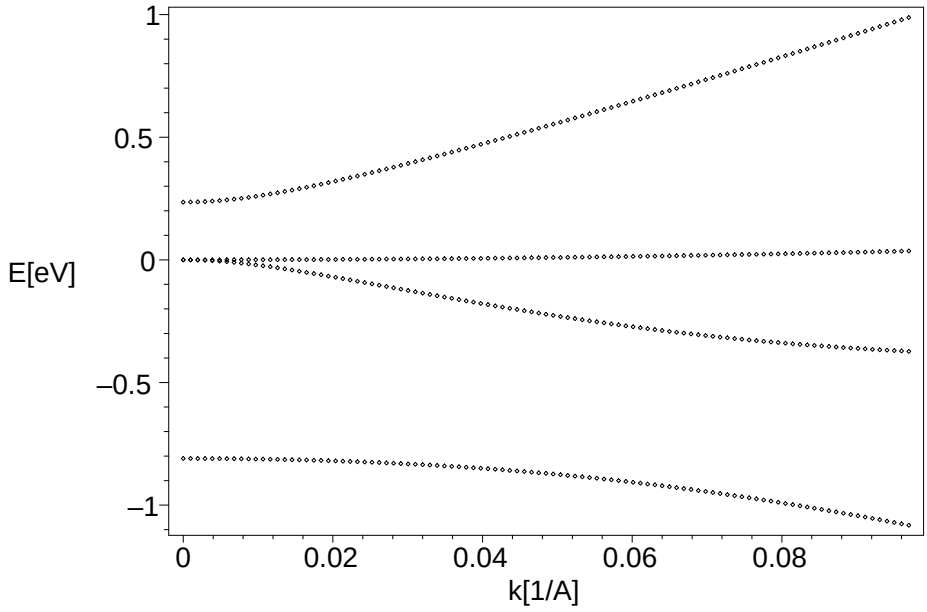

Figure 3.3: Energy bands in 10% of the FBZ for electrons and holes in InSb. Calculation with $\epsilon_o = 0.2352$ [eV], $2P^2/m_o = 22.49$ [eV], $\Delta = 0.81$ [eV], $a = 6.48$ [Å].

in the determinantal equation. When $\mathbf{k} = 0$ the eigenvalues are $E_{CB,\mathbf{0}}$ (twice), $E_{VB,\mathbf{0}} + \Delta/3$ (four times), $E_{VB,\mathbf{0}} - 2\Delta/3$ (twice). We fix the origin of the energy at $E_{VB,\mathbf{0}} + \Delta/3$. Therefore

$$E_{VB,\mathbf{0}} = -\Delta/3, \tag{3.76}$$

$$E_{CB,\mathbf{0}} \equiv \epsilon_o. \tag{3.77}$$

With these definitions the determinantal equation reduces to [18]

$$E'_{n,\mathbf{k}}\left(E'_{n,\mathbf{k}}(E'_{n,\mathbf{k}} - \epsilon_o)(E'_{n,\mathbf{k}} + \Delta) - \frac{\hbar^2 k^2}{m_o^2}P^2(E'_{n,\mathbf{k}} + \frac{2\Delta}{3})\right) = 0, \tag{3.78}$$

where

$$E'_{n,\mathbf{k}} \equiv E_{n,\mathbf{k}} - \frac{\hbar^2 k^2}{2m_o}. \tag{3.79}$$

In Figure 3.3 we see the results of a numerical solution. All four bands are doubly degenerate. The calculations shown here reproduce the results of Kane [18]. The parameters for InSb are taken from Bastard [50]. With the exception of the heavy hole band, which is uncoupled in this model, the energy bands are determined quite well.

3.8 8-band model

This model is an extension of the previous model, when we include contributions from the other energy bands. We include the other bands with the help of Löwdin perturbation theory [23] (see Appendix B).

The basis function which we will use are $u_{n,\mathbf{0}\uparrow}$ and $u_{n,\mathbf{0}\downarrow}$, the eigenfunctions of the Hamiltonian (3.71), with spin added. The functions with $n \in \{s, p_x, p_y, p_z\}$ belong to the A class. The full Hamiltonian

$$H = \frac{p^2}{2m_o} + V(\mathbf{r}) + \frac{\hbar^2 k^2}{2m_o} + \frac{\hbar \mathbf{k}\cdot\mathbf{p}}{m_o} + \frac{\hbar}{4m_o^2c^2}(\sigma \times \nabla V)\cdot(\hbar\mathbf{k} + \mathbf{p}), \tag{3.80}$$

will generate the matrix elements

$$H_{mn} \equiv \langle u_{m,\mathbf{0}}|H|u_{n,\mathbf{0}}\rangle. \tag{3.81}$$

Löwdin perturbation theory requires us to solve self-consistently the system

$$\sum_{n\in A} U_{mn}c_n = Ec_m, \qquad\qquad m \in A, \tag{3.82}$$

where the 'renormalized' matrix elements are

$$U_{mn} \equiv H_{mn} + \sum_{\beta\in B} \frac{H_{m\beta}H_{\beta n}}{E - H_{\beta\beta}} + \ldots\ . \tag{3.83}$$

Several approximations will now be used:

- The $\mathbf{k}$ dependent part of the spin-orbit interaction is ignored.
- The 'renormalized' part of the spin-orbit interaction is ignored.
- The series of the 'renormalized' matrix elements (3.83) is cut after the first order correction.
- The energy E in (3.83) is replaced with the approximate value $(H_{nn} + H_{mm})/2$ [21].

With these approximations the 'renormalized' Hamiltonian becomes

$$U=\begin{pmatrix}H_4 & 0\\ 0 & H_4\end{pmatrix}+\begin{pmatrix}0&0&0&0&0&0&0&0\\0&0&1&0&0&0&0&i\\0&-1&0&0&0&0&0&1\\0&0&0&0&0&-i&-1&0\\0&0&0&0&0&0&0&0\\0&0&0&-i&0&0&-1&0\\0&0&0&1&0&1&0&0\\0&i&-1&0&0&0&0&0\end{pmatrix}\frac{\Delta}{3i}+\begin{pmatrix}H_R & 0\\ 0 & H_R\end{pmatrix}, \tag{3.84}$$

where H_4 is the direct $\mathbf{k}\cdot\mathbf{p}$ interaction

$$H_4=\begin{pmatrix}E_{CB,\mathbf{0}}+\frac{\hbar^2k^2}{2m_o} & i\frac{\hbar}{m_o}k_xP & i\frac{\hbar}{m_o}k_yP & i\frac{\hbar}{m_o}k_zP\\ -i\frac{\hbar}{m_o}k_xP & E_{VB,\mathbf{0}}+\frac{\hbar^2k^2}{2m_o} & 0 & 0\\ -i\frac{\hbar}{m_o}k_yP & 0 & E_{VB,\mathbf{0}}+\frac{\hbar^2k^2}{2m_o} & 0\\ -i\frac{\hbar}{m_o}k_zP & 0 & 0 & E_{VB,\mathbf{0}}+\frac{\hbar^2k^2}{2m_o}\end{pmatrix}, \tag{3.85}$$

and H_R is the 'renormalized' part of the $\mathbf{k}\cdot\mathbf{p}$ interaction [22]

$$H_R=\begin{pmatrix}Ak^2 & Bk_yk_z & Bk_xk_z & Bk_xk_y\\ Bk_yk_z & Lk_x^2+M(k_y^2+k_z^2) & Nk_xk_y & Nk_xk_z\\ Bk_xk_z & Nk_xk_y & Lk_y^2+M(k_x^2+k_z^2) & Nk_yk_z\\ Bk_xk_y & Nk_xk_z & Nk_yk_z & Lk_z^2+M(k_x^2+k_y^2)\end{pmatrix}. \tag{3.86}$$

The definition of the parameter P is

$$P\equiv -i\langle s|p_x|p_x\rangle. \tag{3.87}$$

The parameters L, M, N are closely related to those in the DKK Hamiltonian. The only difference is that now the sum does not include the first CB, which is now taken into account exactly, and not within the perturbation. In these parameters the energy E from (3.83) is replaced by $E_{VB,\mathbf{0}}$.

$$L\equiv\frac{\hbar^2}{m_o^2}\sum_{n\neq s,p_x,p_y,p_z}\frac{\langle p_x|p_x|n\rangle\langle n|p_x|p_x\rangle}{E_{VB,\mathbf{0}}-E_n}, \tag{3.88}$$

$$M\equiv\frac{\hbar^2}{m_o^2}\sum_{n\neq s,p_x,p_y,p_z}\frac{\langle p_x|p_y|n\rangle\langle n|p_y|p_x\rangle}{E_{VB,\mathbf{0}}-E_n}, \tag{3.89}$$

$$N \equiv \frac{\hbar^2}{m_o^2} \sum_{n\neq s,p_x,p_y,p_z} \frac{\langle p_z|p_z|n\rangle\langle n|p_x|p_x\rangle + \langle p_z|p_x|n\rangle\langle n|p_z|p_x\rangle}{E_{VB,\mathbf{0}} - E_n}. \tag{3.90}$$

Consider now the matrix element

$$\frac{\hbar^2}{m_o^2} k_\alpha k_\beta \sum_{n\neq s,p_x,p_y,p_z} \frac{\langle s|p_\alpha|n\rangle\langle n|p_\beta|s\rangle}{E - E_n}. \tag{3.91}$$

In order to have the Cartesian indices paired, we must have $\alpha = \beta$. Because of the symmetry

$$\langle s|p_x|n\rangle\langle n|p_x|s\rangle = \langle s|p_y|n\rangle\langle n|p_y|s\rangle = \langle s|p_z|n\rangle\langle n|p_z|s\rangle. \tag{3.92}$$

Therefore the parameter A is

$$A \equiv \frac{\hbar^2}{m_o^2} \sum_{n\neq s,p_x,p_y,p_z} \frac{\langle s|p_x|n\rangle\langle n|p_x|s\rangle}{E_{CB,\mathbf{0}} - E_n}, \tag{3.93}$$

where the energy E is replaced by $E_{CB,\mathbf{0}}$.

Consider now the matrix element

$$\frac{\hbar^2}{m_o^2} k_\alpha k_\beta \sum_{n\neq s,p_x,p_y,p_z} \frac{\langle s|p_\alpha|n\rangle\langle n|p_\beta|p_z\rangle}{E - E_n}. \tag{3.94}$$

In DM crystals with inversion symmetry this matrix element is zero. In ZB crystals it is non zero. In order to have the Cartesian indices paired, we must have $\{\alpha, \beta\} = \{x, y\}$. The two permutations bring equal contributions.

Because of the symmetry

$$\langle s|p_x|n\rangle\langle n|p_y|p_z\rangle = \langle s|p_y|n\rangle\langle n|p_z|p_x\rangle = \langle s|p_z|n\rangle\langle n|p_x|p_y\rangle. \tag{3.95}$$

Therefore the parameter B is

$$B \equiv \frac{2\hbar^2}{m_o^2} \sum_{n\neq s,p_x,p_y,p_z} \frac{\langle s|p_x|n\rangle\langle n|p_y|p_z\rangle}{(E_{CB,\mathbf{0}} + E_{VB,\mathbf{0}})/2 - E_n}, \tag{3.96}$$

where the energy E is replaced by $(E_{CB,\mathbf{0}} + E_{VB,\mathbf{0}})/2$.

In Figure 3.4 we see the results of a numerical diagonalization. The parameters for InSb are taken from [51]. The double degeneracy of the bands is lifted by the 'renormalized' Hamiltonian. This is due to the B term, which explicitly eliminates the symmetry to inversion in $U(\mathbf{k})$.

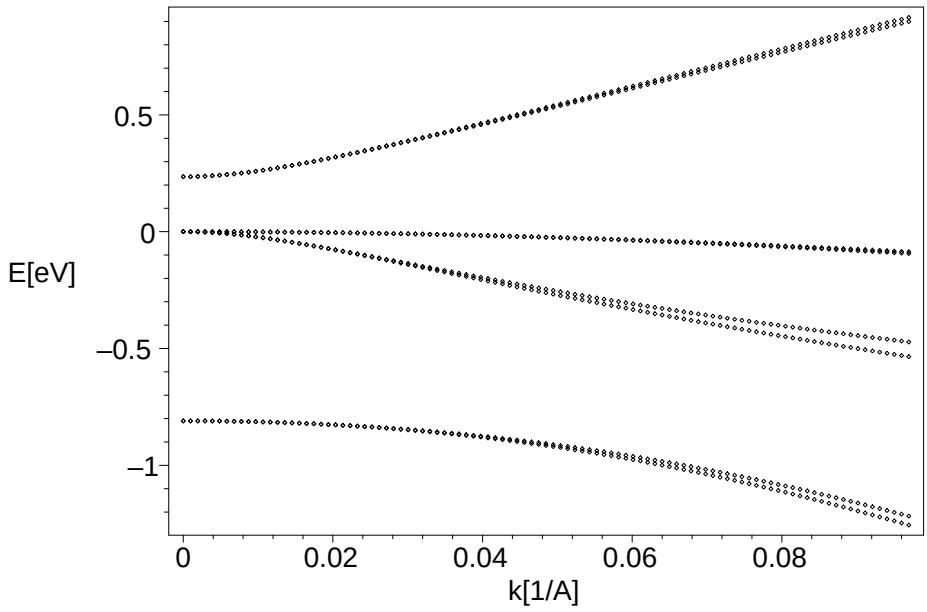

Figure 3.4: Energy bands in 10% of the FBZ for electrons and holes in InSb. Calculation with $\epsilon_o = 0.2352$ [eV], $2P^2/m_o = 22.49$ [eV], $\Delta = 0.81$ [eV], $a = 6.48$ [Å], $A = 0[\hbar^2/2m_o], B = -3.3[\hbar^2/2m_o], L = -2.5[\hbar^2/2m_o], M = -5.6[\hbar^2/2m_o], N = -4.3[\hbar^2/2m_o]$.

3.9 Appendix A. Degenerate perturbation theory

Consider an unperturbed system with degenerate eigenstates. Sometimes the perturbation Hamiltonian consists of two parts: one which contributes in first order, $H^{(1)}$, and one which contributes in second order, $H^{(2)}$. If these two contributions have the same order of magnitude, then it is better to write the perturbation expansion as [17]

$$H(\lambda) = H^{(0)} + \lambda^2 H^{(1)} + \lambda H^{(2)}. \tag{3.97}$$

In this way the first order contribution of $H^{(1)}$ will automatically be paired to the second order contribution of $H^{(2)}$.We write the wave-function as

$$|\psi\rangle = |\psi^{(0)}\rangle + \lambda|\psi^{(1)}\rangle + \lambda^2|\psi^{(2)}\rangle + ... \ , \tag{3.98}$$

and the energy as

$$E(\lambda) = E^{(0)} + \lambda E^{(1)} + \lambda^2 E^{(2)} + ... \ . \tag{3.99}$$

We equate terms with same power in λ in Schrodinger's equation

$$\begin{aligned}(H^{(0)} + \lambda^2 H^{(1)} + \lambda H^{(2)})(|\psi^{(0)}\rangle + \lambda|\psi^{(1)}\rangle + \lambda^2|\psi^{(2)}\rangle + ...) = \\ (E^{(0)} + \lambda E^{(1)} + \lambda^2 E^{(2)} + ...)(|\psi^{(0)}\rangle + \lambda|\psi^{(1)}\rangle + \lambda^2|\psi^{(2)}\rangle + ...).\end{aligned} \tag{3.100}$$

It follows that

$$H^{(0)}|\psi^{(0)}\rangle = E^{(0)}|\psi^{(0)}\rangle, \tag{3.101}$$

$$H^{(0)}|\psi^{(1)}\rangle + H^{(2)}|\psi^{(0)}\rangle = E^{(0)}|\psi^{(1)}\rangle + E^{(1)}|\psi^{(0)}\rangle, \tag{3.102}$$

$$H^{(0)}|\psi^{(2)}\rangle + H^{(2)}|\psi^{(1)}\rangle + H^{(1)}|\psi^{(0)}\rangle = E^{(0)}|\psi^{(2)}\rangle + E^{(1)}|\psi^{(1)}\rangle + E^{(2)}|\psi^{(0)}\rangle. \tag{3.103}$$

Consider the non-perturbed eigenvalue problem for the degenerate level $n, m, ...$, and for the other levels $\alpha, \beta, ...$

$$H^{(0)}|\psi_n\rangle = E_n|\psi_n\rangle, \tag{3.104}$$

$$H^{(0)}|\psi_\alpha\rangle = E_\alpha|\psi_\alpha\rangle. \tag{3.105}$$

The wave-function components will be written as

$$|\psi^{(0)}\rangle = \textstyle\sum_n c_n^{(0)}|\psi_n\rangle, \tag{3.106}$$

$$|\psi^{(1)}\rangle = \textstyle\sum_n c_n^{(1)}|\psi_n\rangle + \sum_\alpha c_\alpha^{(1)}|\psi_\alpha\rangle. \tag{3.107}$$

In writing (3.106) we have used (3.101) and (3.104). In the limit $\lambda \to 0$ we recover the non-perturbed states. Also

$$E^{(0)} = E_n. \tag{3.108}$$

We multiply (3.102) with $\langle\psi^{(0)}|$. Using (3.101) and the fact that $\langle\psi^{(0)}|H^{(2)}|\psi^{(0)}\rangle = 0$, we obtain

$$E^{(1)} = 0. \tag{3.109}$$

We multiply (3.102) with $\langle\psi_\beta|$, and using (3.105) we obtain

$$E_\beta c_\beta^{(1)} + \langle\psi_\beta|H^{(2)}|\psi^{(0)}\rangle = E_n c_\beta^{(1)}. \tag{3.110}$$

Therefore the coefficient $c_\beta^{(1)}$ is

$$c_\beta^{(1)} = \frac{\langle\psi_\beta|H^{(2)}|\psi^{(0)}\rangle}{E_n - E_\beta}. \tag{3.111}$$

We multiply (3.103) with $\langle\psi_m|$, and using (3.104) we obtain

$$\langle\psi_m|H^{(2)}|\psi^{(1)}\rangle + \langle\psi_m|H^{(1)}|\psi^{(0)}\rangle = E^{(2)}c_m^{(0)}. \tag{3.112}$$

Using (3.107) and the fact that $\langle\psi_m|H^{(2)}|\psi_n\rangle = 0$, the first term of (3.82) reduces to

$$\langle\psi_m|H^{(2)}|\psi^{(1)}\rangle = \langle\psi_m|H^{(2)}|\sum_\alpha c_\alpha^{(1)}|\psi_\alpha\rangle. \tag{3.113}$$

Equation (3.112), with the help of (3.113) and (3.111), reduces to

$$\sum_\alpha \frac{\langle\psi_\alpha|H^{(2)}|\psi^{(0)}\rangle}{E_n - E_\alpha}\langle\psi_m|H^{(2)}|\psi_\alpha\rangle + \langle\psi_m|H^{(1)}|\psi^{(0)}\rangle = E^{(2)}c_m^{(0)}. \tag{3.114}$$

By substitution of (3.106) we finally obtain

$$\sum_n \left(\sum_\alpha \frac{\langle\psi_m|H^{(2)}|\psi_\alpha\rangle\langle\psi_\alpha|H^{(2)}|\psi_n\rangle}{E_n - E_\alpha} + \langle\psi_m|H^{(1)}|\psi_n\rangle\right) c_n^{(0)} = E^{(2)}c_m^{(0)}. \tag{3.115}$$

Therefore the coefficients $c_n^{(0)}$ and the energy $E^{(2)}$ are obtained by solving the eigenvalue problem (3.115). In the particular case when $H^{(1)} = 0$ we recover the simpler case of degenerate perturbation theory with second order contributions [52].

3.10 Appendix B. Löwdin perturbation theory

Consider a Hamiltonian H and a finite set of orthonormalized functions $\psi_n^{(0)}$, which are approximate eigenfunctions of H. Suppose the set of functions $\psi_n^{(0)}$ is split into to parts, A and B. We will expand the eigenfunctions of H as

$$\psi = \sum_n c_n \psi_n^{(0)}. \tag{3.116}$$

We substitute (3.116) into the eigenvalue equation

$$H\psi = E\psi. \tag{3.117}$$

We take the scalar product of (3.117) with $\psi_m^{(0)}$ and we obtain

$$\textstyle\sum_n H_{mn} c_n = E c_m, \tag{3.118}$$

$$\textstyle\sum_{n\neq m} H_{mn} c_n = (E - H_{mm}) c_m, \tag{3.119}$$

where

$$H_{mn} \equiv \langle \psi_m^{(0)} | H | \psi_n^{(0)} \rangle. \tag{3.120}$$

From (3.119) we formally extract c_m as

$$c_m = \sum_{\alpha\in A, \alpha\neq m} \frac{H_{m\alpha}}{E - H_{mm}} c_\alpha + \sum_{\beta\in B, \beta\neq m} \frac{H_{m\beta}}{E - H_{mm}} c_\beta. \tag{3.121}$$

From (3.121) we obtain c_β as

$$c_\beta = \sum_{\alpha\in A} \frac{H_{\beta\alpha}}{E - H_{\beta\beta}} c_\alpha + \sum_{\gamma\in B, \gamma\neq\beta} \frac{H_{\beta\gamma}}{E - H_{\beta\beta}} c_\gamma. \tag{3.122}$$

We substitute (3.122) back into (3.121), and we iterate the process, with the ultimate goal of eliminating all the c_δ's with $\delta \in B$.

$$c_m = \sum_{\alpha\in A, \alpha\neq m} \frac{H_{m\alpha}}{E - H_{mm}} c_\alpha + \sum_{\beta\in B, \beta\neq m} \frac{H_{m\beta}}{E - H_{mm}} \sum_{\alpha\in A} \frac{H_{\beta\alpha}}{E - H_{\beta\beta}} c_\alpha + \dots . \tag{3.123}$$

We choose $m \in A$ and we write (3.123) as

$$\sum_{\alpha\in A} U_{m\alpha} c_\alpha = E c_m, \qquad (m \in A), \tag{3.124}$$

with

$$U_{m\alpha} \equiv H_{m\alpha} + \sum_{\beta\in B,\beta\neq m} \frac{H_{m\beta}H_{\beta\alpha}}{E - H_{\beta\beta}} + ..., \qquad (\alpha \in A). \tag{3.125}$$

We have therefore reduced the eigenvalue problem (3.118) on the full $A + B$ space to the restricted eigenvalue problem (3.124) on the A space. The effect of the B space is taken into account through the 'renormalized' matrix elements (3.125). Equations (3.124) and (3.125) are solved iteratively, until convergence is achieved.

We choose $m \in B$ and we write (3.123) as

$$c_m = \sum_{\alpha\in A} \frac{U_{m\alpha}}{E - H_{mm}} c_\alpha, \qquad (m \in B). \tag{3.126}$$

In this way we have completely determined the coefficients of the eigenfunction expansion (3.116).

Chapter 4

$\mathbf{k} \cdot \mathbf{p}$ theory - Burt

4.1 Introduction

The Kane model, developed in the previous chapter, deals with bulk semiconductors. The periodicity characteristic to an infinite lattice has allowed us to apply the Bloch theorem. This periodicity makes $\mathbf{k}$ a good quantum number.

However, when dealing with heterostructures, we no longer have periodicity. The question has arisen, how can we still use Kane's model when dealing with semiconductor quantum wells, wires, and dots? Two empirical changes are applied to Kane's Hamiltonian to extend its range of applicability to heterostructures.

First, recognizing that the k_x, k_y, k_z components have appeared by differentiation of the exponential in the Bloch function

$$\nabla e^{i\mathbf{k}\cdot\mathbf{r}} = i\mathbf{k}e^{i\mathbf{k}\cdot\mathbf{r}}, \tag{4.1}$$

we replace these components by

$$k_x \rightarrow \hat{k_x} = -i\frac{\partial}{\partial x}, \tag{4.2}$$

$$k_y \rightarrow \hat{k_y} = -i\frac{\partial}{\partial y}, \tag{4.3}$$

$$k_z \rightarrow \hat{k_z} = -i\frac{\partial}{\partial z}. \tag{4.4}$$

However, since the Kane parameters in the Hamiltonian now depend on position, being different in different semiconductors, they no longer commute with the differential operators. We

therefore need an ordering of the Kane parameters and of the differentials in the Hamiltonian. A popular choice is to symmetrize each individual element of the 8×8 Hamiltonian matrix. This choice also guarantees that the resulting Hamiltonian is hermitian. The required changes to Kane's Hamiltonian are [53, 54]

$$Tk_x \rightarrow \frac{1}{2}(T\hat{k_x} + \hat{k_x}T), \ldots , \tag{4.5}$$

$$Tk_xk_y \rightarrow \frac{1}{2}(\hat{k_x}T\hat{k_y} + \hat{k_y}T\hat{k_x}), \ldots , \tag{4.6}$$

where T represents any Kane parameter.

Symmetrized Hamiltonians have been successfully applied to the calculation of energy bands in quantum wells [53, 54, 55], wires [56], and dots[57].

4.2 Burt's theory

The arbitrariness of the symmetrization procedure has led Burt to believe that this is not the right theory. Following a different approach, Burt chooses to *derive* the Hamiltonian for a semiconductor heterostructure. He succeeded doing it in a series of papers [5, 6, 7, 8, 9], culminating with a review article [10].

In Burt's theory we start with a complete set of functions $U_n(\mathbf{r})$ that are periodic in the position variable $\mathbf{r}$. We assume that the different semiconductors of the heterojunction have the same lattice constant, and the same Γ point Bloch functions. In fact, these zone-centre eigenfunctions will be the ones used as $U_n(\mathbf{r})$. The wave-function is uniquely expanded as

$$\Psi(\mathbf{r}) = \sum_n F_n(\mathbf{r})U_n(\mathbf{r}), \tag{4.7}$$

where the envelope functions $F_n(\mathbf{r})$ have a plane-wave expansion restricted to the first Brillouin zone (FBZ).

Substitution of (4.7) into Schrödinger's equation, and equating the coefficients of $U_n(\mathbf{r})$, leads to the exact equation

$$\frac{-\hbar^2}{2m}\nabla^2 F_n(\mathbf{r}) + \sum_{n'}\frac{-i\hbar}{m}\mathbf{p}_{nn'}\cdot\nabla F_{n'}(\mathbf{r}) + \sum_{n'}\int_{UC} H_{nn'}(\mathbf{r},\mathbf{r'})F_{n'}(\mathbf{r'})d\mathbf{r'} = EF_n(\mathbf{r}), \tag{4.8}$$

where

$$\mathbf{p}_{nn'} = \tfrac{1}{V_c}\textstyle\int_{UC} U_n^*(\mathbf{r})\mathbf{p}U_{n'}(\mathbf{r})d\mathbf{r}, \tag{4.9}$$

$$H_{nn'}(\mathbf{r},\mathbf{r}') = T_{nn'}\Delta(\mathbf{r}-\mathbf{r}') + V_{nn'}(\mathbf{r},\mathbf{r}'), \tag{4.10}$$

$$T_{nn'} = \tfrac{1}{V_c}\textstyle\int_{UC} U_n^*(\mathbf{r})\frac{p^2}{2m}U_{n'}(\mathbf{r})d\mathbf{r}, \tag{4.11}$$

$$\Delta(\mathbf{r}-\mathbf{r}') = \tfrac{1}{\Omega}\textstyle\sum_{\mathbf{k}\in FBZ} e^{i\mathbf{k}\cdot(\mathbf{r}-\mathbf{r}')}, \tag{4.12}$$

$$V(\mathbf{r})\Psi(\mathbf{r}) = \textstyle\sum_n \left(\sum_{n'}\int_{UC} V_{nn'}(\mathbf{r},\mathbf{r}')F_{n'}(\mathbf{r}')d\mathbf{r}'\right)U_n(\mathbf{r}). \tag{4.13}$$

The volume of a unit cell (UC) in real space is V_c, and in reciprocal space is Ω. The normalization of the functions $U_n(\mathbf{r})$ is

$$\frac{1}{V_c}\int_{UC} U_n^*(\mathbf{r})U_{n'}(\mathbf{r})d\mathbf{r} = \delta_{nn'}. \tag{4.14}$$

We further neglect non-local contributions in $H_{nn'}(\mathbf{r},\mathbf{r}')$, and contributions from the interface regions. We finally obtain the envelope function equation:

$$\frac{-\hbar^2}{2m}\nabla^2 F_n(\mathbf{r}) + \sum_{n'}\frac{-i\hbar}{m}\mathbf{p}_{nn'}\cdot\nabla F_{n'}(\mathbf{r}) + \sum_{n'} H_{nn'}(\mathbf{r})F_{n'}(\mathbf{r}) = EF_n(\mathbf{r}). \tag{4.15}$$

Here $H_{nn'}(\mathbf{r})$ is constant within a given homogeneous semiconductor region, equal to the bulk value

$$H_{nn'} = \frac{1}{V_c}\int_{UC} U_n^*(\mathbf{r})H(\mathbf{r})U_{n'}(\mathbf{r})d\mathbf{r}, \tag{4.16}$$

where $H(\mathbf{r})$ is the Hamiltonian of the bulk semiconductor.

4.3 Envelope function equations

We divide the envelope functions into two categories: dominant ones, labeled with an index s, and small ones, labeled with an index r.

We write the equation (4.15) for $n = r$

$$\frac{-\hbar^2}{2m}\nabla^2 F_r(\mathbf{r}) + \sum_{n'}\frac{-i\hbar}{m}\mathbf{p}_{rn'}\cdot\nabla F_{n'}(\mathbf{r}) + \sum_{n'} H_{rn'}(\mathbf{r})F_{n'}(\mathbf{r}) = EF_r(\mathbf{r}). \tag{4.17}$$

We now expand the sums as

$$\sum_{n'} \to \sum_{s'} + \sum_{r'}. \tag{4.18}$$

We neglect in (4.17) the first term (the small envelope function is slowly varying), and in the sums over n' we keep only the dominant terms (with s') and the term containing $F_r(\mathbf{r})$

$$\sum_{s'} \frac{-i\hbar}{m}\mathbf{p}_{rs'}\cdot\nabla F_{s'}(\mathbf{r}) + \sum_{s'} H_{rs'}(\mathbf{r})F_{s'}(\mathbf{r}) + H_{rr}(\mathbf{r})F_r(\mathbf{r}) = EF_r(\mathbf{r}). \tag{4.19}$$

In the end the envelope function $F_r(\mathbf{r})$ is extracted as

$$F_r(\mathbf{r}) = \frac{1}{E - H_{rr}(\mathbf{r})}\sum_{s'}\left(\frac{-i\hbar}{m}\mathbf{p}_{rs'}\cdot\nabla F_{s'}(\mathbf{r}) + H_{rs'}(\mathbf{r})F_{s'}(\mathbf{r})\right). \tag{4.20}$$

We write the equation (4.15) for $n = s$

$$\frac{-\hbar^2}{2m}\nabla^2 F_s(\mathbf{r}) + \sum_{n'}\frac{-i\hbar}{m}\mathbf{p}_{sn'}\cdot\nabla F_{n'}(\mathbf{r}) + \sum_{n'} H_{sn'}(\mathbf{r})F_{n'}(\mathbf{r}) = EF_s(\mathbf{r}). \tag{4.21}$$

We now expand the sums as

$$\sum_{n'} \to \sum_{s"} + \sum_{r}. \tag{4.22}$$

The expanded equation is

$$\begin{aligned}\frac{-\hbar^2}{2m}\nabla^2 F_s(\mathbf{r}) + \sum_{s"}\frac{-i\hbar}{m}\mathbf{p}_{ss"}\cdot\nabla F_{s"}(\mathbf{r}) + \sum_{s"} H_{ss"}(\mathbf{r})F_{s"}(\mathbf{r})\\ + \sum_{r}\frac{-i\hbar}{m}\mathbf{p}_{sr}\cdot\nabla F_r(\mathbf{r}) + \sum_{r} H_{sr}(\mathbf{r})F_r(\mathbf{r}) = EF_s(\mathbf{r}).\end{aligned} \tag{4.23}$$

We substitute $F_r(\mathbf{r})$ from (4.20) into (4.23)

$$\begin{aligned}&\frac{-\hbar^2}{2m}\nabla^2 F_s(\mathbf{r}) + \sum_{s"}\frac{-i\hbar}{m}\mathbf{p}_{ss"}\cdot\nabla F_{s"}(\mathbf{r}) + \sum_{s"} H_{ss"}(\mathbf{r})F_{s"}(\mathbf{r})\\ &+\sum_{r}\frac{-i\hbar}{m}\mathbf{p}_{sr}\cdot\nabla\left[\frac{1}{E - H_{rr}(\mathbf{r})}\sum_{s'}\left(\frac{-i\hbar}{m}\mathbf{p}_{rs'}\cdot\nabla F_{s'}(\mathbf{r}) + H_{rs'}(\mathbf{r})F_{s'}(\mathbf{r})\right)\right]\\ &+\sum_{r} H_{sr}(\mathbf{r})\frac{1}{E - H_{rr}(\mathbf{r})}\sum_{s'}\left(\frac{-i\hbar}{m}\mathbf{p}_{rs'}\cdot\nabla F_{s'}(\mathbf{r}) + H_{rs'}(\mathbf{r})F_{s'}(\mathbf{r})\right) = EF_s(\mathbf{r}),\end{aligned} \tag{4.24}$$

$$\begin{aligned}&\frac{-\hbar^2}{2m}\nabla^2 F_s(\mathbf{r}) + \sum_{s"}\frac{-i\hbar}{m}\mathbf{p}_{ss"}\cdot\nabla F_{s"}(\mathbf{r}) + \sum_{s"} H_{ss"}(\mathbf{r})F_{s"}(\mathbf{r})\\ &+\sum_{r}\sum_{s'}\frac{-\hbar^2}{m^2}\mathbf{p}_{sr}\cdot\nabla\left(\frac{\mathbf{p}_{rs'}\cdot\nabla F_{s'}(\mathbf{r})}{E - H_{rr}(\mathbf{r})}\right)\\ &+\sum_{r}\sum_{s'}\frac{-i\hbar}{m}\mathbf{p}_{sr}\cdot\nabla\left(\frac{H_{rs'}(\mathbf{r})}{E - H_{rr}(\mathbf{r})}\right)F_{s'}(\mathbf{r})\end{aligned}$$

$$+\sum_r\sum_{s'}\frac{-i\hbar}{m}\frac{H_{rs'}(\mathbf{r})}{E-H_{rr}(\mathbf{r})}\mathbf{p}_{sr}\cdot\nabla F_{s'}(\mathbf{r})$$
$$+\sum_r\sum_{s'}\frac{-i\hbar}{m}\frac{H_{sr}(\mathbf{r})}{E-H_{rr}(\mathbf{r})}\mathbf{p}_{rs'}\cdot\nabla F_{s'}(\mathbf{r})$$
$$+\sum_r\sum_{s'}\frac{H_{sr}(\mathbf{r})H_{rs'}(\mathbf{r})}{E-H_{rr}(\mathbf{r})}F_{s'}(\mathbf{r})=EF_s(\mathbf{r}). \tag{4.25}$$

We now neglect the terms from the 3-rd, 4-th, and 5-th lines in (4.25). The term on the 3-rd line is non-zero only at an interface. The other two terms are also significant only at an interface, being very small in the bulk of the semiconductors. We write the equation as

$$\frac{-\hbar^2}{2m}\nabla^2F_s(\mathbf{r})+\sum_{s"}\frac{-i\hbar}{m}\mathbf{p}_{ss"}\cdot\nabla F_{s"}(\mathbf{r})+\sum_{s"}H_{ss"}(\mathbf{r})F_{s"}(\mathbf{r})$$
$$+\sum_r\sum_{s'}\sum_{\alpha=x,y,z}\sum_{\beta=x,y,z}\frac{-\hbar^2}{m^2}\partial_\alpha\frac{p_{sr\alpha}p_{rs'\beta}}{E-H_{rr}(\mathbf{r})}\partial_\beta F_{s'}(\mathbf{r})$$
$$+\sum_r\sum_{s'}\frac{H_{sr}(\mathbf{r})H_{rs'}(\mathbf{r})}{E-H_{rr}(\mathbf{r})}F_{s'}(\mathbf{r})=EF_s(\mathbf{r}). \tag{4.26}$$

In (4.26) we have moved the momentum matrix element to the right of the differential, since it doesn't depend on position.

4.4 Homogeneous semiconductor

In the simpler case of a homogeneous semiconductor [7] the functions $U_n(\mathbf{r})$ are the zone-centre eigenfunctions. We have only diagonal elements H_{ss}, and the equation (4.26) becomes

$$\frac{-\hbar^2}{2m}\nabla^2F_s(\mathbf{r})+\sum_{s"}\frac{-i\hbar}{m}\mathbf{p}_{ss"}\cdot\nabla F_{s"}(\mathbf{r})+H_{ss}F_s(\mathbf{r})$$
$$+\sum_r\sum_{s'}\sum_{\alpha=x,y,z}\sum_{\beta=x,y,z}\frac{-\hbar^2}{m^2}\partial_\alpha\frac{p_{sr\alpha}p_{rs'\beta}}{E-H_{rr}}\partial_\beta F_{s'}(\mathbf{r})=EF_s(\mathbf{r}). \tag{4.27}$$

Because (4.27) is a differential equation with constant coefficients we can find solutions of the form

$$F_s(\mathbf{r})=A_s(\mathbf{k})e^{i\mathbf{k}\cdot\mathbf{r}}. \tag{4.28}$$

The eigenvalue problem (4.27) becomes

$$\frac{\hbar^2k^2}{2m}A_s(\mathbf{k})+\sum_{s"}\frac{\hbar}{m}\mathbf{p}_{ss"}\cdot\mathbf{k}A_{s"}(\mathbf{k})+H_{ss}A_s(\mathbf{k})$$

$$+\sum_r\sum_{s'}\sum_{\alpha=x,y,z}\sum_{\beta=x,y,z}\frac{\hbar^2}{m^2}k_\alpha\frac{p_{sr\alpha}p_{rs'\beta}}{E-H_{rr}}k_\beta A_{s'}(\mathbf{k})=EA_s(\mathbf{k}), \tag{4.29}$$

which is the well known equation of the Kane model.

4.5 Burt's Hamiltonian

We now apply the most dubious approximation of the Burt model, that the zone centre eigenfunctions are the same in all semiconductors of the quantum microstructure. This will again generate only diagonal elements $H_{ss}(\mathbf{r})$, and the equation (4.26) becomes

$$\frac{-\hbar^2}{2m}\nabla^2F_s(\mathbf{r})+\sum_{s"}\frac{-i\hbar}{m}\mathbf{p}_{ss"}\cdot\nabla F_{s"}(\mathbf{r})+H_{ss}(\mathbf{r})F_s(\mathbf{r})$$
$$+\sum_r\sum_{s'}\sum_{\alpha=x,y,z}\sum_{\beta=x,y,z}\frac{-\hbar^2}{m^2}\partial_\alpha\frac{p_{sr\alpha}p_{rs'\beta}}{E-H_{rr}(\mathbf{r})}\partial_\beta F_{s'}(\mathbf{r})=EF_s(\mathbf{r}). \tag{4.30}$$

4.6 Burt's Hamiltonian for ZB structures

We will investigate in great detail the Hamiltonian matrix element $H^{(int)}_{ss'}$ due to the interaction of the dominant envelope functions with the remote ones.

$$H^{(int)}_{ss'}=\sum_r\sum_{\alpha=x,y,z}\sum_{\beta=x,y,z}\frac{\hbar^2}{m^2}\hat{k_\alpha}\frac{p_{sr\alpha}p_{rs'\beta}}{E-H_{rr}(\mathbf{r})}\hat{k_\beta}. \tag{4.31}$$

We introduce Dirac's notation for the momentum matrix elements. We label the remote bands by their IRR γ, by an index n_γ to distinguish between bands with the same IRR, and by an index m_γ to distinguish between basis functions of the same IRR.

$$H^{(int)}_{ss'}=\sum_\gamma\sum_{n_\gamma}\sum_{m_\gamma}\sum_{\alpha=x,y,z}\sum_{\beta=x,y,z}\frac{\hbar^2}{m^2}\hat{k_\alpha}\frac{\langle s|p_\alpha|\gamma,n_\gamma,m_\gamma\rangle\langle\gamma,n_\gamma,m_\gamma|p_\beta|s'\rangle}{E-H_{\gamma n_\gamma}(\mathbf{r})}\hat{k_\beta}. \tag{4.32}$$

We will now concentrate our attention on

$$\sum_{m_\gamma}\langle s|p_\alpha|\gamma,n_\gamma,m_\gamma\rangle\langle\gamma,n_\gamma,m_\gamma|p_\beta|s'\rangle, \tag{4.33}$$

for a given band (γ,n_γ).

It is useful to notice that, if s or s' belongs to Γ_1, then γ can be only Γ_{15} for non-zero elements. Also, if s and s' belong to Γ_{15}, then γ can be only Γ_1, Γ_{15}, Γ_{25}, or Γ_{12} for non-zero elements.

4.6.1 $s = S, \gamma = \Gamma_{15}, s' = S$

Due to (2.9) the sum (4.33) reduces to

$$\langle S|p_x|X'\rangle\langle X'|p_x|S\rangle\delta_{\alpha x}\delta_{\beta x} + \langle S|p_y|Y'\rangle\langle Y'|p_y|S\rangle\delta_{\alpha y}\delta_{\beta y} + \langle S|p_z|Z'\rangle\langle Z'|p_z|S\rangle\delta_{\alpha z}\delta_{\beta z}, \tag{4.34}$$

which is equal to

$$\langle S|p_x|X'\rangle\langle X'|p_x|S\rangle(\delta_{\alpha x}\delta_{\beta x} + \delta_{\alpha y}\delta_{\beta y} + \delta_{\alpha z}\delta_{\beta z}). \tag{4.35}$$

Also

$$\delta_{\alpha x}\delta_{\beta x} + \delta_{\alpha y}\delta_{\beta y} + \delta_{\alpha z}\delta_{\beta z} = \delta_{\alpha\beta}(\delta_{\alpha x} + \delta_{\alpha y} + \delta_{\alpha z}) = \delta_{\alpha\beta}. \tag{4.36}$$

Therefore

$$\begin{aligned} H_{SS}^{(int)\Gamma_{15}} = \sum_{n_{\Gamma_{15}}}\sum_{\alpha=x,y,z}\frac{\hbar^2}{m^2}\hat{k_\alpha}\frac{\langle S|p_x|\Gamma_{15}, n_{\Gamma_{15}}, X'\rangle\langle\Gamma_{15}, n_{\Gamma_{15}}, X'|p_x|S\rangle}{E - H_{\Gamma_{15}n_{\Gamma_{15}}}(\mathbf{r})}\hat{k_\alpha} \\ = \hat{k_x}A'\hat{k_x} + \hat{k_y}A'\hat{k_y} + \hat{k_z}A'\hat{k_z}, \end{aligned} \tag{4.37}$$

where

$$\begin{aligned} A' \equiv \sum_{n_{\Gamma_{15}}}\frac{\hbar^2}{m^2}\frac{\langle S|p_x|\Gamma_{15}, n_{\Gamma_{15}}, X'\rangle\langle\Gamma_{15}, n_{\Gamma_{15}}, X'|p_x|S\rangle}{E - H_{\Gamma_{15}n_{\Gamma_{15}}}(\mathbf{r})} \\ = \sum_{\nu\in\Gamma_{15}}\frac{\hbar^2}{m^2}\frac{\langle S|p_x|\nu\rangle\langle\nu|p_x|S\rangle}{E - H_\nu(\mathbf{r})}. \end{aligned} \tag{4.38}$$

To get the last line we have artificially inserted the zero matrix elements with Y' and Z'. We thus sum over all basis functions of the IRR. The result is invariant, and does not depend on the basis functions used. This is the expression given by Kane [22].

In the limit of a homogeneous semiconductor we have

$$H_{SS}^{(int)\Gamma_{15}} = A'(k_x^2 + k_y^2 + k_z^2) = A'k^2. \tag{4.39}$$

4.6.2 $s = S, \gamma = \Gamma_{15}, s' = X$

Due to (2.9) and (2.10) the sum (4.33) reduces to

$$\langle S|p_y|Y'\rangle\langle Y'|p_z|X\rangle\delta_{\alpha y}\delta_{\beta z} + \langle S|p_z|Z'\rangle\langle Z'|p_y|X\rangle\delta_{\alpha z}\delta_{\beta y}, \tag{4.40}$$

which is equal to

$$\langle S|p_x|X'\rangle\langle X'|p_y|Z\rangle(\delta_{\alpha y}\delta_{\beta z}+\delta_{\alpha z}\delta_{\beta y}). \tag{4.41}$$

Therefore

$$H_{SX}^{(int)\Gamma_{15}}=\hat{k_y}\frac{B}{2}\hat{k_z}+\hat{k_z}\frac{B}{2}\hat{k_y}, \tag{4.42}$$

where

$$\begin{aligned} B\equiv\sum_{n_{\Gamma_{15}}}\frac{2\hbar^2}{m^2}\frac{\langle S|p_x|\Gamma_{15},n_{\Gamma_{15}},X'\rangle\langle\Gamma_{15},n_{\Gamma_{15}},X'|p_y|Z\rangle}{E-H_{\Gamma_{15}n_{\Gamma_{15}}}(\mathbf{r})} \\ =\sum_{\nu\in\Gamma_{15}}\frac{2\hbar^2}{m^2}\frac{\langle S|p_x|\nu\rangle\langle\nu|p_y|Z\rangle}{E-H_\nu(\mathbf{r})}. \end{aligned} \tag{4.43}$$

In the limit of a homogeneous semiconductor we have

$$H_{SX}^{(int)\Gamma_{15}}=Bk_yk_z. \tag{4.44}$$

4.6.3 $s=X,\gamma=\Gamma_{15},s'=X$

Due to (2.10) the sum (4.33) reduces to

$$\langle X|p_z|Y'\rangle\langle Y'|p_z|X\rangle\delta_{\alpha z}\delta_{\beta z}+\langle X|p_y|Z'\rangle\langle Z'|p_y|X\rangle\delta_{\alpha y}\delta_{\beta y}, \tag{4.45}$$

which is equal to

$$\langle X|p_y|Z'\rangle\langle Z'|p_y|X\rangle(\delta_{\alpha z}\delta_{\beta z}+\delta_{\alpha y}\delta_{\beta y}). \tag{4.46}$$

Therefore

$$H_{XX}^{(int)\Gamma_{15}}=\hat{k_z}H_1\hat{k_z}+\hat{k_y}H_1\hat{k_y}, \tag{4.47}$$

where

$$\begin{aligned} H_1\equiv\sum_{n_{\Gamma_{15}}}\frac{\hbar^2}{m^2}\frac{\langle X|p_y|\Gamma_{15},n_{\Gamma_{15}},Z'\rangle\langle\Gamma_{15},n_{\Gamma_{15}},Z'|p_y|X\rangle}{E-H_{\Gamma_{15}n_{\Gamma_{15}}}(\mathbf{r})} \\ =\sum_{\nu\in\Gamma_{15}}\frac{\hbar^2}{m^2}\frac{\langle X|p_y|\nu\rangle\langle\nu|p_y|X\rangle}{E-H_\nu(\mathbf{r})}. \end{aligned} \tag{4.48}$$

In the limit of a homogeneous semiconductor we have

$$H_{XX}^{(int)\Gamma_{15}}=H_1(k_y^2+k_z^2). \tag{4.49}$$

4.6.4 $s = X, \gamma = \Gamma_{25}, s' = X$

Due to (2.11) the sum (4.33) reduces to

$$\langle X|p_z|S_y\rangle\langle S_y|p_z|X\rangle\delta_{\alpha z}\delta_{\beta z} + \langle X|p_y|S_z\rangle\langle S_z|p_y|X\rangle\delta_{\alpha y}\delta_{\beta y}, \tag{4.50}$$

which is equal to

$$\langle X|p_y|S_z\rangle\langle S_z|p_y|X\rangle(\delta_{\alpha z}\delta_{\beta z} + \delta_{\alpha y}\delta_{\beta y}). \tag{4.51}$$

Therefore

$$H_{XX}^{(int)\Gamma_{25}} = \hat{k_z}H_2\hat{k_z} + \hat{k_y}H_2\hat{k_y}, \tag{4.52}$$

where

$$\begin{aligned} H_2 \equiv \sum_{n_{\Gamma_{25}}} \frac{\hbar^2}{m^2}\frac{\langle X|p_y|\Gamma_{25}, n_{\Gamma_{25}}, S_z\rangle\langle\Gamma_{25}, n_{\Gamma_{25}}, S_z|p_y|X\rangle}{E - H_{\Gamma_{25}n_{\Gamma_{25}}}(\mathbf{r})} \\ = \sum_{\nu\in\Gamma_{25}} \frac{\hbar^2}{m^2}\frac{\langle X|p_y|\nu\rangle\langle\nu|p_y|X\rangle}{E - H_\nu(\mathbf{r})}. \end{aligned} \tag{4.53}$$

In the limit of a homogeneous semiconductor we have

$$H_{XX}^{(int)\Gamma_{25}} = H_2(k_y^2 + k_z^2). \tag{4.54}$$

4.6.5 $s = X, \gamma = \Gamma_1, s' = X$

Due to (2.9) the sum (4.33) reduces to

$$\langle X|p_x|S'\rangle\langle S'|p_x|X\rangle\delta_{\alpha x}\delta_{\beta x}. \tag{4.55}$$

Therefore

$$H_{XX}^{(int)\Gamma_1} = \hat{k_x}F'\hat{k_x}, \tag{4.56}$$

where

$$\begin{aligned} F' \equiv \sum_{n_{\Gamma_1}} \frac{\hbar^2}{m^2}\frac{\langle X|p_x|\Gamma_1, n_{\Gamma_1}, S'\rangle\langle\Gamma_1, n_{\Gamma_1}, S'|p_x|X\rangle}{E - H_{\Gamma_1 n_{\Gamma_1}}(\mathbf{r})} \\ = \sum_{\nu\in\Gamma_1} \frac{\hbar^2}{m^2}\frac{\langle X|p_x|\nu\rangle\langle\nu|p_x|X\rangle}{E - H_\nu(\mathbf{r})}. \end{aligned} \tag{4.57}$$

In the limit of a homogeneous semiconductor we have

$$H_{XX}^{(int)\Gamma_1} = F'k_x^2. \tag{4.58}$$

4.6.6 $s = X, \gamma = \Gamma_{12}, s' = X$

Due to (2.12) the sum (4.33) reduces to

$$\langle X|p_x|A_{12}\rangle\langle A_{12}|p_x|X\rangle\delta_{\alpha x}\delta_{\beta x} + \langle X|p_x|B_{12}\rangle\langle B_{12}|p_x|X\rangle\delta_{\alpha x}\delta_{\beta x}. \tag{4.59}$$

Therefore

$$H_{XX}^{(int)\Gamma_{12}} = \hat{k_x} 2G \hat{k_x}, \tag{4.60}$$

where

$$2G \equiv \sum_{\nu\in\Gamma_{12}} \frac{\hbar^2}{m^2} \frac{\langle X|p_x|\nu\rangle\langle\nu|p_x|X\rangle}{E - H_\nu(\mathbf{r})}. \tag{4.61}$$

In the limit of a homogeneous semiconductor we have

$$H_{XX}^{(int)\Gamma_{12}} = 2Gk_x^2. \tag{4.62}$$

It is usefull to notice that

$$\langle X|p_x|B_{12}\rangle\langle B_{12}|p_x|X\rangle = \frac{1}{3}\langle X|p_x|A_{12}\rangle\langle A_{12}|p_x|X\rangle, \tag{4.63}$$

and therefore

$$2G = \frac{4}{3}\sum_{n_{\Gamma_{12}}} \frac{\hbar^2}{m^2} \frac{\langle X|p_x|\Gamma_{12}, n_{\Gamma_{12}}, A_{12}\rangle\langle\Gamma_{12}, n_{\Gamma_{12}}, A_{12}|p_x|X\rangle}{E - H_{\Gamma_{12}n_{\Gamma_{12}}}(\mathbf{r})}. \tag{4.64}$$

4.6.7 $s = X, \gamma = \Gamma_{15}, s' = Y$

Due to (2.10) the sum (4.33) reduces to

$$\langle X|p_y|Z'\rangle\langle Z'|p_x|Y\rangle\delta_{\alpha y}\delta_{\beta x}, \tag{4.65}$$

which is equal to

$$\langle X|p_y|Z'\rangle\langle Z'|p_y|X\rangle\delta_{\alpha y}\delta_{\beta x}. \tag{4.66}$$

Therefore

$$H_{XY}^{(int)\Gamma_{15}} = \hat{k_y} H_1 \hat{k_x}. \tag{4.67}$$

In the limit of a homogeneous semiconductor we have

$$H_{XY}^{(int)\Gamma_{15}} = H_1 k_x k_y. \tag{4.68}$$

4.6.8 $s = X, \gamma = \Gamma_{25}, s' = Y$

Due to (2.11) the sum (4.33) reduces to

$$\langle X|p_y|S_z\rangle\langle S_z|p_x|Y\rangle\delta_{\alpha y}\delta_{\beta x}, \tag{4.69}$$

which is equal to

$$-\langle X|p_y|S_z\rangle\langle S_z|p_y|X\rangle\delta_{\alpha y}\delta_{\beta x}. \tag{4.70}$$

Therefore

$$H_{XY}^{(int)\Gamma_{25}} = -\hat{k_y}H_2\hat{k_x}. \tag{4.71}$$

In the limit of a homogeneous semiconductor we have

$$H_{XY}^{(int)\Gamma_{25}} = -H_2k_xk_y. \tag{4.72}$$

4.6.9 $s = X, \gamma = \Gamma_1, s' = Y$

Due to (2.9) the sum (4.33) reduces to

$$\langle X|p_x|S'\rangle\langle S'|p_y|Y\rangle\delta_{\alpha x}\delta_{\beta y}, \tag{4.73}$$

which is equal to

$$\langle X|p_x|S'\rangle\langle S'|p_x|X\rangle\delta_{\alpha x}\delta_{\beta y}. \tag{4.74}$$

Therefore

$$H_{XY}^{(int)\Gamma_1} = \hat{k_x}F'\hat{k_y}. \tag{4.75}$$

In the limit of a homogeneous semiconductor we have

$$H_{XY}^{(int)\Gamma_1} = F'k_xk_y. \tag{4.76}$$

4.6.10 $s = X, \gamma = \Gamma_{12}, s' = Y$

Due to (2.12) the sum (4.33) reduces to

$$\langle X|p_x|A_{12}\rangle\langle A_{12}|p_y|Y\rangle\delta_{\alpha x}\delta_{\beta y} + \langle X|p_x|B_{12}\rangle\langle B_{12}|p_y|Y\rangle\delta_{\alpha x}\delta_{\beta y}, \tag{4.77}$$

which is equal to

$$-\langle X|p_x|A_{12}\rangle\langle A_{12}|p_x|X\rangle\delta_{\alpha x}\delta_{\beta y}+\frac{-1}{\sqrt{3}}\frac{-1}{\sqrt{3}}\langle X|p_x|A_{12}\rangle\langle A_{12}|p_x|X\rangle\delta_{\alpha x}\delta_{\beta y}$$
$$=\frac{-2}{3}\langle X|p_x|A_{12}\rangle\langle A_{12}|p_x|X\rangle\delta_{\alpha x}\delta_{\beta y}. \tag{4.78}$$

Therefore, using (4.64)

$$H_{XY}^{(int)\Gamma_{12}}=-\hat{k_x}G\hat{k_y}. \tag{4.79}$$

In the limit of a homogeneous semiconductor we have

$$H_{XY}^{(int)\Gamma_{12}}=-Gk_xk_y. \tag{4.80}$$

4.7 Conclusions

By summing up all contributions to the Hamiltonian we obtain

$$H_{SS}^{(int)}=\hat{k_x}A'\hat{k_x}+\hat{k_y}A'\hat{k_y}+\hat{k_z}A'\hat{k_z}, \tag{4.81}$$
$$H_{SX}^{(int)}=\hat{k_y}\frac{B}{2}\hat{k_z}+\hat{k_z}\frac{B}{2}\hat{k_y}, \tag{4.82}$$
$$H_{XX}^{(int)}=\hat{k_x}(F'+2G)\hat{k_x}+\hat{k_y}(H_1+H_2)\hat{k_y}+\hat{k_z}(H_1+H_2)\hat{k_z}, \tag{4.83}$$
$$H_{XY}^{(int)}=\hat{k_y}(H_1-H_2)\hat{k_x}+\hat{k_x}(F'-G)\hat{k_y}, \tag{4.84}$$

with the other elements obtained in a similar fashion.

In the case of a homogeneous semiconductor we obtain

$$H_{SS}^{(int)}=A'(k_x^2+k_y^2+k_z^2), \tag{4.85}$$
$$H_{SX}^{(int)}=Bk_yk_z, \tag{4.86}$$
$$H_{XX}^{(int)}=(F'+2G)k_x^2+(H_1+H_2)(k_y^2+k_z^2), \tag{4.87}$$
$$H_{XY}^{(int)}=(H_1-H_2+F'-G)k_xk_y, \tag{4.88}$$

and we recover Kane's parameters

$$L'=F'+2G, \tag{4.89}$$
$$M=H_1+H_2, \tag{4.90}$$
$$N'=F'-G+H_1-H_2. \tag{4.91}$$

In all these parameters the summation is over the remote bands, and excludes the valence bands and the first conduction band.

4.7.1 Foreman's notation

Foreman [11] uses the following notation

$$F \equiv -\frac{\hbar^2}{m_o}3\sigma, \tag{4.92}$$

$$H_1 \equiv -\frac{\hbar^2}{m_o}3\pi, \tag{4.93}$$

$$G \equiv -\frac{\hbar^2}{m_o}3\delta, \tag{4.94}$$

$$H_2 \approx 0. \tag{4.95}$$

In all these parameters the summation is over the remote bands, and excludes the valence bands.

4.8 Symmetrization versus Burt's Hamiltonian

We now see clearly the difference between the two procedures. The element (4.84) in the Burt Hamiltonian corresponds to the element (4.88) in a homogeneous semiconductor. The symmetrization procedure generates an element

$$\frac{1}{2}\hat{k_y}(H_1 - H_2 + F' - G)\hat{k_x} + \frac{1}{2}\hat{k_x}(H_1 - H_2 + F' - G)\hat{k_y}, \tag{4.96}$$

quite different from (4.84).

Comparisons between calculations using the symmetrized and the non-symmetrized Hamiltonians have been made for quantum wells [11, 24, 25, 26], wires [27], and dots [28].

Chapter 5

Momentum Matrix Elements

5.1 Introduction

Assuming that the eigenvalue problem has been solved, and that we know the wavefunctions, we can now proceed to the calculation of the momentum matrix elements (MME). The MME are the main quantities that we need in order to determine optical properties, like absorption or gain.

Consider two wavefunctions $\Psi^{(N)}(\mathbf{r})$ and $\Psi^{(M)}(\mathbf{r})$, corresponding to eigenstates N and M. In general:

$$\Psi^{(N)}(\mathbf{r}) = \sum_n F_n^{(N)}(\mathbf{r})U_n(\mathbf{r}) = \sum_s F_s^{(N)}(\mathbf{r})U_s(\mathbf{r}) + \sum_r F_r^{(N)}(\mathbf{r})U_r(\mathbf{r}), \tag{5.1}$$

$$\Psi^{(M)}(\mathbf{r}) = \sum_\nu F_\nu^{(M)}(\mathbf{r})U_\nu(\mathbf{r}) = \sum_\sigma F_\sigma^{(M)}(\mathbf{r})U_\sigma(\mathbf{r}) + \sum_\rho F_\rho^{(M)}(\mathbf{r})U_\rho(\mathbf{r}), \tag{5.2}$$

where the sum has been broken down into main bands (s, σ) and remote bands (r, ρ) contributions. We need to calculate

$$\langle \Psi^{(N)}(\mathbf{r}) | \hat{p_\epsilon} | \Psi^{(M)}(\mathbf{r}) \rangle, \tag{5.3}$$

where the momentum operator is

$$\hat{p_\epsilon} \equiv -i\hbar \frac{\partial}{\partial \epsilon}, \qquad \epsilon \in \{x, y, z\}. \tag{5.4}$$

The calculation is complicated by the fact that, after solving the eigenvalue problem for the folded-down Hamiltonian, we only know the eight (for an eight bands model) envelope functions

for the main bands

$$\bar{\Psi}^{(N)}(\mathbf{r}) = \left(F_1^{(N)}(\mathbf{r}), F_2^{(N)}(\mathbf{r}), ..., F_8^{(N)}(\mathbf{r})\right), \tag{5.5}$$

$$\bar{\Psi}^{(M)}(\mathbf{r}) = \left(F_1^{(M)}(\mathbf{r}), F_2^{(M)}(\mathbf{r}), ..., F_8^{(M)}(\mathbf{r})\right). \tag{5.6}$$

The solution to this problem, as we will show, is to ignore contributions second order or higher in $\hat{k_\alpha} F_s$, where the operator $\hat{k_\alpha}$ is

$$\hat{k_\alpha} \equiv -i\frac{\partial}{\partial \alpha}, \qquad \alpha \in \{x, y, z\}. \tag{5.7}$$

5.2 Calculation of $\langle \Psi^{(N)}(\mathbf{r}) | \hat{p_\epsilon} | \Psi^{(M)}(\mathbf{r}) \rangle$

From Burt's approximation that the zone center eigenfunctions are the same in all semiconductors of the quantum microstructure it follows that $H_{rs'} = 0$. Therefore the envelope functions for the remote bands (4.20) are

$$F_r(\mathbf{r}) = \frac{1}{E - H_{rr}(\mathbf{r})} \sum_{s'} \frac{-i\hbar}{m} \mathbf{p}_{rs'} \cdot \nabla F_{s'}(\mathbf{r}). \tag{5.8}$$

The equations (5.1) and (5.2) now become

$$\Psi^{(N)}(\mathbf{r}) = \sum_s F_s^{(N)}(\mathbf{r}) U_s(\mathbf{r}) + \sum_r \left(\frac{1}{E - H_{rr}(\mathbf{r})} \sum_{s'} \frac{-i\hbar}{m} \mathbf{p}_{rs'} \cdot \nabla F_{s'}^{(N)}(\mathbf{r}) \right) U_r(\mathbf{r}), \tag{5.9}$$

$$\Psi^{(M)}(\mathbf{r}) = \sum_\sigma F_\sigma^{(M)}(\mathbf{r}) U_\sigma(\mathbf{r}) + \sum_\rho \left(\frac{1}{E - H_{\rho\rho}(\mathbf{r})} \sum_{\sigma'} \frac{-i\hbar}{m} \mathbf{p}_{\rho\sigma'} \cdot \nabla F_{\sigma'}^{(M)}(\mathbf{r}) \right) U_\rho(\mathbf{r}). \tag{5.10}$$

We now use the approximation of slowly varying envelope functions:

$$\begin{aligned}
&\langle F_n(\mathbf{r}) U_n(\mathbf{r}) | \hat{p_\epsilon} | F_\nu(\mathbf{r}) U_\nu(\mathbf{r}) \rangle \\
&= \int F_n^*(\mathbf{r}) U_n^*(\mathbf{r}) \hat{p_\epsilon} F_\nu(\mathbf{r}) U_\nu(\mathbf{r}) d\mathbf{r} \\
&= \int F_n^*(\mathbf{r}) U_n^*(\mathbf{r}) (\hat{p_\epsilon} F_\nu(\mathbf{r})) U_\nu(\mathbf{r}) d\mathbf{r} + \int F_n^*(\mathbf{r}) U_n^*(\mathbf{r}) F_\nu(\mathbf{r}) (\hat{p_\epsilon} U_\nu(\mathbf{r})) d\mathbf{r} \\
&\approx \left(\int F_n^*(\mathbf{r}) \hat{p_\epsilon} F_\nu(\mathbf{r}) d\mathbf{r} \right) \left(\int_{UC} U_n^*(\mathbf{r}) U_\nu(\mathbf{r}) d\mathbf{r} \right) + \left(\int F_n^*(\mathbf{r}) F_\nu(\mathbf{r}) d\mathbf{r} \right) \left(\int_{UC} U_n^*(\mathbf{r}) \hat{p_\epsilon} U_\nu(\mathbf{r}) d\mathbf{r} \right) \\
&= \langle F_n(\mathbf{r}) | \hat{p_\epsilon} | F_\nu(\mathbf{r}) \rangle \delta_{n\nu} + \langle F_n(\mathbf{r}) | F_\nu(\mathbf{r}) \rangle p_{n\nu,\epsilon}.
\end{aligned} \tag{5.11}$$

With the approximation (5.11), the MME becomes

$$
\begin{aligned}
&\langle\Psi^{(N)}(\mathbf{r})|\hat{p_\epsilon}|\Psi^{(M)}(\mathbf{r})\rangle \\
&= \langle\sum_s F_s^{(N)}(\mathbf{r})U_s(\mathbf{r}) + \sum_r F_r^{(N)}(\mathbf{r})U_r(\mathbf{r})|\hat{p_\epsilon}|\sum_\sigma F_\sigma^{(M)}(\mathbf{r})U_\sigma(\mathbf{r}) + \sum_\rho F_\rho^{(M)}(\mathbf{r})U_\rho(\mathbf{r})\rangle \\
&\approx \sum_s\sum_\sigma\langle F_s^{(N)}(\mathbf{r})|\hat{p_\epsilon}|F_\sigma^{(M)}(\mathbf{r})\rangle\delta_{s\sigma} + \sum_s\sum_\sigma\langle F_s^{(N)}(\mathbf{r})|F_\sigma^{(M)}(\mathbf{r})\rangle p_{s\sigma,\epsilon} \\
&+ \sum_s\sum_\rho\langle F_s^{(N)}(\mathbf{r})|\hat{p_\epsilon}|F_\rho^{(M)}(\mathbf{r})\rangle\delta_{s\rho} + \sum_s\sum_\rho\langle F_s^{(N)}(\mathbf{r})|F_\rho^{(M)}(\mathbf{r})\rangle p_{s\rho,\epsilon} \\
&+ \sum_r\sum_\sigma\langle F_r^{(N)}(\mathbf{r})|\hat{p_\epsilon}|F_\sigma^{(M)}(\mathbf{r})\rangle\delta_{r\sigma} + \sum_r\sum_\sigma\langle F_r^{(N)}(\mathbf{r})|F_\sigma^{(M)}(\mathbf{r})\rangle p_{r\sigma,\epsilon} \\
&+ \sum_r\sum_\rho\langle F_r^{(N)}(\mathbf{r})|\hat{p_\epsilon}|F_\rho^{(M)}(\mathbf{r})\rangle\delta_{r\rho} + \sum_r\sum_\rho\langle F_r^{(N)}(\mathbf{r})|F_\rho^{(M)}(\mathbf{r})\rangle p_{r\rho,\epsilon} \\
&= \sum_s\langle F_s^{(N)}(\mathbf{r})|\hat{p_\epsilon}|F_s^{(M)}(\mathbf{r})\rangle + \sum_s\sum_\sigma\langle F_s^{(N)}(\mathbf{r})|F_\sigma^{(M)}(\mathbf{r})\rangle p_{s\sigma,\epsilon} + \sum_s\sum_\rho\langle F_s^{(N)}(\mathbf{r})|F_\rho^{(M)}(\mathbf{r})\rangle p_{s\rho,\epsilon} \\
&+ \sum_r\sum_\sigma\langle F_r^{(N)}(\mathbf{r})|F_\sigma^{(M)}(\mathbf{r})\rangle p_{r\sigma,\epsilon} + \sum_r\langle F_r^{(N)}(\mathbf{r})|\hat{p_\epsilon}|F_r^{(M)}(\mathbf{r})\rangle + \sum_r\sum_\rho\langle F_r^{(N)}(\mathbf{r})|F_\rho^{(M)}(\mathbf{r})\rangle p_{r\rho,\epsilon},
\end{aligned}
\tag{5.12}
$$

where we have used the fact that $\delta_{s\rho} = \delta_{r\sigma} = 0$. In (5.12) there are terms with a single summation over the remote bands. These terms will be reduced to Kane parameters, which also contain a single summation over remote bands. There are also terms of second order in $F_r \sim \hat{k}F_s$. These terms will be ignored, as second order contributions in $\hat{k}$. Therefore

$$
\begin{aligned}
&\langle\Psi^{(N)}(\mathbf{r})|\hat{p_\epsilon}|\Psi^{(M)}(\mathbf{r})\rangle \\
&\approx \sum_s\langle F_s^{(N)}(\mathbf{r})|\hat{p_\epsilon}|F_s^{(M)}(\mathbf{r})\rangle + \sum_s\sum_\sigma\langle F_s^{(N)}(\mathbf{r})|F_\sigma^{(M)}(\mathbf{r})\rangle p_{s\sigma,\epsilon} \\
&+ \sum_s\sum_\rho\langle F_s^{(N)}(\mathbf{r})|F_\rho^{(M)}(\mathbf{r})\rangle p_{s\rho,\epsilon} + \sum_r\sum_\sigma\langle F_r^{(N)}(\mathbf{r})|F_\sigma^{(M)}(\mathbf{r})\rangle p_{r\sigma,\epsilon} \\
&= \sum_s\langle F_s^{(N)}(\mathbf{r})|\hat{p_\epsilon}|F_s^{(M)}(\mathbf{r})\rangle + \sum_s\sum_\sigma\langle F_s^{(N)}(\mathbf{r})|F_\sigma^{(M)}(\mathbf{r})\rangle p_{s\sigma,\epsilon} \\
&+ \sum_s\sum_\rho\langle F_s^{(N)}(\mathbf{r})|\frac{1}{E - H_{\rho\rho}(\mathbf{r})}\sum_{\sigma'}\frac{-i\hbar}{m}\mathbf{p}_{\rho\sigma'}\cdot\nabla F_{\sigma'}^{(M)}(\mathbf{r})\rangle p_{s\rho,\epsilon} \\
&+ \sum_r\sum_\sigma\langle\frac{1}{E - H_{rr}(\mathbf{r})}\sum_{s'}\frac{-i\hbar}{m}\mathbf{p}_{rs'}\cdot\nabla F_{s'}^{(N)}(\mathbf{r})|F_\sigma^{(M)}(\mathbf{r})\rangle p_{r\sigma,\epsilon}.
\end{aligned}
\tag{5.13}
$$

We now work a little bit on the last term of (5.13).

$$
\langle\frac{1}{E - H_{rr}(\mathbf{r})}\frac{-i\hbar}{m}\mathbf{p}_{rs'}\cdot\nabla F_{s'}^{(N)}(\mathbf{r})|F_\sigma^{(M)}(\mathbf{r})\rangle
$$

$$
\begin{aligned}
&= \int \left(\frac{1}{E - H_{rr}(\mathbf{r})} \frac{-i\hbar}{m} \mathbf{p}_{rs'} \cdot \nabla F_{s'}^{(N)}(\mathbf{r}) \right)^* F_{\sigma}^{(M)}(\mathbf{r}) d\mathbf{r} \\
&= \int \frac{1}{E - H_{rr}(\mathbf{r})} \frac{+i\hbar}{m} \mathbf{p}_{s'r} \cdot \nabla \left(F_{s'}^{(N)}(\mathbf{r}) \right)^* F_{\sigma}^{(M)}(\mathbf{r}) d\mathbf{r} \\
&= \int \left(F_{s'}^{(N)}(\mathbf{r}) \right)^* \nabla \cdot \left(\mathbf{p}_{s'r} \frac{1}{E - H_{rr}(\mathbf{r})} \frac{-i\hbar}{m} F_{\sigma}^{(M)}(\mathbf{r}) \right) d\mathbf{r} \\
&= \langle F_{s'}^{(N)}(\mathbf{r}) | \nabla \cdot \mathbf{p}_{s'r} \frac{1}{E - H_{rr}(\mathbf{r})} \frac{-i\hbar}{m} | F_{\sigma}^{(M)}(\mathbf{r}) \rangle, \qquad (5.14)
\end{aligned}
$$

where we have used the fact that, due to the hermiticity of $\hat{H}$ and $\hat{\mathbf{p}}$, we have $H_{rr}^* = H_{rr}$ and $\mathbf{p}_{rs'}^* = \mathbf{p}_{s'r}$. We have also integrated by parts.

The third term in (5.13) can be written as:

$$
\sum_s \sum_{\sigma'} \langle F_s^{(N)}(\mathbf{r}) | \sum_{\beta} \sum_{\rho} \frac{\hbar}{m} \frac{p_{s\rho,\epsilon} p_{\rho\sigma',\beta}}{E - H_{\rho\rho}(\mathbf{r})} \hat{k_\beta} | F_{\sigma'}^{(M)}(\mathbf{r}) \rangle = \sum_s \sum_{\sigma'} \langle F_s^{(N)}(\mathbf{r}) | \sum_{\beta} D_{s\sigma'}^{\epsilon\beta}(\mathbf{r}) \hat{k_\beta} | F_{\sigma'}^{(M)}(\mathbf{r}) \rangle, \qquad (5.15)
$$

where

$$
D_{s\sigma'}^{\epsilon\beta}(\mathbf{r}) \equiv \sum_{\rho} \frac{\hbar}{m} \frac{p_{s\rho,\epsilon} p_{\rho\sigma',\beta}}{E - H_{\rho\rho}(\mathbf{r})}. \qquad (5.16)
$$

The fourth term in (5.13), using (5.14), can be written as:

$$
\sum_{s'} \sum_{\sigma} \langle F_{s'}^{(N)}(\mathbf{r}) | \sum_{\alpha} \sum_{r} \hat{k_\alpha} \frac{\hbar}{m} \frac{p_{s'r,\alpha} p_{r\sigma,\epsilon}}{E - H_{rr}(\mathbf{r})} | F_{\sigma}^{(M)}(\mathbf{r}) \rangle = \sum_{s'} \sum_{\sigma} \langle F_{s'}^{(N)}(\mathbf{r}) | \sum_{\alpha} \hat{k_\alpha} D_{s'\sigma}^{\alpha\epsilon}(\mathbf{r}) | F_{\sigma}^{(M)}(\mathbf{r}) \rangle, \qquad (5.17)
$$

where

$$
D_{s'\sigma}^{\alpha\epsilon}(\mathbf{r}) \equiv \sum_{r} \frac{\hbar}{m} \frac{p_{s'r,\alpha} p_{r\sigma,\epsilon}}{E - H_{rr}(\mathbf{r})}. \qquad (5.18)
$$

We now substitute (5.15) and (5.17) into (5.13) and obtain

$$
\begin{aligned}
&\langle \Psi^{(N)}(\mathbf{r}) | \hat{p_\epsilon} | \Psi^{(M)}(\mathbf{r}) \rangle \\
&= \sum_s \langle F_s^{(N)}(\mathbf{r}) | \hat{p_\epsilon} | F_s^{(M)}(\mathbf{r}) \rangle + \sum_s \sum_{\sigma} \langle F_s^{(N)}(\mathbf{r}) | F_{\sigma}^{(M)}(\mathbf{r}) \rangle p_{s\sigma,\epsilon} \\
&+ \sum_s \sum_{\sigma'} \langle F_s^{(N)}(\mathbf{r}) | \sum_{\beta} D_{s\sigma'}^{\epsilon\beta}(\mathbf{r}) \hat{k_\beta} | F_{\sigma'}^{(M)}(\mathbf{r}) \rangle \\
&+ \sum_{s'} \sum_{\sigma} \langle F_{s'}^{(N)}(\mathbf{r}) | \sum_{\alpha} \hat{k_\alpha} D_{s'\sigma}^{\alpha\epsilon}(\mathbf{r}) | F_{\sigma}^{(M)}(\mathbf{r}) \rangle \\
&= \sum_s \sum_{\sigma} \langle F_s^{(N)}(\mathbf{r}) | \hat{p_\epsilon} \delta_{s\sigma} + p_{s\sigma,\epsilon} + \sum_{\beta} D_{s\sigma}^{\epsilon\beta}(\mathbf{r}) \hat{k_\beta} + \sum_{\alpha} \hat{k_\alpha} D_{s\sigma}^{\alpha\epsilon}(\mathbf{r}) | F_{\sigma}^{(M)}(\mathbf{r}) \rangle. \qquad (5.19)
\end{aligned}
$$

5.3 Calculation of $\langle\bar{\Psi}^{(N)}(\mathbf{r})|\frac{\partial\bar{H}}{\partial\hat{k_\epsilon}}|\bar{\Psi}^{(M)}(\mathbf{r})\rangle$

In Burt's theory, the folded-down Hamiltonian, acting in the envelope space, is (4.30)

$$\begin{aligned}\bar{H}_{s\sigma} &= \frac{-\hbar^2}{2m}\delta_{s\sigma}\nabla^2 + \frac{-i\hbar}{m}\mathbf{p}_{s\sigma}\cdot\nabla + H_{s\sigma}(\mathbf{r}) + \sum_r\sum_\alpha\sum_\beta \frac{-\hbar^2}{m^2}\partial_\alpha\frac{p_{sr,\alpha}p_{r\sigma,\beta}}{E-H_{rr}(\mathbf{r})}\partial_\beta \\ &= \frac{\hbar^2}{2m}\delta_{s\sigma}\sum_\alpha \hat{k_\alpha}\hat{k_\alpha} + \frac{\hbar}{m}\sum_\alpha p_{s\sigma,\alpha}\hat{k_\alpha} + H_{s\sigma}(\mathbf{r}) + \sum_\alpha\sum_\beta \frac{\hbar}{m}\hat{k_\alpha}D^{\alpha\beta}_{s\sigma}(\mathbf{r})\hat{k_\beta}. \qquad (5.20)\end{aligned}$$

We now calculate the partial derivative of the Hamiltonian

$$\begin{aligned}\frac{\partial\bar{H}_{s\sigma}}{\partial\hat{k_\epsilon}} &= \frac{\hbar^2}{2m}\delta_{s\sigma}\sum_\alpha(\delta_{\alpha\epsilon}\hat{k_\alpha} + \hat{k_\alpha}\delta_{\alpha\epsilon}) + \frac{\hbar}{m}\sum_\alpha p_{s\sigma,\alpha}\delta_{\alpha\epsilon} \\ &+ \sum_\alpha\sum_\beta \frac{\hbar}{m}\left(\delta_{\alpha\epsilon}D^{\alpha\beta}_{s\sigma}(\mathbf{r})\hat{k_\beta} + \hat{k_\alpha}D^{\alpha\beta}_{s\sigma}(\mathbf{r})\delta_{\beta\epsilon}\right) \\ &= \frac{\hbar^2}{m}\delta_{s\sigma}\hat{k_\epsilon} + \frac{\hbar}{m}p_{s\sigma,\epsilon} + \sum_\beta \frac{\hbar}{m}D^{\epsilon\beta}_{s\sigma}(\mathbf{r})\hat{k_\beta} + \sum_\alpha \frac{\hbar}{m}\hat{k_\alpha}D^{\alpha\epsilon}_{s\sigma}(\mathbf{r}). \qquad (5.21)\end{aligned}$$

The matrix element, computed in the envelope space, is

$$\begin{aligned}&\langle\bar{\Psi}^{(N)}(\mathbf{r})|\frac{\partial\bar{H}}{\partial\hat{k_\epsilon}}|\bar{\Psi}^{(M)}(\mathbf{r})\rangle \\ &= \sum_s\sum_\sigma\langle F^{(N)}_s(\mathbf{r})|\frac{\partial\bar{H}_{s\sigma}}{\partial\hat{k_\epsilon}}|F^{(M)}_\sigma(\mathbf{r})\rangle \\ &= \sum_s\sum_\sigma\langle F^{(N)}_s(\mathbf{r})|\frac{\hbar^2}{m}\delta_{s\sigma}\hat{k_\epsilon} + \frac{\hbar}{m}p_{s\sigma,\epsilon} + \sum_\beta \frac{\hbar}{m}D^{\epsilon\beta}_{s\sigma}(\mathbf{r})\hat{k_\beta} + \sum_\alpha \frac{\hbar}{m}\hat{k_\alpha}D^{\alpha\epsilon}_{s\sigma}(\mathbf{r})|F^{(M)}_\sigma(\mathbf{r})\rangle. \qquad (5.22)\end{aligned}$$

Comparison of (5.19) and (5.22) gives directly the formula [29, 30]

$$\langle\Psi^{(N)}(\mathbf{r})|\hat{p_\epsilon}|\Psi^{(M)}(\mathbf{r})\rangle = \frac{m}{\hbar}\langle\bar{\Psi}^{(N)}(\mathbf{r})|\frac{\partial\bar{H}}{\partial\hat{k_\epsilon}}|\bar{\Psi}^{(M)}(\mathbf{r})\rangle, \qquad (5.23)$$

where we have used the fact that $\hat{p_\epsilon} = \hbar\hat{k_\epsilon}$.

5.4 Normalization of the Wave Function

In the approximation of slowly varying envelope functions:

$$\langle F_n(\mathbf{r})U_n(\mathbf{r})|F_\nu(\mathbf{r})U_\nu(\mathbf{r})\rangle$$

$$\begin{aligned}
&\approx \left(\int F_n^*(\mathbf{r})F_\nu(\mathbf{r})d\mathbf{r}\right)\left(\int_{UC} U_n^*(\mathbf{r})U_\nu(\mathbf{r})d\mathbf{r}\right)\\
&= \langle F_n(\mathbf{r})|F_\nu(\mathbf{r})\rangle\delta_{n\nu}. \qquad (5.24)
\end{aligned}$$

With the approximation (5.24), the scalar product $\langle\Psi^{(N)}(\mathbf{r})|\Psi^{(M)}(\mathbf{r})\rangle$ becomes

$$\begin{aligned}
&\langle\Psi^{(N)}(\mathbf{r})|\Psi^{(M)}(\mathbf{r})\rangle\\
&= \langle\sum_s F_s^{(N)}(\mathbf{r})U_s(\mathbf{r}) + \sum_r F_r^{(N)}(\mathbf{r})U_r(\mathbf{r})|\sum_\sigma F_\sigma^{(M)}(\mathbf{r})U_\sigma(\mathbf{r}) + \sum_\rho F_\rho^{(M)}(\mathbf{r})U_\rho(\mathbf{r})\rangle\\
&\approx \sum_s\sum_\sigma\langle F_s^{(N)}(\mathbf{r})|F_\sigma^{(M)}(\mathbf{r})\rangle\delta_{s\sigma} + \sum_s\sum_\rho\langle F_s^{(N)}(\mathbf{r})|F_\rho^{(M)}(\mathbf{r})\rangle\delta_{s\rho}\\
&+ \sum_r\sum_\sigma\langle F_r^{(N)}(\mathbf{r})|F_\sigma^{(M)}(\mathbf{r})\rangle\delta_{r\sigma} + \sum_r\sum_\rho\langle F_r^{(N)}(\mathbf{r})|F_\rho^{(M)}(\mathbf{r})\rangle\delta_{r\rho}\\
&= \sum_s\sum_\sigma\langle F_s^{(N)}(\mathbf{r})|F_\sigma^{(M)}(\mathbf{r})\rangle\delta_{s\sigma} + \sum_r\sum_\rho\langle F_r^{(N)}(\mathbf{r})|F_\rho^{(M)}(\mathbf{r})\rangle\delta_{r\rho}, \qquad (5.25)
\end{aligned}$$

where we have used the fact that $\delta_{s\rho} = \delta_{r\sigma} = 0$. In (5.25) there are terms with a single summation over the remote bands. There are also terms of second order in $F_r \sim \hat{k}F_s$. These terms will be ignored, as second order contributions in $\hat{k}$. Therefore

$$\langle\Psi^{(N)}(\mathbf{r})|\Psi^{(M)}(\mathbf{r})\rangle = \sum_s\langle F_s^{(N)}(\mathbf{r})|F_s^{(M)}(\mathbf{r})\rangle = \langle\bar{\Psi}^{(N)}(\mathbf{r})|\bar{\Psi}^{(M)}(\mathbf{r})\rangle. \qquad (5.26)$$

5.5 The Effect of Symmetrization on the MME

Consider the Burt Hamiltonian quadratic in $\mathbf{k}$

$$\bar{H}_{s\sigma} = \sum_\alpha\sum_\beta \frac{\hbar}{m}\hat{k_\alpha}D_{s\sigma}^{\alpha\beta}(\mathbf{r})\hat{k_\beta}. \qquad (5.27)$$

The MME is given by [58]

$$\begin{aligned}
\frac{m}{\hbar}\frac{\partial\bar{H}_{s\sigma}}{\partial\hat{k_\epsilon}} &= \sum_\alpha\sum_\beta\delta_{\alpha\epsilon}D_{s\sigma}^{\alpha\beta}(\mathbf{r})\hat{k_\beta} + \sum_\alpha\sum_\beta\hat{k_\alpha}D_{s\sigma}^{\alpha\beta}(\mathbf{r})\delta_{\beta\epsilon}\\
&= \sum_\beta D_{s\sigma}^{\epsilon\beta}(\mathbf{r})\hat{k_\beta} + \sum_\alpha\hat{k_\alpha}D_{s\sigma}^{\alpha\epsilon}(\mathbf{r}). \qquad (5.28)
\end{aligned}$$

Consider the symmetrized Hamiltonian

$$\bar{H}_{s\sigma} = \sum_\alpha\sum_\beta\frac{\hbar}{m}\hat{k_\alpha}\frac{D_{s\sigma}^{\alpha\beta}(\mathbf{r}) + D_{s\sigma}^{\beta\alpha}(\mathbf{r})}{2}\hat{k_\beta}. \qquad (5.29)$$

The MME is given by [58]

$$\begin{aligned}\frac{m}{\hbar}\frac{\partial \bar{H}_{s\sigma}}{\partial \hat{k_\epsilon}} &= \sum_\alpha \sum_\beta \delta_{\alpha\epsilon}\frac{D_{s\sigma}^{\alpha\beta}(\mathbf{r}) + D_{s\sigma}^{\beta\alpha}(\mathbf{r})}{2}\hat{k_\beta} + \sum_\alpha \sum_\beta \hat{k_\alpha}\frac{D_{s\sigma}^{\alpha\beta}(\mathbf{r}) + D_{s\sigma}^{\beta\alpha}(\mathbf{r})}{2}\delta_{\beta\epsilon} \\ &= \sum_\beta \frac{D_{s\sigma}^{\epsilon\beta}(\mathbf{r}) + D_{s\sigma}^{\beta\epsilon}(\mathbf{r})}{2}\hat{k_\beta} + \sum_\alpha \hat{k_\alpha}\frac{D_{s\sigma}^{\alpha\epsilon}(\mathbf{r}) + D_{s\sigma}^{\epsilon\alpha}(\mathbf{r})}{2}. \end{aligned} \tag{5.30}$$

5.6 Appendix. The Projection Operator Method

The projection operator method [59] is an alternative way of calculating the optical matrix elements entering the oscillator strength. The method is remarkable because it does not require the eigenfunctions of the Hamiltonian.

Consider the general Schrödinger equation

$$\hat{H}(\mathbf{r})|\psi_{\nu\rho\mathbf{k}}(\mathbf{r})\rangle = E_{\nu\mathbf{k}}|\psi_{\nu\rho\mathbf{k}}(\mathbf{r})\rangle, \tag{5.31}$$

where ν is an energy band index and ρ is a degeneracy index.

The projection operator is by definition

$$\hat{P}_{\nu\mathbf{k}}(\mathbf{r},\mathbf{r}') = \sum_{\rho} |\psi_{\nu\rho\mathbf{k}}(\mathbf{r})\rangle\langle\psi_{\nu\rho\mathbf{k}}(\mathbf{r}')|. \tag{5.32}$$

It follows that

$$\begin{aligned}\hat{P}_{\nu\mathbf{k}}(\mathbf{r},\mathbf{r}')|\psi_{\mu\sigma\mathbf{k}}(\mathbf{r}')\rangle &= \sum_{\rho} |\psi_{\nu\rho\mathbf{k}}(\mathbf{r})\rangle\langle\psi_{\nu\rho\mathbf{k}}(\mathbf{r}')|\psi_{\mu\sigma\mathbf{k}}(\mathbf{r}')\rangle \\ &= \sum_{\rho} |\psi_{\nu\rho\mathbf{k}}(\mathbf{r})\rangle\delta_{\nu\mu}\delta_{\rho\sigma} = \delta_{\nu\mu}|\psi_{\nu\sigma\mathbf{k}}(\mathbf{r})\rangle = \delta_{\nu\mu}|\psi_{\mu\sigma\mathbf{k}}(\mathbf{r})\rangle.\end{aligned} \tag{5.33}$$

The projection Hamiltonian operator is by definition

$$\hat{H}(\mathbf{r},\mathbf{r}') = \sum_{\mu} \hat{P}_{\mu\mathbf{k}}(\mathbf{r},\mathbf{r}')\hat{H}(\mathbf{r}'). \tag{5.34}$$

It follows that

$$\begin{aligned}\hat{H}(\mathbf{r},\mathbf{r}')|\psi_{\nu\rho\mathbf{k}}(\mathbf{r}')\rangle &= \sum_{\mu} \hat{P}_{\mu\mathbf{k}}(\mathbf{r},\mathbf{r}')\hat{H}(\mathbf{r}')|\psi_{\nu\rho\mathbf{k}}(\mathbf{r}')\rangle \\ &= \sum_{\mu}\sum_{\sigma} |\psi_{\mu\sigma\mathbf{k}}(\mathbf{r})\rangle\langle\psi_{\mu\sigma\mathbf{k}}(\mathbf{r}')|\hat{H}(\mathbf{r}')|\psi_{\nu\rho\mathbf{k}}(\mathbf{r}')\rangle \\ &= \sum_{\mu}\sum_{\sigma} |\psi_{\mu\sigma\mathbf{k}}(\mathbf{r})\rangle\langle\psi_{\mu\sigma\mathbf{k}}(\mathbf{r}')|\psi_{\nu\rho\mathbf{k}}(\mathbf{r}')\rangle E_{\nu\mathbf{k}} \\ &= \sum_{\mu}\sum_{\sigma} |\psi_{\mu\sigma\mathbf{k}}(\mathbf{r})\rangle\delta_{\mu\nu}\delta_{\sigma\rho}E_{\nu\mathbf{k}} \\ &= E_{\nu\mathbf{k}}|\psi_{\nu\rho\mathbf{k}}(\mathbf{r})\rangle.\end{aligned} \tag{5.35}$$

The optical matrix elements entering the oscillator strength can be expressed as follows:

$$\begin{aligned}&\sum_{\rho\sigma} |\langle\psi_{\mu\sigma\mathbf{k}}(\mathbf{r})|\hat{p}(\mathbf{r})|\psi_{\nu\rho\mathbf{k}}(\mathbf{r})\rangle|^2 \\ &= \sum_{\rho\sigma}\langle\psi_{\mu\sigma\mathbf{k}}(\mathbf{r})|\hat{p}(\mathbf{r})|\psi_{\nu\rho\mathbf{k}}(\mathbf{r})\rangle\langle\psi_{\nu\rho\mathbf{k}}(\mathbf{r}')|\hat{p}(\mathbf{r}')|\psi_{\mu\sigma\mathbf{k}}(\mathbf{r}')\rangle.\end{aligned} \tag{5.36}$$

At the same time:

$$
\begin{aligned}
&Trace(\hat{P}_{\mu\mathbf{k}}(\mathbf{r}',\mathbf{r})\hat{p}(\mathbf{r})\hat{P}_{\nu\mathbf{k}}(\mathbf{r},\mathbf{r}')\hat{p}(\mathbf{r}')) \\
&= \sum_{\omega\tau}\langle\psi_{\omega\tau\mathbf{k}}(\mathbf{r}')|\hat{P}_{\mu\mathbf{k}}(\mathbf{r}',\mathbf{r})\hat{p}(\mathbf{r})\hat{P}_{\nu\mathbf{k}}(\mathbf{r},\mathbf{r}')\hat{p}(\mathbf{r}')|\psi_{\omega\tau\mathbf{k}}(\mathbf{r}')\rangle \\
&= \sum_{\omega\tau}\langle\psi_{\omega\tau\mathbf{k}}(\mathbf{r}')|\sum_{\rho}|\psi_{\mu\rho\mathbf{k}}(\mathbf{r}')\rangle\langle\psi_{\mu\rho\mathbf{k}}(\mathbf{r})|\hat{p}(\mathbf{r})|\sum_{\sigma}|\psi_{\nu\sigma\mathbf{k}}(\mathbf{r})\rangle\langle\psi_{\nu\sigma\mathbf{k}}(\mathbf{r}')|\hat{p}(\mathbf{r}')|\psi_{\omega\tau\mathbf{k}}(\mathbf{r}')\rangle \\
&= \sum_{\omega\tau\rho\sigma}\langle\psi_{\omega\tau\mathbf{k}}(\mathbf{r}')|\psi_{\mu\rho\mathbf{k}}(\mathbf{r}')\rangle\langle\psi_{\mu\rho\mathbf{k}}(\mathbf{r})|\hat{p}(\mathbf{r})|\psi_{\nu\sigma\mathbf{k}}(\mathbf{r})\rangle\langle\psi_{\nu\sigma\mathbf{k}}(\mathbf{r}')|\hat{p}(\mathbf{r}')|\psi_{\omega\tau\mathbf{k}}(\mathbf{r}')\rangle \\
&= \sum_{\omega\tau\rho\sigma}\delta_{\omega\mu}\delta_{\tau\rho}\langle\psi_{\mu\rho\mathbf{k}}(\mathbf{r})|\hat{p}(\mathbf{r})|\psi_{\nu\sigma\mathbf{k}}(\mathbf{r})\rangle\langle\psi_{\nu\sigma\mathbf{k}}(\mathbf{r}')|\hat{p}(\mathbf{r}')|\psi_{\omega\tau\mathbf{k}}(\mathbf{r}')\rangle \\
&= \sum_{\rho\sigma}\langle\psi_{\mu\rho\mathbf{k}}(\mathbf{r})|\hat{p}(\mathbf{r})|\psi_{\nu\sigma\mathbf{k}}(\mathbf{r})\rangle\langle\psi_{\nu\sigma\mathbf{k}}(\mathbf{r}')|\hat{p}(\mathbf{r}')|\psi_{\mu\rho\mathbf{k}}(\mathbf{r}')\rangle. \qquad (5.37)
\end{aligned}
$$

From (5.36) and (5.37) it follows that

$$
\sum_{\rho\sigma}|\langle\psi_{\mu\sigma\mathbf{k}}(\mathbf{r})|\hat{p}(\mathbf{r})|\psi_{\nu\rho\mathbf{k}}(\mathbf{r})\rangle|^2 = Trace(\hat{P}_{\mu\mathbf{k}}(\mathbf{r}',\mathbf{r})\hat{p}(\mathbf{r})\hat{P}_{\nu\mathbf{k}}(\mathbf{r},\mathbf{r}')\hat{p}(\mathbf{r}')). \qquad (5.38)
$$

The *Trace* opens alternative calculational options, because it is representation independent. There is also another formula for the projection operator, which is independent of the eigenfunctions of the Hamiltonian.

$$
\hat{P}_{\nu\mathbf{k}}(\mathbf{r},\mathbf{r}') = \prod_{\mu\neq\nu}\frac{\hat{H}(\mathbf{r},\mathbf{r}') - E_{\mu\mathbf{k}}\times\hat{1}(\mathbf{r},\mathbf{r}')}{E_{\nu\mathbf{k}} - E_{\mu\mathbf{k}}}, \qquad (5.39)
$$

where $\hat{1}(\mathbf{r},\mathbf{r}')$ is the unit operator.

We will derive equation (5.39) by applying the operators from both sides to a general wavefunction.

$$
|\psi_{\mathbf{k}}(\mathbf{r}')\rangle = \sum_{\alpha\beta}c_{\alpha\beta}|\psi_{\alpha\beta\mathbf{k}}(\mathbf{r}')\rangle. \qquad (5.40)
$$

Using (5.33) we have

$$
\begin{aligned}
&\hat{P}_{\nu\mathbf{k}}(\mathbf{r},\mathbf{r}')|\psi_{\mathbf{k}}(\mathbf{r}')\rangle \\
&= \hat{P}_{\nu\mathbf{k}}(\mathbf{r},\mathbf{r}')\sum_{\alpha\beta}c_{\alpha\beta}|\psi_{\alpha\beta\mathbf{k}}(\mathbf{r}') \\
&= \sum_{\alpha\beta}c_{\alpha\beta}\hat{P}_{\nu\mathbf{k}}(\mathbf{r},\mathbf{r}')|\psi_{\alpha\beta\mathbf{k}}(\mathbf{r}') \\
&= \sum_{\alpha\beta}c_{\alpha\beta}\delta_{\nu\alpha}|\psi_{\alpha\beta\mathbf{k}}(\mathbf{r}) \\
&= \sum_{\beta}c_{\nu\beta}|\psi_{\nu\beta\mathbf{k}}(\mathbf{r}). \qquad (5.41)
\end{aligned}
$$

Using (5.37) we have

$$\begin{aligned}
&\hat{H}(\mathbf{r},\mathbf{r}')|\psi_{\mathbf{k}}(\mathbf{r}')\rangle \\
&= \hat{H}(\mathbf{r},\mathbf{r}')\sum_{\alpha\beta} c_{\alpha\beta}|\psi_{\alpha\beta\mathbf{k}}(\mathbf{r}')\rangle \\
&= \sum_{\alpha\beta} c_{\alpha\beta}\hat{H}(\mathbf{r},\mathbf{r}')|\psi_{\alpha\beta\mathbf{k}}(\mathbf{r}')\rangle \\
&= \sum_{\alpha\beta} c_{\alpha\beta}E_{\alpha\mathbf{k}}|\psi_{\alpha\beta\mathbf{k}}(\mathbf{r})\rangle. \qquad (5.42)
\end{aligned}$$

Also

$$\begin{aligned}
&E_{\mu\mathbf{k}} \times \hat{1}(\mathbf{r},\mathbf{r}')|\psi_{\mathbf{k}}(\mathbf{r}')\rangle \\
&= E_{\mu\mathbf{k}}|\psi_{\mathbf{k}}(\mathbf{r})\rangle \\
&= E_{\mu\mathbf{k}}\sum_{\alpha\beta} c_{\alpha\beta}|\psi_{\alpha\beta\mathbf{k}}(\mathbf{r})\rangle. \qquad (5.43)
\end{aligned}$$

From (5.42) and (5.43) we have

$$\left(\hat{H}(\mathbf{r},\mathbf{r}') - E_{\mu\mathbf{k}} \times \hat{1}(\mathbf{r},\mathbf{r}')\right)|\psi_{\mathbf{k}}(\mathbf{r}')\rangle = \sum_{\alpha\beta}(E_{\alpha\mathbf{k}} - E_{\mu\mathbf{k}})c_{\alpha\beta}|\psi_{\alpha\beta\mathbf{k}}(\mathbf{r})\rangle. \qquad (5.44)$$

For $\mu \neq \nu$ from (5.44) we get

$$\frac{\hat{H}(\mathbf{r},\mathbf{r}') - E_{\mu\mathbf{k}} \times \hat{1}(\mathbf{r},\mathbf{r}')}{E_{\nu\mathbf{k}} - E_{\mu\mathbf{k}}}|\psi_{\mathbf{k}}(\mathbf{r}')\rangle = \sum_{\alpha\beta}\frac{E_{\alpha\mathbf{k}} - E_{\mu\mathbf{k}}}{E_{\nu\mathbf{k}} - E_{\mu\mathbf{k}}}c_{\alpha\beta}|\psi_{\alpha\beta\mathbf{k}}(\mathbf{r})\rangle. \qquad (5.45)$$

We now look at the right side of (5.45), to see what happens with the sum over α.

$$\alpha = \mu \quad \rightarrow \quad 0, \qquad (5.46)$$

$$\alpha = \nu \quad \rightarrow \quad \sum_{\beta} c_{\nu\beta}|\psi_{\nu\beta\mathbf{k}}(\mathbf{r})\rangle, \qquad (5.47)$$

$$\alpha \neq \mu, \alpha \neq \nu \quad \rightarrow \quad \sum_{\beta}\frac{E_{\alpha\mathbf{k}} - E_{\mu\mathbf{k}}}{E_{\nu\mathbf{k}} - E_{\mu\mathbf{k}}}c_{\alpha\beta}|\psi_{\alpha\beta\mathbf{k}}(\mathbf{r})\rangle. \qquad (5.48)$$

The result is that the terms with $\psi_{\mu\beta\mathbf{k}}(\mathbf{r})$ have been eliminated, the terms with $\psi_{\nu\beta\mathbf{k}}(\mathbf{r})$ have been preserved unchanged, and the other terms have been changed. However, by repeatedly applying the operator on the right of (5.45) for all possible values of μ (with the exception of

ν) we succeed in eliminating all the terms in the wavefunction, with the exception of the terms with $\psi_{\nu\beta\mathbf{k}}(\mathbf{r})$. These last terms are left unchanged. As a result

$$\left(\prod_{\mu\neq\nu}\frac{\hat{H}(\mathbf{r},\mathbf{r}')-E_{\mu\mathbf{k}}\times\hat{1}(\mathbf{r},\mathbf{r}')}{E_{\nu\mathbf{k}}-E_{\mu\mathbf{k}}}\right)|\psi_{\mathbf{k}}(\mathbf{r}')\rangle=\sum_{\beta}c_{\nu\beta}|\psi_{\nu\beta\mathbf{k}}(\mathbf{r}). \tag{5.49}$$

Comparing (5.41) and (5.49), and because of the arbitrariness of the wavefunction $|\psi_{\mathbf{k}}(\mathbf{r}')\rangle$, we end up with (5.39).

Chapter 6

$\mathbf{k} \cdot \mathbf{p}$ Theory under a Change of Basis

6.1 Introduction

Although the derivations presented in the previous chapters assume a semiconductor crystal with the crystallographic axes parallel to the reference frame axes, this is not always the case in practice. To deal with arbitrary orientations we need to know what happens with the Hamiltonian matrix when the reference axes are rotated. This question is answered using the formalism of linear algebra, described in this chapter. The same formalism is also used when we have a change of basis required to diagonalize the spin-orbit interaction.

6.2 Mathematical Formalism

In the $\mathbf{k} \cdot \mathbf{p}$ method the wave-function is expanded in terms of zone-center eigenfunctions:

$$\begin{aligned} \psi(\mathbf{r}) = F_1(\mathbf{r})|S\uparrow\rangle + F_2(\mathbf{r})|X\uparrow\rangle + F_3(\mathbf{r})|Y\uparrow\rangle + F_4(\mathbf{r})|Z\uparrow\rangle \\ + F_5(\mathbf{r})|S\downarrow\rangle + F_6(\mathbf{r})|X\downarrow\rangle + F_7(\mathbf{r})|Y\downarrow\rangle + F_8(\mathbf{r})|Z\downarrow\rangle \\ + \text{remote bands.} \end{aligned} \tag{6.1}$$

These zone-center eigenfunctions form an orthonormal basis. Hamiltonian elements are defined by, e.g.,

$$H_{12} = \langle S\uparrow|\hat{H}|X\uparrow\rangle, \tag{6.2}$$

where $\hat{H}$ is the folded down Hamiltonian, with the contributions from the remote bands included. The eigenvalue equation

$$\hat{H}\psi(\mathbf{r}) = E\psi(\mathbf{r}), \tag{6.3}$$

becomes

$$\begin{pmatrix} H_{11} & H_{12} & ... & H_{1n} \\ H_{21} & H_{22} & ... & H_{2n} \\ ... & ... & ... & ... \\ H_{n1} & H_{n2} & ... & H_{nn} \end{pmatrix} \begin{pmatrix} F_1 \\ F_2 \\ ... \\ F_n \end{pmatrix} = E \begin{pmatrix} F_1 \\ F_2 \\ ... \\ F_n \end{pmatrix}. \tag{6.4}$$

It is clear that the general theory of linear algebra applies to $\mathbf{k}\cdot\mathbf{p}$ theory, and that under a change to a new orthonormal basis ($S^{-1} = S^{\dagger}$) given by

$$\begin{pmatrix} U_1 \\ U_2 \\ U_3 \\ U_4 \\ U_5 \\ U_6 \\ U_7 \\ U_8 \end{pmatrix} = (S^T) \begin{pmatrix} |S\uparrow\rangle \\ |X\uparrow\rangle \\ |Y\uparrow\rangle \\ |Z\uparrow\rangle \\ |S\downarrow\rangle \\ |X\downarrow\rangle \\ |Y\downarrow\rangle \\ |Z\downarrow\rangle \end{pmatrix}, \tag{6.5}$$

the Hamiltonian will become

$$(H_{new}) = (S^{-1})(H)(S). \tag{6.6}$$

Since

$$(F_{new}) = (S^{-1})(F), \tag{6.7}$$

equation (5.23) shows us that the MME is left invariant by the change of basis, as long as the matrix S does not depend on $\mathbf{k}$, result also derived in Ref. [60].

6.3 Diagonalization of the Spin-Orbit Interaction

Imagine a ZB crystal in which we can change the lattice constant. The spin-orbit interaction Hamiltonian will only change through the multiplicative constant Δ. In the tight-binding limit

the $|J\ m_j\rangle$ representation will diagonalize the spin-orbit interaction. Because the diagonalization does not depend on the value of Δ, the same transformation will diagonalize the spin-orbit interaction even when tight-binding is not a good approximation [17].

6.3.1 ZB semiconductors

The 6-band spin-orbit Hamiltonian for bulk ZB semiconductors is [17]

$$
(H_{so}) = \begin{array}{c} \\ |X\uparrow\rangle \\ |Y\uparrow\rangle \\ |Z\uparrow\rangle \\ |X\downarrow\rangle \\ |Y\downarrow\rangle \\ |Z\downarrow\rangle \end{array}
\begin{array}{c}
\begin{array}{cccccc} |X\uparrow\rangle & |Y\uparrow\rangle & |Z\uparrow\rangle & |X\downarrow\rangle & |Y\downarrow\rangle & |Z\downarrow\rangle \end{array} \\
\begin{pmatrix}
0 & 1 & 0 & 0 & 0 & i \\
-1 & 0 & 0 & 0 & 0 & 1 \\
0 & 0 & 0 & -i & -1 & 0 \\
0 & 0 & -i & 0 & -1 & 0 \\
0 & 0 & 1 & 1 & 0 & 0 \\
i & -1 & 0 & 0 & 0 & 0
\end{pmatrix}
\end{array}
\frac{\Delta}{3i}. \tag{6.8}
$$

A change of basis given by [11]

$$
\begin{pmatrix} |\frac{3}{2},\frac{3}{2}\rangle \\ |\frac{3}{2},\frac{1}{2}\rangle \\ |\frac{3}{2},\frac{-1}{2}\rangle \\ |\frac{3}{2},\frac{-3}{2}\rangle \\ |\frac{1}{2},\frac{1}{2}\rangle \\ |\frac{1}{2},\frac{-1}{2}\rangle \end{pmatrix}
=
\begin{pmatrix}
\frac{1}{\sqrt{2}} & \frac{i}{\sqrt{2}} & 0 & 0 & 0 & 0 \\
0 & 0 & \frac{-\sqrt{2}}{\sqrt{3}} & \frac{1}{\sqrt{6}} & \frac{i}{\sqrt{6}} & 0 \\
\frac{-1}{\sqrt{6}} & \frac{i}{\sqrt{6}} & 0 & 0 & 0 & \frac{-\sqrt{2}}{\sqrt{3}} \\
0 & 0 & 0 & \frac{1}{\sqrt{2}} & \frac{-i}{\sqrt{2}} & 0 \\
0 & 0 & \frac{1}{\sqrt{3}} & \frac{1}{\sqrt{3}} & \frac{i}{\sqrt{3}} & 0 \\
\frac{-1}{\sqrt{3}} & \frac{i}{\sqrt{3}} & 0 & 0 & 0 & \frac{1}{\sqrt{3}}
\end{pmatrix}
\begin{pmatrix} |X\uparrow\rangle \\ |Y\uparrow\rangle \\ |Z\uparrow\rangle \\ |X\downarrow\rangle \\ |Y\downarrow\rangle \\ |Z\downarrow\rangle \end{pmatrix}, \tag{6.9}
$$

transforms the spin-orbit Hamiltonian into

$$
(H_{so}^{(new)}) = \begin{pmatrix}
1 & 0 & 0 & 0 & 0 & 0 \\
0 & 1 & 0 & 0 & 0 & 0 \\
0 & 0 & 1 & 0 & 0 & 0 \\
0 & 0 & 0 & 1 & 0 & 0 \\
0 & 0 & 0 & 0 & -2 & 0 \\
0 & 0 & 0 & 0 & 0 & -2
\end{pmatrix} \frac{\Delta}{3}. \tag{6.10}
$$

6.3.2 WZ semiconductors

The 6-band spin-orbit Hamiltonian for bulk WZ semiconductors is [31]

$$(H_{so}) = \begin{array}{c} \\ |X\uparrow\rangle \\ |Y\uparrow\rangle \\ |Z\uparrow\rangle \\ |X\downarrow\rangle \\ |Y\downarrow\rangle \\ |Z\downarrow\rangle \end{array} \begin{array}{c} \begin{array}{cccccc} |X\uparrow\rangle & |Y\uparrow\rangle & |Z\uparrow\rangle & |X\downarrow\rangle & |Y\downarrow\rangle & |Z\downarrow\rangle \end{array} \\ \begin{pmatrix} \Delta_1 & -i\Delta_2 & 0 & 0 & 0 & \Delta_3 \\ i\Delta_2 & \Delta_1 & 0 & 0 & 0 & -i\Delta_3 \\ 0 & 0 & 0 & -\Delta_3 & i\Delta_3 & 0 \\ 0 & 0 & -\Delta_3 & \Delta_1 & i\Delta_2 & 0 \\ 0 & 0 & -i\Delta_3 & -i\Delta_2 & \Delta_1 & 0 \\ \Delta_3 & i\Delta_3 & 0 & 0 & 0 & 0 \end{pmatrix} \end{array}. \tag{6.11}$$

A change of basis given by [31]

$$\begin{pmatrix} |u_1\rangle \\ |u_2\rangle \\ |u_3\rangle \\ |u_4\rangle \\ |u_5\rangle \\ |u_6\rangle \end{pmatrix} = \begin{pmatrix} \frac{-1}{\sqrt{2}} & \frac{-i}{\sqrt{2}} & 0 & 0 & 0 & 0 \\ \frac{1}{\sqrt{2}} & \frac{-i}{\sqrt{2}} & 0 & 0 & 0 & 0 \\ 0 & 0 & 1 & 0 & 0 & 0 \\ 0 & 0 & 0 & \frac{1}{\sqrt{2}} & \frac{-i}{\sqrt{2}} & 0 \\ 0 & 0 & 0 & \frac{-1}{\sqrt{2}} & \frac{-i}{\sqrt{2}} & 0 \\ 0 & 0 & 0 & 0 & 0 & 1 \end{pmatrix} \begin{pmatrix} |X\uparrow\rangle \\ |Y\uparrow\rangle \\ |Z\uparrow\rangle \\ |X\downarrow\rangle \\ |Y\downarrow\rangle \\ |Z\downarrow\rangle \end{pmatrix}, \tag{6.12}$$

transforms the spin-orbit Hamiltonian into

$$(H_{so}^{(new)}) = \begin{pmatrix} \Delta_1+\Delta_2 & 0 & 0 & 0 & 0 & 0 \\ 0 & \Delta_1-\Delta_2 & 0 & 0 & 0 & \sqrt{2}\Delta_3 \\ 0 & 0 & 0 & 0 & \sqrt{2}\Delta_3 & 0 \\ 0 & 0 & 0 & \Delta_1+\Delta_2 & 0 & 0 \\ 0 & 0 & \sqrt{2}\Delta_3 & 0 & \Delta_1-\Delta_2 & 0 \\ 0 & \sqrt{2}\Delta_3 & 0 & 0 & 0 & 0 \end{pmatrix}. \tag{6.13}$$

6.4 Rotation of the Cartesian Axes

Whenever the semiconductor structure is periodic in the x, y, or z directions the wave-function is given by the Bloch theorem, and the operators $\hat{k}_x$, $\hat{k}_y$, or $\hat{k}_z$ are replaced by real numbers. This greatly simplifies the calculation. When the structure is periodic in a different direction

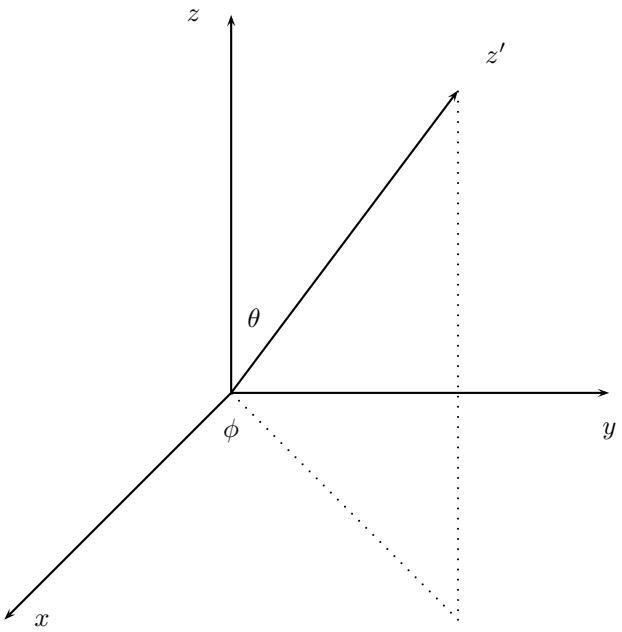

Figure 6.1: The polar angles θ and ϕ.

we need to use a rotated reference frame, in which the z' axis goes in the direction of the periodicity [18]. The direction of the z' axis is given by the polar angles θ and ϕ, as shown in Figure 6.1.

In the rotated reference frame the new spin basis vectors are [18]

$$\begin{pmatrix} |\uparrow'\rangle \\ |\downarrow'\rangle \end{pmatrix} = \begin{pmatrix} \exp(-i\phi/2)\cos(\theta/2) & \exp(i\phi/2)\sin(\theta/2) \\ -\exp(-i\phi/2)\sin(\theta/2) & \exp(i\phi/2)\cos(\theta/2) \end{pmatrix} \begin{pmatrix} |\uparrow\rangle \\ |\downarrow\rangle \end{pmatrix}, \tag{6.14}$$

and the new zone-center basis vectors are

$$\begin{pmatrix} |X'\rangle \\ |Y'\rangle \\ |Z'\rangle \end{pmatrix} = \begin{pmatrix} \cos(\theta)\cos(\phi) & \cos(\theta)\sin(\phi) & -\sin(\theta) \\ -\sin(\phi) & \cos(\phi) & 0 \\ \sin(\theta)\cos(\phi) & \sin(\theta)\sin(\phi) & \cos(\theta) \end{pmatrix} \begin{pmatrix} |X\rangle \\ |Y\rangle \\ |Z\rangle \end{pmatrix}. \tag{6.15}$$

If

$$\begin{pmatrix} S_{11} & S_{12} \\ S_{21} & S_{22} \end{pmatrix} = \begin{pmatrix} \exp(-i\phi/2)\cos(\theta/2) & \exp(i\phi/2)\sin(\theta/2) \\ -\exp(-i\phi/2)\sin(\theta/2) & \exp(i\phi/2)\cos(\theta/2) \end{pmatrix}, \tag{6.16}$$

$$\begin{pmatrix} R_{11} & R_{12} & R_{13} \\ R_{21} & R_{22} & R_{23} \\ R_{31} & R_{32} & R_{33} \end{pmatrix} = \begin{pmatrix} \cos(\theta)\cos(\phi) & \cos(\theta)\sin(\phi) & -\sin(\theta) \\ -\sin(\phi) & \cos(\phi) & 0 \\ \sin(\theta)\cos(\phi) & \sin(\theta)\sin(\phi) & \cos(\theta) \end{pmatrix}, \tag{6.17}$$

then

$$\begin{pmatrix} |X'\uparrow\rangle \\ |Y'\uparrow\rangle \\ |Z'\uparrow\rangle \\ |X'\downarrow\rangle \\ |Y'\downarrow\rangle \\ |Z'\downarrow\rangle \end{pmatrix} = \begin{pmatrix} R_{11}S_{11} & R_{12}S_{11} & R_{13}S_{11} & R_{11}S_{12} & R_{12}S_{12} & R_{13}S_{12} \\ R_{21}S_{11} & R_{22}S_{11} & R_{23}S_{11} & R_{21}S_{12} & R_{22}S_{12} & R_{23}S_{12} \\ R_{31}S_{11} & R_{32}S_{11} & R_{33}S_{11} & R_{31}S_{12} & R_{32}S_{12} & R_{33}S_{12} \\ R_{11}S_{21} & R_{12}S_{21} & R_{13}S_{21} & R_{11}S_{22} & R_{12}S_{22} & R_{13}S_{22} \\ R_{21}S_{21} & R_{22}S_{21} & R_{23}S_{21} & R_{21}S_{22} & R_{22}S_{22} & R_{23}S_{22} \\ R_{31}S_{21} & R_{32}S_{21} & R_{33}S_{21} & R_{31}S_{22} & R_{32}S_{22} & R_{33}S_{22} \end{pmatrix} \begin{pmatrix} |X\uparrow\rangle \\ |Y\uparrow\rangle \\ |Z\uparrow\rangle \\ |X\downarrow\rangle \\ |Y\downarrow\rangle \\ |Z\downarrow\rangle \end{pmatrix}. \tag{6.18}$$

Under this change of basis the spin-orbit interaction Hamiltonian matrix for ZB remains unchanged. The spin-orbit interaction Hamiltonian matrix for WZ is however modified [26].

The matrix (R) has the property that $(R)^T = (R)^{-1}$. Under the rotation of the axes the components of a vector will change as

$$\begin{pmatrix} k'_x \\ k'_y \\ k'_z \end{pmatrix} = (R) \begin{pmatrix} k_x \\ k_y \\ k_z \end{pmatrix}. \tag{6.19}$$

6.4.1 Hamiltonian with no spin

Under the rotation of the axes the matrix of a three-band Hamiltonian will change as

$$(H') = (R)(H)(R^T), \tag{6.20}$$

$$H'_{\alpha'\beta'} = R_{\alpha'\alpha}H_{\alpha\beta}R_{\beta'\beta}. \tag{6.21}$$

When the Hamiltonian is given by

$$H_{\alpha\beta} = k_i D^{ij}_{\alpha\beta} k_j, \tag{6.22}$$

because

$$(k) = (R^T)(k'), \tag{6.23}$$

$$k_i = R_{i'i}k'_{i'}, \tag{6.24}$$

the rotated Hamiltonian becomes [27]

$$H'_{\alpha'\beta'} = R_{\alpha'\alpha}R_{i'i}k'_{i'}D^{ij}_{\alpha\beta}R_{j'j}k'_{j'}R_{\beta'.\beta} \tag{6.25}$$

6.4.2 Hamiltonian with spin

Consider

$$(U) \equiv \begin{pmatrix} R_{11}S_{11} & R_{12}S_{11} & R_{13}S_{11} & R_{11}S_{12} & R_{12}S_{12} & R_{13}S_{12} \\ R_{21}S_{11} & R_{22}S_{11} & R_{23}S_{11} & R_{21}S_{12} & R_{22}S_{12} & R_{23}S_{12} \\ R_{31}S_{11} & R_{32}S_{11} & R_{33}S_{11} & R_{31}S_{12} & R_{32}S_{12} & R_{33}S_{12} \\ R_{11}S_{21} & R_{12}S_{21} & R_{13}S_{21} & R_{11}S_{22} & R_{12}S_{22} & R_{13}S_{22} \\ R_{21}S_{21} & R_{22}S_{21} & R_{23}S_{21} & R_{21}S_{22} & R_{22}S_{22} & R_{23}S_{22} \\ R_{31}S_{21} & R_{32}S_{21} & R_{33}S_{21} & R_{31}S_{22} & R_{32}S_{22} & R_{33}S_{22} \end{pmatrix}. \tag{6.26}$$

Under the rotation of the axes the matrix of the Hamiltonian will change as

$$(H') = (U^*)(H)(U^T), \tag{6.27}$$

$$H'_{\alpha'\beta'} = U^*_{\alpha'\alpha} H_{\alpha\beta} U_{\beta'\beta}. \tag{6.28}$$

When the Hamiltonian is given by

$$H_{\alpha\beta} = k_i D^{ij}_{\alpha\beta} k_j, \tag{6.29}$$

because

$$(k) = (R^T)(k'), \tag{6.30}$$

$$k_i = R_{i'i} k'_{i'}, \tag{6.31}$$

the rotated Hamiltonian becomes

$$H'_{\alpha'\beta'} = U^*_{\alpha'\alpha} R_{i'i} k'_{i'} D^{ij}_{\alpha\beta} R_{j'j} k'_{j'} U_{\beta'\beta}. \tag{6.32}$$

Chapter 7

Strain in Cylindrical Heterostructures

7.1 Elasticity Theory in Cartesian Coordinates

The basic quantity in elasticity theory is the deformation vector field $\mathbf{u} = \mathbf{x}' - \mathbf{x}$ relating the position $\mathbf{x}$ of a point before the deformation to the position $\mathbf{x}'$ of the point after the deformation. For a pair of two close points $d\mathbf{u} = d\mathbf{x}' - d\mathbf{x}$, and the distance between the two points after the deformation can be written as [61]

$$(dx')^2 = (dx)^2 + 2\epsilon_{ij} dx_i dx_j, \tag{7.1}$$

where the symmetric strain tensor is defined as

$$\epsilon_{ij} = \frac{1}{2}\left(\frac{\partial u_i}{\partial x_j} + \frac{\partial u_j}{\partial x_i} + \frac{\partial u_k}{\partial x_i}\frac{\partial u_k}{\partial x_j}\right). \tag{7.2}$$

When the deformations are small the derivatives $\partial u_i/\partial x_j$ are small, and we keep only linear terms in these derivatives. This is how we end up with the expression for the linear strain:

$$\epsilon_{ij} = \frac{1}{2}\left(\frac{\partial u_i}{\partial x_j} + \frac{\partial u_j}{\partial x_i}\right). \tag{7.3}$$

The strain-displacement equations (7.3) can be integrated, to obtain the deformation from the strain tensor. Since the six stress tensor components are more than the three displacement

components, extra conditions need to be imposed to make sure that the solution is consistent. The displacement field at a given point does not depend on the integration path. Stokes theorem is applied to the integrand, and the following compatibility conditions are obtained [62] :

$$\frac{\partial}{\partial x_l}\left[\epsilon_{ik} - x_j\left(\frac{\partial \epsilon_{ik}}{\partial x_j} - \frac{\partial \epsilon_{jk}}{\partial x_i}\right)\right] = \frac{\partial}{\partial x_k}\left[\epsilon_{il} - x_j\left(\frac{\partial \epsilon_{il}}{\partial x_j} - \frac{\partial \epsilon_{jl}}{\partial x_i}\right)\right]. \tag{7.4}$$

Consider a small volume element inside a solid body. There are two kind of forces acting on this volume element: the body forces (e.g. gravity) and the surface tractions. The surface tractions are the forces due to the remaining of the solid, acting on the small volume element at its surface. Since the surface tractions act only at the surface, they must be given by a surface integral, which is then converted to a volume integral:

$$F_i = \oint \sigma_{ik} df_k = \int \frac{\partial \sigma_{ik}}{\partial x_k} dV, \tag{7.5}$$

where σ_{ik} is the stress tensor. $\sigma_{ik}df_k$ is the F_i component of the force acting on a surface element df_k perpendicular to the x_k axis. For a body in rotational equilibrium the stress tensor must be symmetric [61]. When the body is in translational motion the net force acting on the volume element gives its acceleration:

$$\frac{\partial \sigma_{ik}}{\partial x_k} + f_i = \rho a_i, \tag{7.6}$$

where f is the body force density (e.g. ρg), ρ is the mass density, and a is the acceleration. In general there is a proportionality relation between force and elongation (between stress and strain), called Hooke's Law. In the most general case this relation takes the form:

$$\sigma_{ij} = C_{ijmn}\epsilon_{mn}, \tag{7.7}$$

where C_{ijmn} is the stiffness matrix. Although the 4 indices suggest 81 stiffness elements, due to symmetry $C_{ijmn} = C_{jimn}$ and $C_{ijmn} = C_{ijnm}$. The existence of a strain energy density function, when the system is adiabatic or isothermal, leads to $C_{ijmn} = C_{mnij}$. As a result there are only 21 independent stiffness elements. For an isotropic material, due to symmetry considerations, only 2 independent stiffness elements (μ and λ) are left. The stress-strain relations take the form:

$$\sigma_{ij} = 2\mu\epsilon_{ij} + \lambda\epsilon_{nn}\delta_{ij}. \tag{7.8}$$

7.2 Elasticity Theory in Cylindrical Coordinates

In cylindrical coordinates the strain-displacement equations (7.3) take the form:

$$\epsilon_{rr} = \frac{\partial u_r}{\partial r}, \tag{7.9}$$

$$\epsilon_{\theta\theta} = \frac{1}{r}\frac{\partial u_\theta}{\partial \theta} + \frac{u_r}{r}, \tag{7.10}$$

$$\epsilon_{zz} = \frac{\partial u_z}{\partial z}, \tag{7.11}$$

$$\epsilon_{r\theta} = \frac{1}{2}\left(\frac{1}{r}\frac{\partial u_r}{\theta} + \frac{\partial u_\theta}{\partial r} - \frac{u_\theta}{r}\right), \tag{7.12}$$

$$\epsilon_{rz} = \frac{1}{2}\left(\frac{\partial u_r}{\partial z} + \frac{\partial u_z}{\partial r}\right), \tag{7.13}$$

$$\epsilon_{\theta z} = \frac{1}{2}\left(\frac{\partial u_\theta}{\partial z} + \frac{1}{r}\frac{\partial u_z}{\partial \theta}\right). \tag{7.14}$$

The compatibility relations (7.4) take the form:

$$\frac{\partial^2 \epsilon_{\theta\theta}}{\partial r^2} + \frac{1}{r^2}\frac{\partial^2 \epsilon_{rr}}{\partial \theta^2} + \frac{2}{r}\frac{\partial \epsilon_{\theta\theta}}{\partial r} - \frac{1}{r}\frac{\partial \epsilon_{rr}}{\partial r} = 2\left(\frac{1}{r}\frac{\partial^2 \epsilon_{r\theta}}{\partial r \partial \theta} + \frac{1}{r^2}\frac{\partial \epsilon_{r\theta}}{\partial \theta}\right), \tag{7.15}$$

$$\frac{\partial^2 \epsilon_{\theta\theta}}{\partial z^2} + \frac{1}{r^2}\frac{\partial^2 \epsilon_{zz}}{\partial \theta^2} + \frac{1}{r}\frac{\partial \epsilon_{zz}}{\partial r} = 2\left(\frac{1}{r}\frac{\partial^2 \epsilon_{\theta z}}{\partial z \partial \theta} + \frac{1}{r}\frac{\partial \epsilon_{zr}}{\partial z}\right), \tag{7.16}$$

$$\frac{\partial^2 \epsilon_{zz}}{\partial r^2} + \frac{\partial^2 \epsilon_{rr}}{\partial z^2} = 2\frac{\partial^2 \epsilon_{rz}}{\partial z \partial r}, \tag{7.17}$$

$$\frac{1}{r}\frac{\partial^2 \epsilon_{zz}}{\partial r \partial \theta} - \frac{1}{r^2}\frac{\partial \epsilon_{zz}}{\partial \theta} = \frac{\partial}{\partial z}\left(\frac{1}{r}\frac{\partial \epsilon_{zr}}{\partial \theta} + \frac{\partial \epsilon_{\theta z}}{\partial r} - \frac{\partial \epsilon_{r\theta}}{\partial z}\right) - \frac{\partial}{\partial z}\left(\frac{\epsilon_{\theta z}}{r}\right), \tag{7.18}$$

$$\frac{1}{r}\frac{\partial^2 \epsilon_{rr}}{\partial \theta \partial z} = \frac{\partial}{\partial r}\left(\frac{1}{r}\frac{\partial \epsilon_{zr}}{\partial \theta} - \frac{\partial \epsilon_{\theta z}}{\partial r} + \frac{\partial \epsilon_{r\theta}}{\partial z}\right) - \frac{\partial}{\partial r}\left(\frac{\epsilon_{\theta z}}{r}\right) + \frac{2}{r}\frac{\partial \epsilon_{r\theta}}{\partial z}, \tag{7.19}$$

$$\frac{\partial^2 \epsilon_{\theta\theta}}{\partial r \partial z} - \frac{1}{r}\frac{\partial \epsilon_{rr}}{\partial z} + \frac{1}{r}\frac{\partial \epsilon_{\theta\theta}}{\partial z} = \frac{1}{r}\frac{\partial}{\partial \theta}\left(-\frac{1}{r}\frac{\partial \epsilon_{zr}}{\partial \theta} + \frac{\partial \epsilon_{\theta z}}{\partial r} + \frac{\partial \epsilon_{r\theta}}{\partial z}\right) + \frac{1}{r}\frac{\partial}{\partial \theta}\left(\frac{\epsilon_{\theta z}}{r}\right). \tag{7.20}$$

The equilibrium relations (7.6) take the form:

$$\frac{\partial \sigma_{rr}}{\partial r} + \frac{1}{r}\frac{\partial \sigma_{\theta r}}{\partial \theta} + \frac{\partial \sigma_{zr}}{\partial z} + \frac{1}{r}(\sigma_{rr} - \sigma_{\theta\theta}) + f_r = \rho a_r, \tag{7.21}$$

$$\frac{\partial \sigma_{r\theta}}{\partial r} + \frac{1}{r}\frac{\partial \sigma_{\theta\theta}}{\partial \theta} + \frac{\partial \sigma_{z\theta}}{\partial z} + \frac{2}{r}\sigma_{r\theta} + f_\theta = \rho a_\theta, \tag{7.22}$$

$$\frac{\partial \sigma_{rz}}{\partial r} + \frac{1}{r}\frac{\partial \sigma_{\theta z}}{\partial \theta} + \frac{\partial \sigma_{zz}}{\partial z} + \frac{1}{r}\sigma_{rz} + f_z = \rho a_z. \tag{7.23}$$

The stress-strain relations (7.8) take the form:

$$\sigma_{rr} = 2\mu\epsilon_{rr} + \lambda(\epsilon_{rr} + \epsilon_{\theta\theta} + \epsilon_{zz}), \tag{7.24}$$

$$\sigma_{\theta\theta} = 2\mu\epsilon_{\theta\theta} + \lambda(\epsilon_{rr} + \epsilon_{\theta\theta} + \epsilon_{zz}), \tag{7.25}$$

$$\sigma_{zz} = 2\mu\epsilon_{zz} + \lambda(\epsilon_{rr} + \epsilon_{\theta\theta} + \epsilon_{zz}), \tag{7.26}$$

$$\sigma_{r\theta} = 2\mu\epsilon_{r\theta}, \tag{7.27}$$

$$\sigma_{rz} = 2\mu\epsilon_{rz}, \tag{7.28}$$

$$\sigma_{\theta z} = 2\mu\epsilon_{\theta z}. \tag{7.29}$$

7.3 Plane Deformation with Cylindrical Symmetry

A state of plane deformation is defined by $u_r = u_r(r,\theta)$, $u_\theta = u_\theta(r,\theta)$, $u_z = u_z(z)$. If the problem has cylindrical symmetry (no dependence on θ), and if there is no torsion ($u_\theta = 0$), the deformation is given by $u_r = u_r(r)$, $u_\theta = 0$, $u_z = u_z(z)$. In this situation the strain-displacement equations take the form:

$$\epsilon_{rr} = \frac{\partial u_r}{\partial r}, \tag{7.30}$$

$$\epsilon_{\theta\theta} = \frac{u_r}{r}, \tag{7.31}$$

$$\epsilon_{zz} = \frac{\partial u_z}{\partial z}, \tag{7.32}$$

$$\epsilon_{r\theta} = 0, \tag{7.33}$$

$$\epsilon_{rz} = 0, \tag{7.34}$$

$$\epsilon_{\theta z} = 0. \tag{7.35}$$

The compatibility relations are reduced to:

$$\frac{\partial^2\epsilon_{\theta\theta}}{\partial r^2} + \frac{2}{r}\frac{\partial\epsilon_{\theta\theta}}{\partial r} - \frac{1}{r}\frac{\partial\epsilon_{rr}}{\partial r} = 0. \tag{7.36}$$

The stress-strain relations take the form:

$$\sigma_{rr} = 2\mu\epsilon_{rr} + \lambda(\epsilon_{rr} + \epsilon_{\theta\theta} + \epsilon_{zz}), \tag{7.37}$$

$$\sigma_{\theta\theta} = 2\mu\epsilon_{\theta\theta} + \lambda(\epsilon_{rr} + \epsilon_{\theta\theta} + \epsilon_{zz}), \tag{7.38}$$

$$\sigma_{zz} = 2\mu\epsilon_{zz} + \lambda(\epsilon_{rr} + \epsilon_{\theta\theta} + \epsilon_{zz}), \tag{7.39}$$

$$\sigma_{r\theta} = 0, \tag{7.40}$$

$$\sigma_{rz} = 0, \tag{7.41}$$

$$\sigma_{\theta z} = 0. \tag{7.42}$$

Suppose that the body is in translational equilibrium, and that there are no body forces. The equilibrium relations take the form:

$$\frac{\partial \sigma_{rr}}{\partial r} + \frac{1}{r}(\sigma_{rr} - \sigma_{\theta\theta}) = 0, \tag{7.43}$$

$$\frac{\partial \sigma_{zz}}{\partial z} = 0. \tag{7.44}$$

Since

$$\frac{\partial \sigma_{zz}}{\partial z} = (2\mu + \lambda)\frac{\partial \epsilon_{zz}}{\partial z} = 0, \tag{7.45}$$

we conclude that $\epsilon_{zz} \equiv \epsilon_o$ is constant, and that $u_z = \epsilon_o z$.

7.4 Infinite Embedded Cylindrical Wire with Cubic Structure

We are now ready to analyze the strain distribution in an infinitely long cylindrical wire embedded in an infinite substrate. In the following the label "*in*" refers to the wire, and the label "*out*" refers to the substrate. Let's start with the wire and the substrate separated and unstrained, as shown in Figure 7.1. The radius of the unstrained wire is greater than the radius of the hole in the unstrained substrate. This difference is called δ. Because $\epsilon_{zz}^{(out)}$ at infinity is zero, and because it is constant, we conclude that $\epsilon_{zz}^{(out)} = 0$. The wire is first compressed, in such a way as to preserve the cubic structure, until the lattice constant of the wire matches the lattice constant of the substrate. Therefore

$$\frac{\delta}{r_o} = \frac{u_z}{z} = \epsilon_o = \frac{a^{(out)} - a^{(in)}}{a^{(out)}}. \tag{7.46}$$

The compressed wire is then inserted into the cavity, and the radial strain in allowed to relax. This procedure is known as "shrink fit" [63]. As a result the wire will end up with a deformation $u_r^{(in)}(r)$ and the substrate will end up with a deformation $u_r^{(out)}(r)$. It is clear from the figure that

$$u_r^{(in)}(r_o) - u_r^{(out)}(r_o) = \delta. \tag{7.47}$$

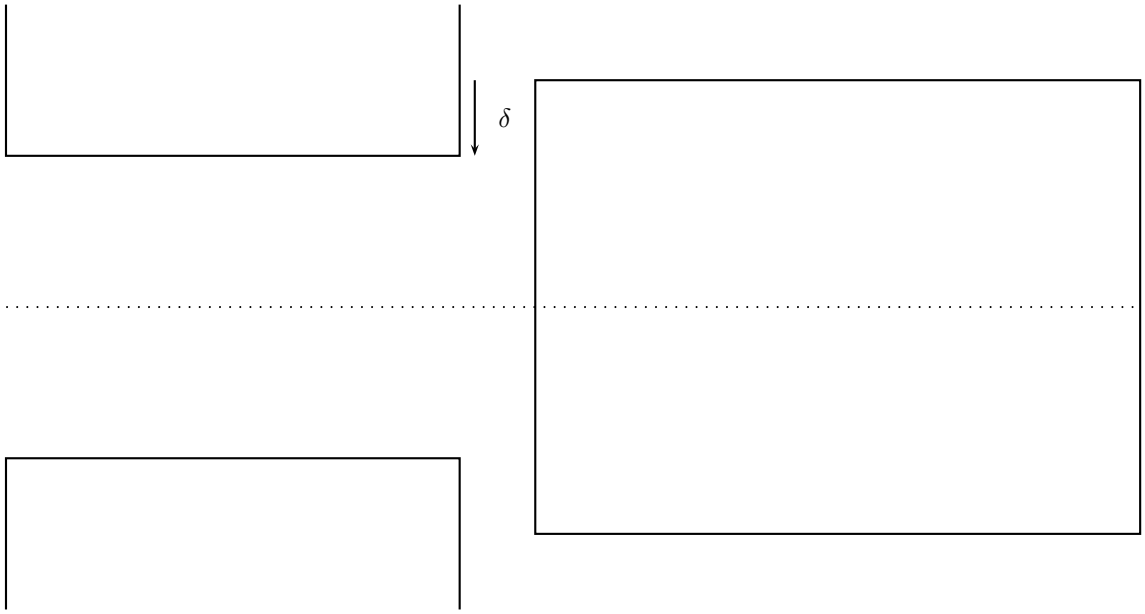

Figure 7.1: The wire and the substrate before embedding.

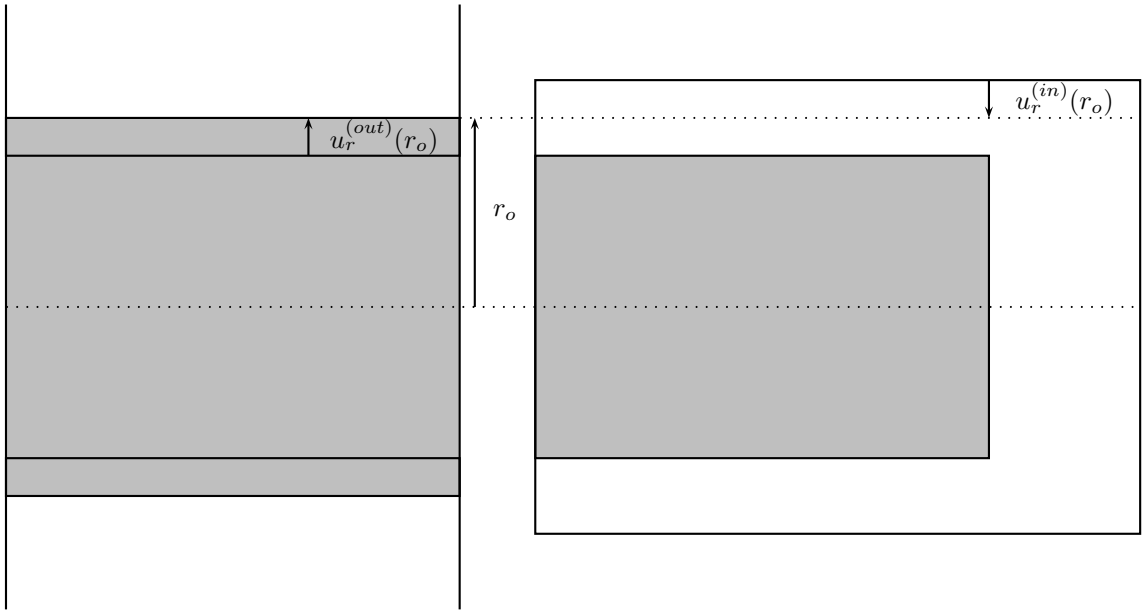

Figure 7.2: The wire and the substrate after the "shrink fit" embedding. The shaded regions are the compressed wire before insertion (right) and the relaxed wire after insertion (left).

The equation (7.47) is used to determine the pressure P at the wire-substrate interface, the key to solving the strain distribution.

In a first step we substitute the stress components from (7.37) and (7.38) into (7.43).

$$2\mu\frac{\partial\epsilon_{rr}}{\partial r}+\lambda\frac{\partial\epsilon_{rr}}{\partial r}+\lambda\frac{\partial\epsilon_{\theta\theta}}{\partial r}+\frac{2\mu}{r}(\epsilon_{rr}-\epsilon_{\theta\theta}). \tag{7.48}$$

In a second step we substitute the strain components from (7.30) and (7.31) into (7.48).

$$\frac{\partial^2 u_r}{\partial r^2}+\frac{1}{r}\frac{\partial u_r}{\partial r}-\frac{u_r}{r^2}=0. \tag{7.49}$$

The general solution of the equation (7.49) is

$$u_r(r)=C_1 r+\frac{C_2}{r}. \tag{7.50}$$

7.4.1 The Wire

In the wire $C_2=0$, to prevent the divergence when the radius is zero. Therefore:

$$u_r=C_1 r, \tag{7.51}$$

$$\epsilon_{rr}=C_1, \tag{7.52}$$

$$\epsilon_{\theta\theta}=C_1, \tag{7.53}$$

$$\sigma_{rr}=2(\mu+\lambda)C_1+\lambda\epsilon_o. \tag{7.54}$$

At the wire-substrate interface the radial stress is the negative pressure. This is the boundary condition.

$$-P=2(\mu+\lambda)C_1+\lambda\epsilon_o. \tag{7.55}$$

As a consequence:

$$C_1=-\frac{P+\lambda\epsilon_o}{2(\mu+\lambda)}, \tag{7.56}$$

$$u_r^{(in)}(r)=-\frac{P+\lambda\epsilon_o}{2(\mu+\lambda)}r. \tag{7.57}$$

7.4.2 The Substrate

In the substrate $C_1 = 0$, to prevent the divergence when the radius goes to infinity. Therefore:

$$u_r = \frac{C_2}{r}, \tag{7.58}$$

$$\epsilon_{rr} = -\frac{C_2}{r^2}, \tag{7.59}$$

$$\epsilon_{\theta\theta} = \frac{C_2}{r^2}, \tag{7.60}$$

$$\sigma_{rr} = -\frac{2\mu C_2}{r^2}. \tag{7.61}$$

At the wire-substrate interface the radial stress is the negative pressure. This is the boundary condition.

$$-P = -\frac{2\mu C_2}{r_o^2}. \tag{7.62}$$

As a consequence:

$$C_2 = \frac{P r_o^2}{2\mu}, \tag{7.63}$$

$$u_r^{(out)}(r) = \frac{P r_o^2}{2\mu r}. \tag{7.64}$$

7.4.3 The Shrink Fit

We now substitute (7.57) and (7.64) into (7.47). For simplicity we assume that μ and λ are the same in both materials [32].

$$-\frac{P + \lambda\epsilon_o}{2(\mu + \lambda)} r_o - \frac{P r_o^2}{2\mu r_o} = \epsilon_o r_o. \tag{7.65}$$

From (7.65) we find the pressure P, needed in (7.57) and (7.64) to give the strain distribution.

$$P = -\epsilon_o \frac{(2\mu + 3\lambda)\mu}{2\mu + \lambda}. \tag{7.66}$$

Chapter 8

One-Band $\mathbf{k} \cdot \mathbf{p}$ Calculations - Quantum Ice Cream Dot

8.1 Introduction

Modeling the electron states in semiconductor nanostructures remains a difficult computational task. Various computational methods such as the transfer matrix method [64], the finite element method [65], the finite difference method [66, 67, 68], and the fast Fourier transform technique [69] have been used. Other methods, the effective index method and numerical relaxation, have also been used to calculate the ground state of a cylindrical quantum dot (QD) [70]. The finite difference method (FDM) has been, by far, the most commonly used method. Nevertheless, implementation details are rarely given. One exception is in the study of GaN quantum wells by Chuang and Chang [71].

The shape and size of a quantum dot determine the number of eigenstates and their degeneracy [72]. We investigated whether we can have a bound state in a very narrow quantum dot with the shape of an ice cream cone (QIC dot). In this calculation the QIC dot is embedded into a cube, with a potential barrier of 0.5 eV, as shown in Figure 8.1.

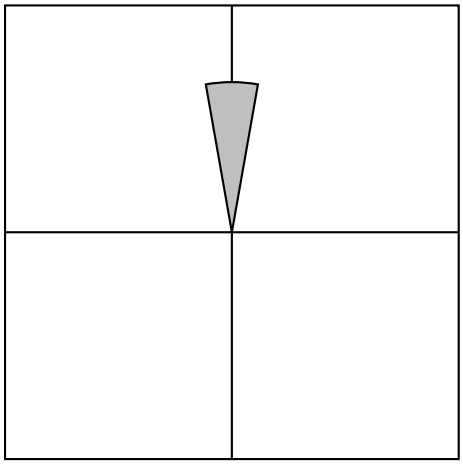

Figure 8.1: The 10^o QIC dot embedded into a cubical substrate.

8.2 Effect of Dirichlet and van Neumann boundary conditions

On the faces of the cube Dirichlet or van Neumann boundary conditions are imposed. When the state is truly bound, then of course both the wave function and its derivative are zero on the outer boundary of the substrate. If van Neumann boundary conditions are used then the magnitude of the wave function on the outer boundary of the substrate can be used as a check: only when it is zero we truly have a bound state [66].

In order to see the effect of applying Dirichlet or van Neumann boundary conditions on the boundary, we have solved the 10^o QIC, with a radius of 100 Å, enclosed in a cubical barrier of side 300 Å. The grid is 31×31×31, with the tip of the QIC at the center of the grid. The grid step is 10 Å. Inside the dot the effective mass is 0.067 m_o, and the potential is 0 eV. In the barrier the effective mass is 0.0919 m_o, and the potential is 0.5 eV. Our calculation with van Neumann boundary conditions resulted in only one bounded state, with energy 0.461 eV, about 3% higher than the one obtained with Dirichlet boundary conditions. This value is pretty close to 0.5 eV, the potential of the barrier, therefore it is of legitimate interest to see whether the wave function is zero on the boundary of the cubical grid, as required for a bound state. The wave function for the only bound state is plotted in Figures 8.2 and 8.3.

It can be seen that the wave-function is not concentrated closer to the tip of the QIC. It can

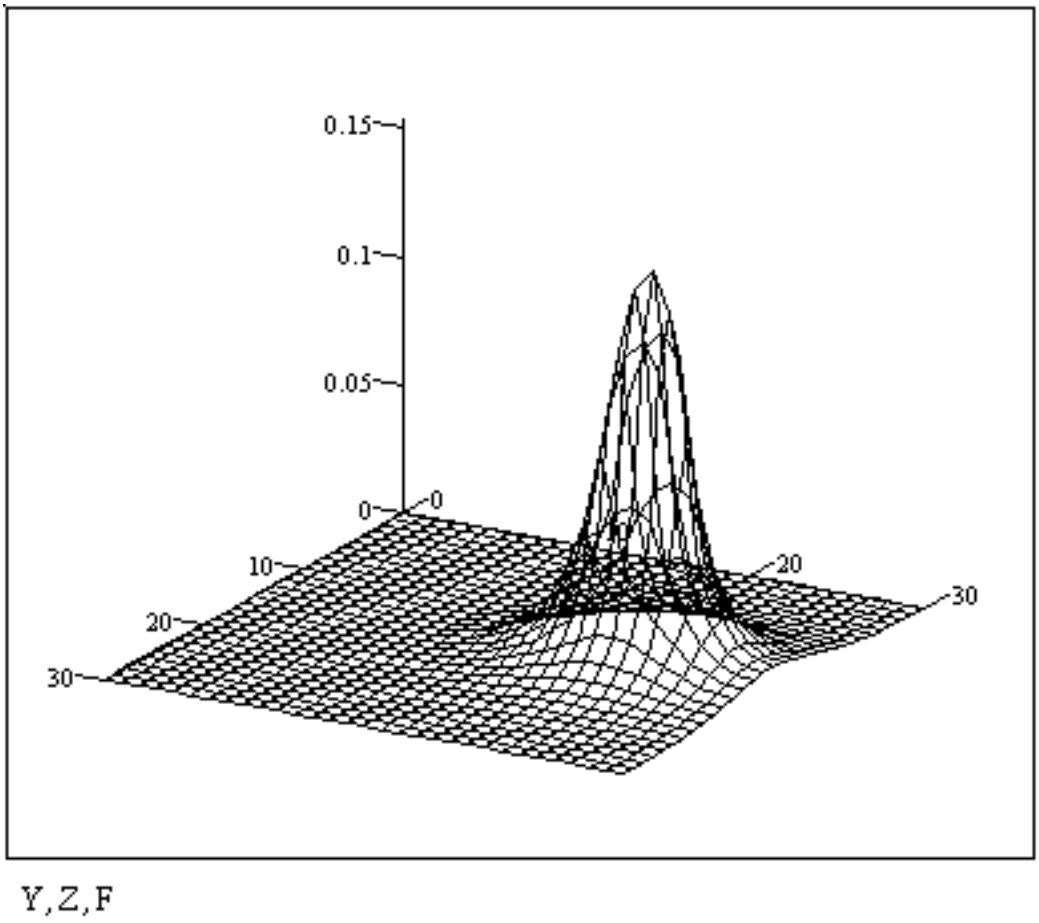

Figure 8.2: The 10^o QIC wave-function in a YZ cross-section, at half X.

also be seen that the wave-function is not zero on the grid boundary closer to the cap of the QIC. This can be most easily seen from Figure 8.4. Therefore a better calculation should be done, with the QIC better centered within the cubical grid. By imposing Dirichlet boundary conditions we have affected the wave-function in a rather dramatic way, forcing it towards the center of the grid. The bound state found is not bound by the barrier's potential outside the QIC dot, but by the infinite potential applied by the Dirichlet boundary conditions on the faces of the cube.

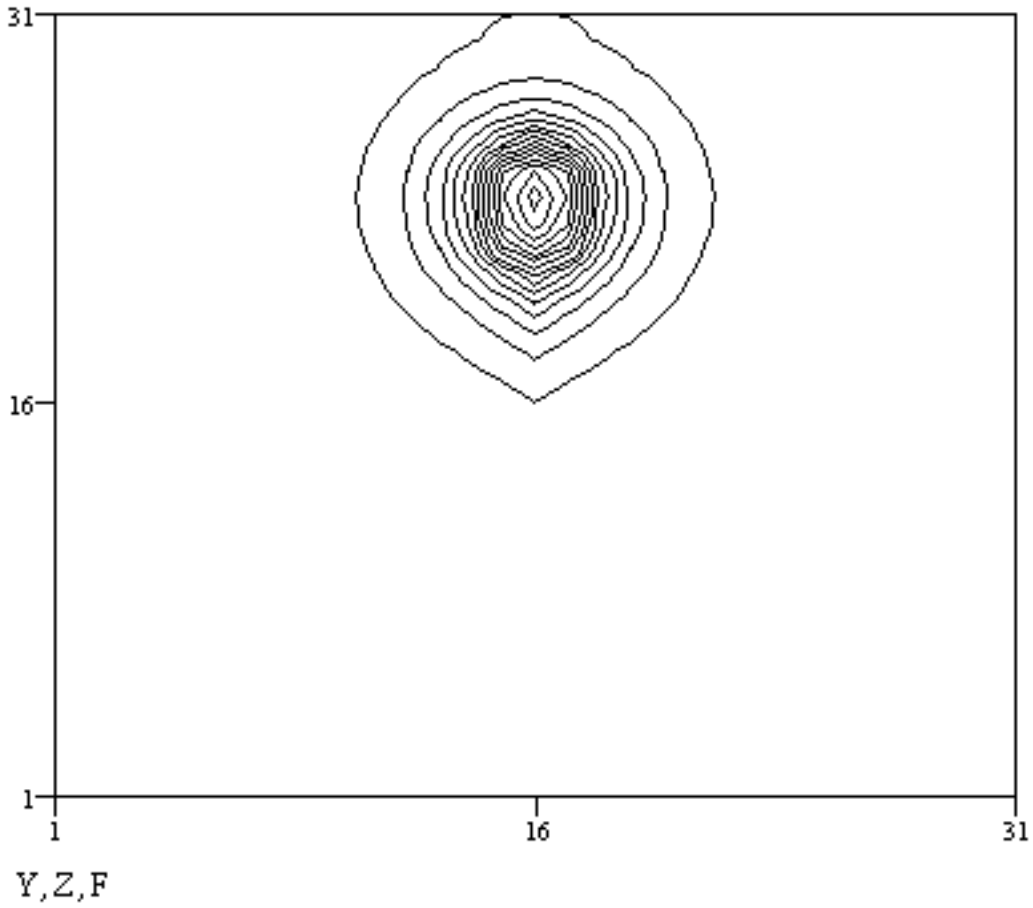

Figure 8.3: The 10^o QIC wave-function in a YZ cross-section, at half X. Contour plot lines at 0.01, 0.02, etc.

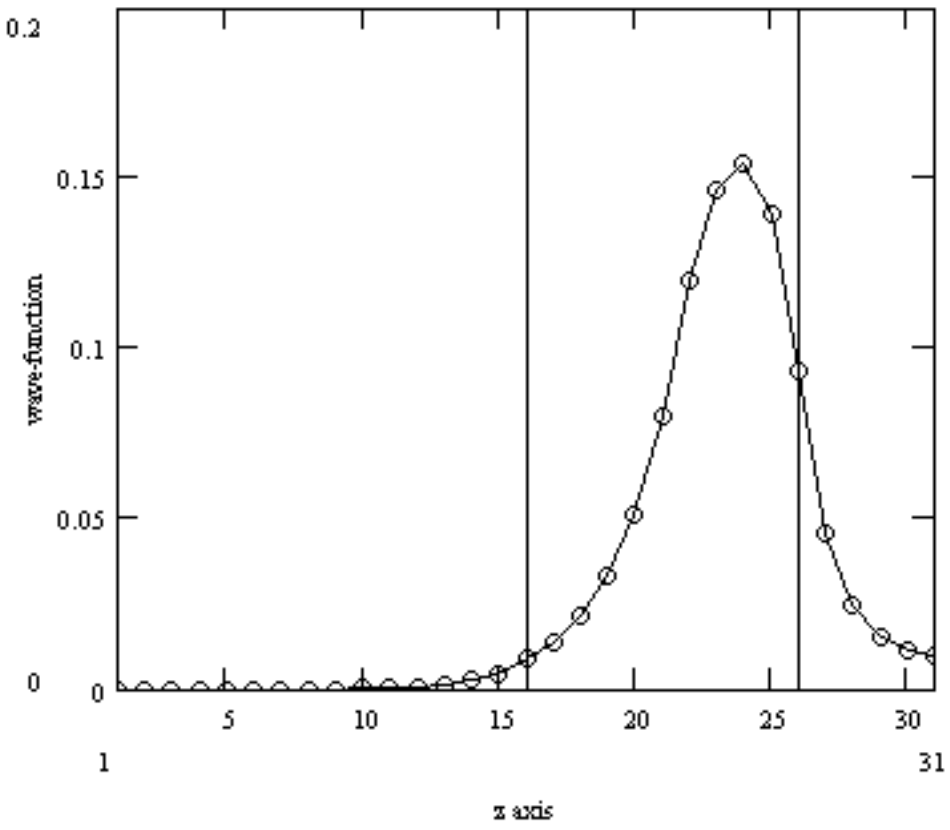

Figure 8.4: The 10^o QIC wave-function along the Z axis. The three vertical domains are the barrier, the quantum dot, and the barrier.

Chapter 9

One-Band $\mathbf{k} \cdot \mathbf{p}$ Calculations - Elliptical Dot

9.1 Introduction

There are 11 coordinate systems with orthogonal coordinate lines [73]. Depending on the symmetry of the domain, and also on the boundary conditions, the Schrödinger equation can or cannot be simplified and solved exactly in the coordinate system compatible with the symmetry of the quantum dot. The separability of the Schrödinger equation is very important when studying shape effects, for it allows us to better understand why we get degeneracies in the eigenfunctions [72].

In a recent paper [35], it is stated that the two-dimensional elliptic quantum dot (QD) problem with finite barrier can be exactly solved. The purpose of our work [34] is to point out that the above assertion is incorrect and to correct the energy spectra presented in Ref. [35].

9.2 The Eigenstates of an Elliptical Quantum Dot

The separation of the Schrödinger equation for an elliptic QD in elliptical coordinates leads to the Mathieu and modified Mathieu differential equations (Eqs. (3a) and (3b) of Ref. [35]). For the infinite barrier problem, it is correctly stated that the energy eigenvalues E are determined

by the boundary condition imposed upon the even or odd radial Mathieu functions

$$\mathrm{Mc}_l^{(1)}(c, q_1, U) = 0, \tag{9.1}$$

$$\mathrm{Ms}_l^{(1)}(c, q_1, U) = 0, \tag{9.2}$$

where c is a separation constant, $q_1 = f^2k^2/4$ with $f = \sqrt{a^2 - b^2}$ the focal length and $k^2 = 2m^*E/\hbar^2$, and $U = \mathrm{arctanh}(b/a)$ is the dot boundary. Periodicity of the angular Mathieu function determines the separation constant c, while the zeroes of the radial Mathieu function at $u = U$ determine the energy eigenvalues [73].

For the finite barrier problem the even and odd wave functions (Eqs. (11) and (12) of Ref. [35]) are assumed to have the form

$$\Psi^{\mathrm{e}}_{n,l}(u, v) = \begin{cases} N^{\mathrm{e}}_{n,l}\mathrm{Mc}_l^{(1)}(u, q_{1_{n,l}})\mathrm{ce}_l(v, q_{1_{n,l}}), & u \le U, \\ N^{\mathrm{e}}_{n,l}\mathrm{Mc}_l^{(3)}(u, -q_{2_{n,l}})\mathrm{ce}_l(v, -q_{2_{n,l}}), & u > U, \end{cases} \tag{9.3}$$

and

$$\Psi^{\mathrm{o}}_{n,l}(u, v) = \begin{cases} N^{\mathrm{o}}_{n,l}\mathrm{Ms}_l^{(1)}(u, q_{1_{n,l}})\mathrm{se}_l(v, q_{1_{n,l}}), & u \le U, \\ N^{\mathrm{o}}_{n,l}\mathrm{Ms}_l^{(3)}(u, -q_{2_{n,l}})\mathrm{se}_l(v, -q_{2_{n,l}}), & u > U. \end{cases} \tag{9.4}$$

These functions lead to a simple boundary condition (Eq. (5) of Ref. [35]), which is solved similarly to the infinite barrier case.

That the wave functions (3) and (4) cannot be right can be seen by rewriting the continuity of the wave function on the ellipse boundary. For example, Eq. (3) gives

$$\begin{aligned} \mathrm{ce}_l(v, q_{1_{n,l}}) &= \frac{\mathrm{Mc}_l^{(3)(U, -q_{2_{n,l}})}}{\mathrm{Mc}_l^{(1)(U, q_{1_{n,l}})}}\mathrm{ce}_l(v, -q_{2_{n,l}}) \\ &\equiv \text{constant} \times \mathrm{ce}_l(v, -q_{2_{n,l}}). \end{aligned} \tag{9.5}$$

The latter equation cannot be satisfied for an arbitrary v. If the angular Mathieu functions were the same for all v (apart from a proportionality constant) then, in particular, the following

set of equations would be fulfilled:

$$c_{l,q_1} - 2q_1\cos(2v) = \frac{1}{\mathrm{ce}_l(v,q_1)}\frac{d^2\mathrm{ce}_l(v,q_1)}{dv^2}$$
$$= \frac{1}{\mathrm{ce}_l(v,-q_2)}\frac{d^2\mathrm{ce}_l(v,-q_2)}{dv^2} = c_{l,-q_2} - 2q_2\cos(2v). \tag{9.6}$$

From Eq. (9.6) it follows that:

$$2(q_1 - q_2)\cos(2v) = c_{l,q_1} - c_{l,-q_2}. \tag{9.7}$$

The latter equation cannot be fulfilled for all v since $q_1 - q_2 = f^2 m^* V_o/(2\hbar^2) \neq 0$. The origin of the problem is, obviously, that the problem is not separable, contrary to what is stated in Ref. [35].

The correct wave function for the finite barrier problem can be written in the form (for the even states as example)

$$\Psi_n^{\mathrm{e}}(u,v)$$
$$= \begin{cases} \sum_l A_{n,l}^{\mathrm{e}}\mathrm{Mc}_l^{(1)}(u,q_{1_n})\mathrm{ce}_l(v,q_{1_n}), & u \leq U, \\ \sum_l B_{n,l}^{\mathrm{e}}\mathrm{Mc}_l^{(3)}(u,-q_{2_n})\mathrm{ce}_l(v,-q_{2_n}), & u > U. \end{cases} \tag{9.8}$$

In addition to the summation, we note that the q's should not be functions of l.

In the absence of a simple exact solution, we present a numerical solution. We have used the finite-difference method on a 400 $\times$ 400 uniform rectangular grid. Different eccentricities have been achieved by changing the mesh sizes in the two directions. The algebraic eigenvalue problem for the resulting large sparse matrix has been solved with the help of the ARPACK library [74]. For the infinite-barrier problem, we have obtained a spectrum identical to Fig. 5 of Ref. [35]. However, for a finite barrier, our results are different. For example, we have reproduced in our Fig. 9.1, results of our calculations corresponding to Fig. 3 of Ref. [35]. While we get the same limiting eigenvalues for the circular dot (due to the separability of the problem), our results differ for increasing eccentricity. In particular, we get a more rapid increase in the energies with increasing eccentricity. This is the same trend seen for the infinite barrier QD.

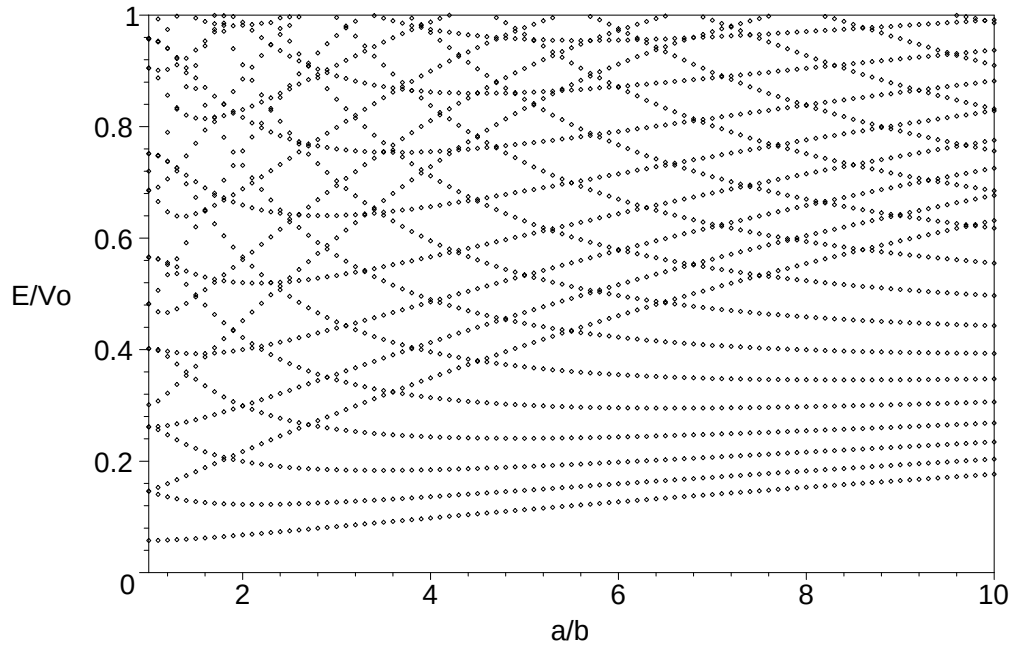

Figure 9.1: Energy of the bound states for an elliptic quantum dot as a function of the eccentricity a/b. The effective electron mass is m^*=0.041 m_o, the product of the two semi-axes is $(ab)^{1/2}$ = 10 nm, the potential in the barrier is V_o = 0.7527 eV. The strength of the well, deffined by $\gamma = \sqrt{(2m^*/\hbar^2)abV_o}$, is $\gamma = 9$.

Chapter 10

One-Band $\mathbf{k} \cdot \mathbf{p}$ Calculations - Nanowire Superlattice

10.1 Introduction

In this chapter we apply the finite difference method in cylindrical polar coordinates to solve the Schrödinger equation for a nanowire superlattice. Our work [36] is motivated by two recent sets of papers. In the first one, most of which were published in *Comp. Phys. Comm.*, various authors have applied the FDM in cylindrical polar coordinates (CPC) to study quantum dots using the one-band effective mass equation [75, 76, 77], but details of the FDM were not given. In particular, complications of the formulation near the cylinder axis were not mentioned. In the second one, there has been a flurry of experimental activity on the growth of free-standing semiconductor nanowire superlattices (NWSL's) [37, 38, 78, 79, 80]. These NWSL are characterized by a cylindrical cross-section, a periodicity along the cylinder axis, and an effectively infinite potential barrier for the electrons outside the wire. Extremely polarized photoluminescence is one characteristic that makes NWSL likely candidates for practical applications. In addition, a recent one-dimensional theory predicted the remarkable existence of an inversion regime when the localization of the electron states can be reversed [39].

Our central goal is to demonstrate the applicability of the FDM in CPC for the novel study of NWSL's. FDM in CPC is needed since using the admitted more flexible Cartesian system will

lead to a three-dimensional problem rather than two-dimensional for a cylindrical cross-section. Also, we show how to solve a periodic problem and formulate the FDM in the presence of Bloch periodicity; this leads to a nonsymmetric, complex matrix eigenvalue problem. In the process, we report the correct formalism for treating the boundary condition near the cylinder axis. One application is to answer the question of how many periods are required before the finite-length structure is a good approximation to the infinitely periodic structure (superlattice). We also compare the FDM to an implementation of the finite element method (FEM) using FEMLAB as a further check on the correctness of the implementation. Finally, the technique is used to confirm the existence of an inversion regime and to obtain the energy spectrum of an embedded system for which there are no analytical solutions.

10.2 Theory

The theory of the electron state used here is the one-band envelope function theory [68, 50]. In our calculations, the effective mass of the electron is position dependent, but does not depend on energy. Non-parabolicity is not important for the systems studied, GaAs/AlGaAs nanostructures, due to the large band gap present but it can be introduced as proposed by Li *et al.* [75, 76, 77]. Similarly, strain can be introduced by renormalizing the effective mass and potential energy. However, we ignore both effects here in order to focus on our novel computational implementation. The task is to solve the one-electron BenDaniel-Duke equation [50],

$$\frac{-\hbar^2}{2}\nabla\cdot\left[\frac{1}{m(\mathbf{r})}\nabla\psi_n(\mathbf{r})\right]+V(\mathbf{r})\psi_n(\mathbf{r})=E_n\psi_n(\mathbf{r}), \tag{10.1}$$

when the effective mass $m(\mathbf{r})$ and the potential $V(\mathbf{r})$ have cylindrical symmetry. The NWSL is modeled as a cylinder of infinite length, with alternating layers of GaAs (the well) and AlGaAs (the barrier) (see Fig. 10.1). The NWSL's currently being grown are free standing. An accurate modeling of such a structure is achieved by using an infinite potential barrier outside, where the wavefunction is therefore zero. In this paper, we use the term wavefunction in a loose sense to refer to the envelope function [50].

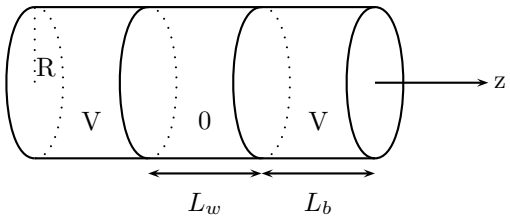

Figure 10.1: A model nanowire superlattice. The parameters are: radius R, well width L_w, barrier width L_b, effective mass in the well m_w, effective mass in the barrier m_b, and the band offset V.

10.3 Computational Models

Three methods are used: the finite difference method (FDM) applied to a unit cell (well + barrier) with periodic boundary conditions (PBC) (see Fig. 10.2a), the FDM applied to a finite number of unit cells (see Fig. 10.2b), and the exact solution of the equivalent Kronig-Penney model. The FDM was implemented using a non-uniform grid and is two-dimensional (in the radial and z directions). When studying a finite sequence of wells and barriers, with infinite potential barriers at the ends, three patterns are possible: the ends are both wells, at one end there is a well and at the other there is a barrier, and the ends are both barriers. In the first and third case, the structure is symmetric with respect to a center plane, and the wavefunctions are symmetric or antisymmetric. In the second case, the structure is asymmetric with respect to a center plane. In the first (or second) case, the infinite potential adjacent to the wells will produce extra quantum confinement, increasing the energy of two (or one) states localized at the well–vacuum interface. The remaining eigenvalues will converge to the infinite superlattice values. The finite structures studied in this article have either two barriers at the ends, or one barrier and one well.

The FDM described in this paper can be applied to other problems, e.g., cylindrical QDs, conical QDs, and spherical QDs. The method is also suitable for analyzing electronic states in a semiconductor nanostructure embedded in a semiconductor substrate, a region of finite potential, where the wavefunction has an exponential decay. This is the situation when our FDM method is most useful, since analytical methods based on separation of variables in the

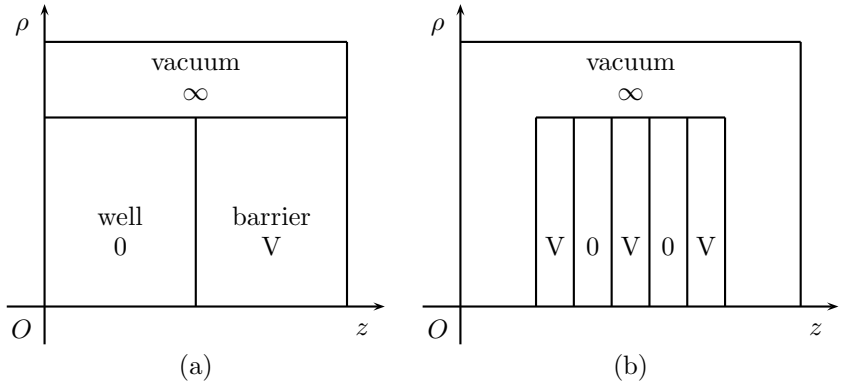

Figure 10.2: The domain for (a) a unit cell with periodic boundary conditions and (b) a finite number of unit cells, with barrier layers at both ends.

BenDaniel-Duke equation do not apply.

For a planar superlattice of finite length, Kolbas and Holonyak have developed a transfer matrix method (TMM) [81]. The TMM can also be applied for a cylindrical superlattice of finite length, provided it is surrounded by vacuum. In the TMM method, the first and last barrier regions are extended to infinity, which gives a slightly different structure from the one studied here. We also note that they used an incorrect boundary condition, though this is not expected to impact the numerical convergence.

10.4 FDM applied to a unit cell with PBC

This method has the advantage of a smaller grid and, therefore, significantly reduced memory and computing time requirements. The disadvantage is the presence of complex numbers in the Hamiltonian matrix, due to the use of Bloch's theorem.

We write the gradient and the divergence operators in cylindrical coordinates. The BenDaniel-Duke equation, Eq. (10.1), becomes

$$\begin{aligned}&\frac{-\hbar^2}{2}\left[\frac{1}{\rho}\frac{1}{m}\frac{\partial\psi}{\partial\rho}+\frac{\partial}{\partial\rho}\left(\frac{1}{m}\frac{\partial\psi}{\partial\rho}\right)+\frac{1}{\rho}\frac{\partial}{\partial\phi}\left(\frac{1}{m}\frac{1}{\rho}\frac{\partial\psi}{\partial\phi}\right)+\frac{\partial}{\partial z}\left(\frac{1}{m}\frac{\partial\psi}{\partial z}\right)\right] \\ &+V\psi=E\psi.\end{aligned} \tag{10.2}$$

Due to the cylindrical symmetry, $V = V(\rho, z)$, $m = m(\rho, z)$, and $\psi = F(\rho, z)e^{iL\phi}$. The

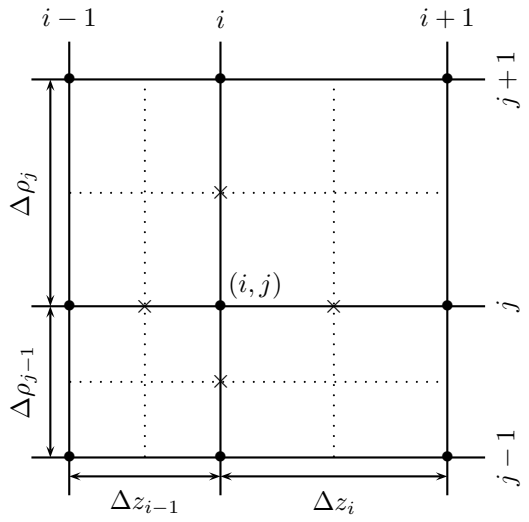

Figure 10.3: Indexing of points on the non-uniform grid. • at grid points. × at midway points.

BenDaniel-Duke equation becomes

$$\frac{-\hbar^2}{2}\left[\frac{1}{\rho}\frac{1}{m}\frac{\partial F}{\partial \rho}+\frac{\partial}{\partial \rho}\left(\frac{1}{m}\frac{\partial F}{\partial \rho}\right)+\frac{-L^2}{m\rho^2}F+\frac{\partial}{\partial z}\left(\frac{1}{m}\frac{\partial F}{\partial z}\right)\right]+VF=EF. \tag{10.3}$$

Away from the z axis, the equation is discretized the usual way. Let i label grid points along the z direction, and let j label grid points along the radial direction (see Fig. 10.3). With the notation $F_{i,j}\equiv F(z_i,\rho_j)$, etc., the derivatives are calculated with a central difference scheme on the non-uniform grid as

$$\frac{\partial F_{i,j}}{\partial z}=F_{i-1,j}A_i+F_{i,j}B_i+F_{i+1,j}C_i, \tag{10.4}$$

where

$$\begin{aligned} A_i &\equiv \frac{-\Delta z_i}{\Delta z_{i-1}(\Delta z_{i-1}+\Delta z_i)},\\ B_i &\equiv \frac{\Delta z_i-\Delta z_{i-1}}{\Delta z_{i-1}\Delta z_i},\\ C_i &\equiv \frac{\Delta z_{i-1}}{\Delta z_i(\Delta z_{i-1}+\Delta z_i)}, \end{aligned} \tag{10.5}$$

and as

$$\frac{\partial F_{i,j}}{\partial \rho}=F_{i,j-1}D_j+F_{i,j}E_j+F_{i,j+1}G_j, \tag{10.6}$$

where

$$\begin{aligned} D_j &\equiv \frac{-\Delta\rho_j}{\Delta\rho_{j-1}(\Delta\rho_{j-1}+\Delta\rho_j)}, \\ E_j &\equiv \frac{\Delta\rho_j-\Delta\rho_{j-1}}{\Delta\rho_{j-1}\Delta\rho_j}, \\ G_j &\equiv \frac{\Delta\rho_{j-1}}{\Delta\rho_j(\Delta\rho_{j-1}+\Delta\rho_j)}. \end{aligned} \tag{10.7}$$

To avoid problems due to the discontinuous jumps of the effective mass, we expand the derivatives using midway points [2]. In this way the differential operator is applied only to the continuous functions F, $\frac{1}{m}\frac{\partial F}{\partial\rho}$, and $\frac{1}{m}\frac{\partial F}{\partial z}$. The discretized terms are

$$\begin{aligned} &\frac{\partial}{\partial z}\left(\frac{1}{m_{i,j}}\frac{\partial F_{i,j}}{\partial z}\right) \\ &= \frac{1}{m_{i-1/2,j}}\frac{\partial F_{i-1/2,j}}{\partial z}2A_i + \frac{1}{m_{i,j}}\frac{\partial F_{i,j}}{\partial z}2B_i + \frac{1}{m_{i+1/2,j}}\frac{\partial F_{i+1/2,j}}{\partial z}2C_i \\ &= \frac{1}{m_{i-1/2,j}}\frac{F_{i,j}-F_{i-1,j}}{\Delta z_{i-1}}2A_i + \frac{1}{m_{i,j}}\frac{F_{i+1,j}-F_{i-1,j}}{\Delta z_{i-1}+\Delta z_i}2B_i \\ &+\frac{1}{m_{i+1/2,j}}\frac{F_{i+1,j}-F_{i,j}}{\Delta z_i}2C_i, \end{aligned} \tag{10.8}$$

and

$$\begin{aligned} &\frac{\partial}{\partial\rho}\left(\frac{1}{m_{i,j}}\frac{\partial F_{i,j}}{\partial\rho}\right) \\ &= \frac{1}{m_{i,j-1/2}}\frac{\partial F_{i,j-1/2}}{\partial\rho}2D_j + \frac{1}{m_{i,j}}\frac{\partial F_{i,j}}{\partial\rho}2E_j + \frac{1}{m_{i,j+1/2}}\frac{\partial F_{i,j+1/2}}{\partial\rho}2G_j \\ &= \frac{1}{m_{i,j-1/2}}\frac{F_{i,j}-F_{i,j-1}}{\Delta\rho_{j-1}}2D_j + \frac{1}{m_{i,j}}\frac{F_{i,j+1}-F_{i,j-1}}{\Delta\rho_{j-1}+\Delta\rho_j}2E_j \\ &+\frac{1}{m_{i,j+1/2}}\frac{F_{i,j+1}-F_{i,j}}{\Delta\rho_j}2G_j. \end{aligned} \tag{10.9}$$

The discretized BenDaniel-Duke equation is obtained as

$$\begin{aligned} &F_{i-1,j}\frac{\hbar^2}{2}\left(\frac{2A_i}{m_{i-1/2,j}\Delta z_{i-1}}+\frac{2B_i}{m_{i,j}(\Delta z_{i-1}+\Delta z_i)}\right) \\ &+F_{i+1,j}\frac{\hbar^2}{2}\left(-\frac{2B_i}{m_{i,j}(\Delta z_{i-1}+\Delta z_i)}-\frac{2C_i}{m_{i+1/2,j}\Delta z_i}\right) \\ &+F_{i,j-1}\frac{\hbar^2}{2}\left(-\frac{D_j}{\rho_j m_{i,j}}+\frac{2D_j}{m_{i,j-1/2}\Delta\rho_{j-1}}+\frac{2E_j}{m_{i,j}(\Delta\rho_{j-1}+\Delta\rho_j)}\right) \end{aligned}$$

$$
\begin{aligned}
&+F_{i,j+1}\frac{\hbar^2}{2}\left(-\frac{G_j}{\rho_j m_{i,j}}-\frac{2E_j}{m_{i,j}(\Delta\rho_{j-1}+\Delta\rho_j)}-\frac{2G_j}{m_{i,j+1/2}\Delta\rho_j}\right) \\
&+F_{i,j}\frac{\hbar^2}{2}\left(-\frac{E_j}{\rho_j m_{i,j}}-\frac{2A_i}{m_{i-1/2,j}\Delta z_{i-1}}+\frac{2C_i}{m_{i+1/2,j}\Delta z_i}\right. \\
&\left.-\frac{2D_j}{m_{i,j-1/2}\Delta\rho_{j-1}}+\frac{2G_j}{m_{i,j+1/2}\Delta\rho_j}+\frac{L^2}{m_{i,j}\rho_j^2}\right) \\
&+V_{i,j}F_{i,j}=EF_{i,j}.
\end{aligned}
\tag{10.10}
$$

Equation (10.10) applies for points in the bulk of the structure. At midway points on the interfaces, the mass is calculated as an arithmetic average of the masses on the neighboring grid points. The points on the boundary of the domain require a special treatment, since Eq. (10.10) does not apply for points with $\rho_j = 0$, as ρ_j appears in the denominator. A different approach is needed to determine the function $F(\rho = 0, z)$. Equation (10.3) is multiplied by ρ^2, then the terms are evaluated in the limit $\rho \to 0$. We are left with $L^2F(\rho = 0, z) = 0$. Therefore, if $L \neq 0$ then $F(\rho = 0, z) = 0$. For the case $L = 0$, Eq. (10.3) is multiplied by ρ, then the terms are evaluated in the limit $\rho \to 0$. We are left with $\frac{\partial F}{\partial \rho}|_{\rho=0} = 0$. The derivative calculated with a forward difference scheme on the non-uniform grid is

$$
\begin{aligned}
&\frac{\partial F_{i,j-1}}{\partial\rho}=F_{i,j-1}\frac{-(2\Delta\rho_{j-1}+\Delta\rho_j)}{\Delta\rho_{j-1}(\Delta\rho_{j-1}+\Delta\rho_j)} \\
&+F_{i,j}\frac{\Delta\rho_{j-1}+\Delta\rho_j}{\Delta\rho_{j-1}\Delta\rho_j}+F_{i,j+1}\frac{-\Delta\rho_{j-1}}{\Delta\rho_j(\Delta\rho_{j-1}+\Delta\rho_j)}=0.
\end{aligned}
\tag{10.11}
$$

In summary, for points with $\rho_{j-1} = 0$, if $L \neq 0$ the discretized equation is obtained from Eq. (10.10) with $F_{i,j-1} = 0$. If $L = 0$ the discretized equation is obtained from Eq. (10.10) with

$$
F_{i,j-1}=F_{i,j}\frac{(\Delta\rho_{j-1}+\Delta\rho_j)^2}{\Delta\rho_j(2\Delta\rho_{j-1}+\Delta\rho_j)}-F_{i,j+1}\frac{(\Delta\rho_{j-1})^2}{\Delta\rho_j(2\Delta\rho_{j-1}+\Delta\rho_j)}. \tag{10.12}
$$

The above treatment of Schrödinger's equation in CPC does not appear to have been previously reported. For completeness, we note, however, that the Navier-Stokes equation in cylindrical coordinates is not as easy, and one needs to use a staggered grid in order to deal with the $\rho = 0$ axis [82].

For points with $\rho_j = \rho_{\max}$ (see Fig. 10.2), we apply Neumann boundary conditions: $\frac{\partial F}{\partial \rho} = 0$. The discretized equation is obtained from Eq. (10.10) with $M_{i,j+1/2} = M_{i,j-1/2}$ and with $F_{i,j+1} = F_{i,j-1}$.

Since for bound states both the wave function and its derivative vanish at the radial edge of the computational domain, Dirichlet and Neumann boundary conditions are equivalent. It is more useful to use Neumann conditions since in this way we can check the value of the wave function on the boundary [66]. Spurious states, with energy just below the barrier but which do not vanish on the boundary, are in this way identified and discarded.

Assume that inside the domain the index i takes values from 1 to N_z. For points with $z_i = z_1$, in order to substitute for z_0 in Eq. (10.10), we use Bloch's theorem:

$$F(\rho, z_0) = e^{-iKZ} F(\rho, z_{N_z}), \tag{10.13}$$

where K is the wave number associated with the periodicity in the z direction, and the period is Z. Therefore we replace $M_{i-1,j}$ with $M_{i-1+N_z,j}$ and $F_{i-1,j}$ with $F_{i-1+N_z,j}e^{-iKZ}$. For points with $z_i = z_{N_z}$, in order to substitute for z_{N_z+1} in Eq. (10.10), we use Bloch's theorem again:

$$F(\rho, z_{N_z+1}) = e^{iKZ} F(\rho, z_1). \tag{10.14}$$

Therefore we replace $M_{i+1,j}$ with $M_{i+1-N_z,j}$ and $F_{i+1,j}$ with $F_{i+1-N_z,j}e^{iKZ}$.

10.5 FDM applied to a finite number of unit cells

This method applies well to semiconductor nanostructures of finite length, e.g. quantum dots. It has the advantage that only real numbers appear in the Hamiltonian matrix. However, for large structures, memory requirements can be a problem. The periodic structure of the NWSL is generated by a finite sequence of unit cells (well + barrier). The discretized equation and boundary conditions are as discussed previously, with the exception of the points with $z = 0$ or $z = z_{\max}$. These points are in the vacuum layer; in order to be able to use the same program for structures embedded in a semiconductor substrate (i.e., finite barrier), we do not use Dirichlet boundary conditions. Bound states are then easily authenticated, by inspection of the magnitude of the wavefunction on the boundary [66].

For points with $z = 0$ (see Fig. 10.2) we apply Neumann boundary conditions: $\frac{\partial F}{\partial z} = 0$. The discretized equation is obtained from Eq. (10.10) with $M_{i-1/2,j} = M_{i+1/2,j}$ and with $F_{i-1,j} = F_{i+1,j}$. For points with $z = z_{\max}$ we apply Neumann boundary conditions: $\frac{\partial F}{\partial z} = 0$.

The discretized equation is obtained from Eq. (10.10) with $M_{i+1/2,j} = M_{i-1/2,j}$ and with $F_{i+1,j} = F_{i-1,j}$.

10.6 Equivalent Kronig-Penney model

In order to validate our computational models, we now obtain the exact solutions, only possible when the outside layer is vacuum. We solve Eq. (10.3) by separation of variables, with $F(\rho, z) = J(\rho)Z(z)$. We also use the fact that, for the NWSL under investigation, $m = m(z)$ and V = V(z). Solution of the decoupled radial equation gives $J(\rho) = J_L(\rho q)$, where q is the separation constant and J_L is the cylindrical Bessel function of order L. The separation constant q is determined by the condition that Rq be a zero of the Bessel function. The decoupled equation for z is [39]

$$\frac{-\hbar^2}{2}\frac{\partial}{\partial z}\left(\frac{1}{m}\frac{\partial Z}{\partial z}\right) + \left(V + \frac{\hbar^2 q^2}{2m}\right) Z = EZ. \tag{10.15}$$

This equation describes a Kronig-Penney model with a potential $V_{eq:KP} = V + \hbar^2 q^2/2m$. We increase the origin of the energy by $\hbar^2 q^2/2m_w$, such that the potential in the well is zero and in the barrier is $V' = V + \hbar^2 q^2/2m_b - \hbar^2 q^2/2m_w$. Equation (10.15) is solved by writing the wavefunctions in the well and in the barrier, and then imposing the matching boundary conditions for the functions and their derivatives [83]. When writing the boundary conditions, we use Bloch's theorem and introduce the quantum number K. We are left with a system of four linear homogeneous equations. A zero determinant is obtained only when

$$\begin{aligned}&\cos[K(L_w + L_b)] = \cos(k_w L_w) cos(k_b L_b) \\ &+\frac{k_b^2 m_w/m_b - k_w^2 m_b/m_w}{2k_w k_b} sin(k_w L_w) cos(k_b L_b),\end{aligned} \tag{10.16}$$

where $k_w \equiv \sqrt{2m_w E'}/\hbar$ and $k_b \equiv \sqrt{2m_b(V' - E')}/\hbar$. The energy of the NWSL is given by $E = E' + \hbar^2 q^2/2m_w$. The transcendental equation [Eq. (10.16)] is solved numerically. In summary, four indices label the energy eigenvalues: the angular momentum number L, an index N to label the roots $q_{L,N}$ of the Bessel function, the quantum number K due to the translational periodicity in the z direction, and an index M to label the roots of the transcendental equation [Eq. (10.16)].

Figure 10.4: Detailed structure of the non-uniform grid at the well-barrier interface. Grid steps of 1, 0.5, 0.25, 0.125, 0.0625, 0.03125, and 0.025 Å are used.

10.7 Results and Discussions

A representative set of parameters used for the calculations were as follows: radius $R = 100$ Å, well (L_W) and barrier (L_B) widths of 50 Å, well (m_W) and barrier (m_B) effective masses of $0.067m_0$ and $0.0919m_0$, and a barrier height of 0.23 eV. These parameters correspond to a $GaAs/Al_{0.3}Ga_{0.7}As$ structure [69]. In the radial direction the infinite barrier extended for 10 Å. When modeling a finite lattice, two 10 Å wide regions of infinite potential were used to pack the structure in the z direction. In practice the infinite potential is approximated by 10^6 eV, and a region of finite dimension is needed to allow the exponentially decaying wave function to vanish. Free standing NWSL have been grown [37], and the complete localization of electrons inside these NWSL justifies our approximation of infinite surrounding potential.

We used a non-uniform grid with a grid step varying from 1 Å to 0.025 Å (see Fig. 10.4). The non-uniform grid is used at the interfaces, and also near the z axis. No grid point lies on the well-barrier interface, where the effective mass is discontinuous. The total number of grid points is $140 \times (40 + 70N)$ for the non-uniform grid, and $110 \times (20 + 50N)$ for the uniform grid, where N is the number of semiconductor layers. A simple uniform grid (of 1 Å) could not reproduce the discontinuous jump of the derivative of the wavefunction at the well-barrier interface. This discontinuity, due to the abrupt change in the effective mass, has dramatic effects; in particular, it validates the Heisenberg uncertainty principle [84].

A calculation using the finite element method (FEM) has also been performed, using FEMLAB. The FEM is a variational reformulation of the problem, so we do not need to treat the interfaces in any special way. The FEM solves partial differential equations (PDE) in weak form by integrating the PDEs. Thus slope discontinuities are captured, as calculations reveal, and

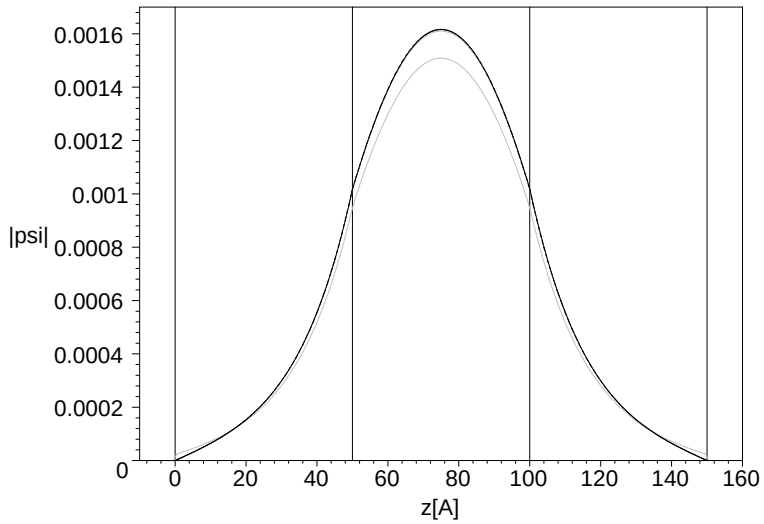

Figure 10.5: Ground state for the NWSL calculated with the FEM (dotted black curve), the FDM with uniform grid (solid gray curve), the FDM with non-uniform grid (dotted gray curve), and the equivalent Kronig-Penney model (solid black curve).

one can get the correct result even with a fairly sparse grid. In Figure 10.5 we have plotted a cross section, at $\rho = 0.5\,\dot{\mathrm{A}}$, of the ground-state wavefunction of the simplest barrier-well-barrier structure. The FEM calculation overlaps perfectly over the exact solution, the FDM calculation with non-uniform grid is also very accurate, while the FDM calculation with uniform grid but with about the same number of total grid points is not very good, due to the poor grid around the interfaces. As a practical calculational detail, the wavefunctions have been normalized to unit cell: $\int_\Omega |\psi|^2 \rho d\rho d\theta dz = 1$. In contrast, the eigenvector resulted from the numerical procedure is normalized as $\sum_{i,j} |\psi_{i,j}|^2 = 1$.

The eigenvalue problem for the large sparse matrix was solved using ARPACK [74]. The LU decomposition, external to the ARPACK library, has been performed with UMFPACK. On a computer with 2 GB RAM running at 2 GHz, the computation took from a few seconds to a few minutes. Results for the electron energies obtained using the above methods are given in Figs. 10.5–10.9. The FDM provided the energy eigenvalues with an error $< 0.5\%$. In Figs. 10.6 and 10.7 we study finite NWSL structures, with barrier layers at both ends and, respectively, with one barrier and one well layer at the ends. We find that the finite-length NWSL structure

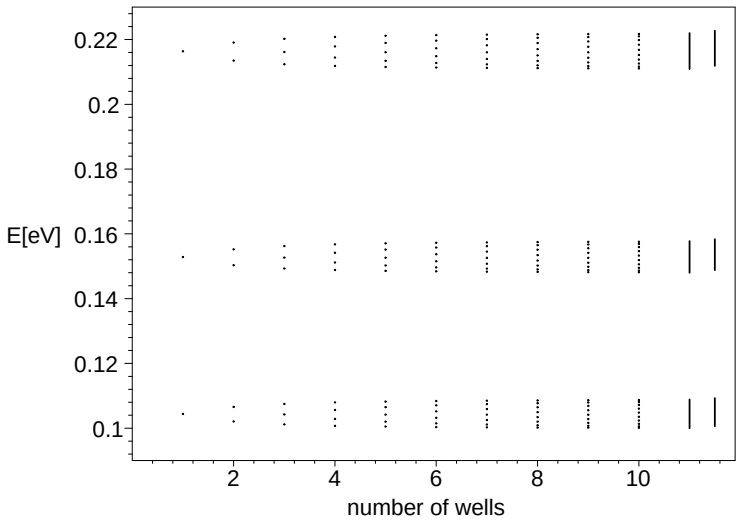

Figure 10.6: Miniband formation in a symmetric NWSL structure. Energy levels as a function of the number of wells. The segments on the right side are the energy bands for the infinite NWSL, calculated with the FDM with non-uniform grid (left segments) and with the equivalent Kronig-Penney model (right segments). $L = 0$, $L = 1$, and $L = 2$, in increasing order of the energy.

with barrier layers at both ends approaches the superlattice energy bands when the number of unit cells is of the order of 6. Note, however, that the infinite NWSL (with PBC) reproduces the exact solution (given on the right-hand side) a lot faster.

The miniband formation in Fig. 10.6 can be understood from a perturbative point of view. Indeed, consider the case of barriers of length much larger than the wells. In this situation the wells are practically decoupled, and in each one we have the eigenstates of the single well. As the length of the barriers is decreased, the states interact more strongly with each other, and their energies shift, forming the miniband. It is clear that the number of states in one miniband is equal to the number of wells in the superlattice structure. Each energy level of the single well will correspond to a miniband in the infinite superlattice structure. The miniband formation in Fig. 10.7 can be understood in the same way. Here, however, the state localized at the well-vacuum interface is higher in energy, due to the increased quantum confinement, and does not mix with the other states in the miniband. A similar state sandwiched between

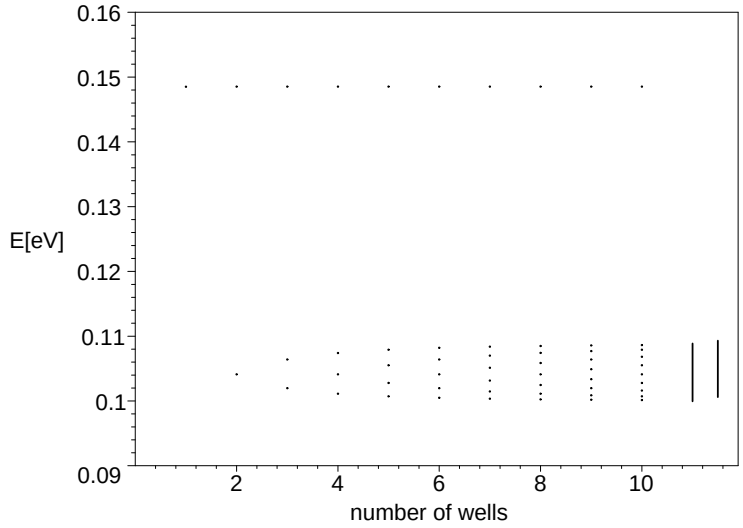

Figure 10.7: Miniband formation in an asymmetric NWSL structure. Energy levels as a function of the number of wells. The segments on the right side are the energy bands for the infinite NWSL, calculated with the FDM with non-uniform grid (left segment) and with the equivalent Kronig-Penney model (right segment). $L = 0$.

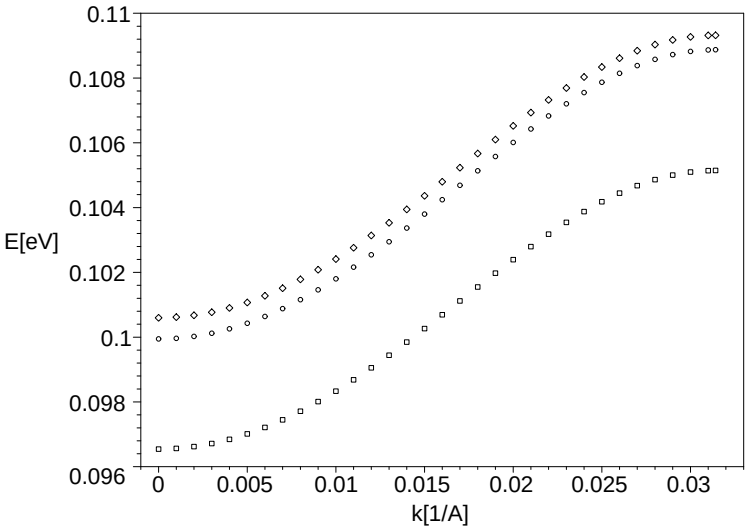

Figure 10.8: An energy band in the full Brillouin zone, calculated using the FDM with uniform grid (squares), the FDM with non-uniform grid (circles), and the equivalent Kronig-Penney model (diamonds). The quantum numbers are $L = 0$, $N = 1$, $M = 1$.

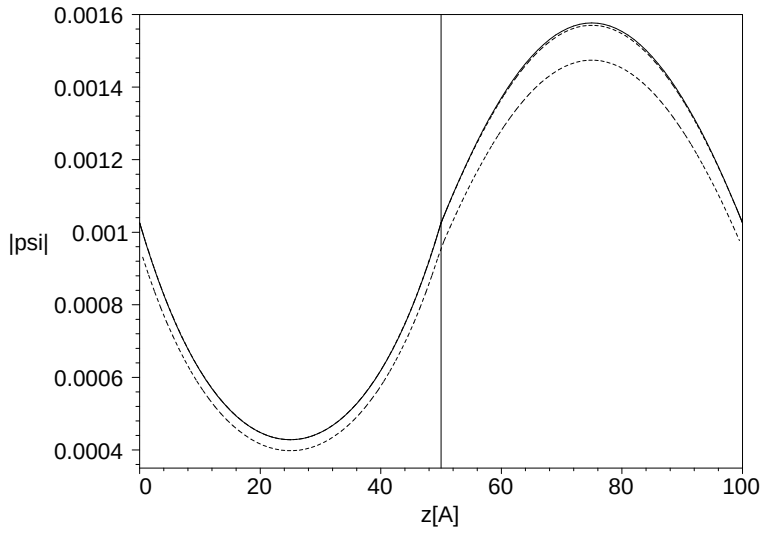

Figure 10.9: Ground state for the NWSL calculated with the FDM with uniform grid (lower dotted curve), the FDM with non-uniform grid (upper dotted curve), and the equivalent Kronig-Penney model (solid curve).

AlGaAs and vacuum does not exist in the symmetrical structure (Fig. 10.2b).

The lowest set of points on the left-hand side of Fig. 10.6, lying between 0.10 eV and 0.11 eV, corresponds to the solutions with quantum numbers $L = 0$, $N = 1$, $M = 1$. In fact, they are the discretized version of the miniband present in the superlattice calculation, shown in Fig. 10.8. The clustering of the levels towards the top and bottom of a miniband can be readily explained in terms of the density of states of the miniband. As shown in Fig. 10.8, at the top and bottom of a miniband the derivative $\partial E/\partial K$ is at a minimum, and therefore the number of states N in an energy interval $\partial N/\partial E = (\partial N/\partial K)/(\partial E/\partial K)$ is at a maximum.

In Fig. 10.9, we show a cross section, at $\rho = 0.5$ Å, of the NWSL ground-state wavefunction. The wavefunction $|\psi|$ plotted clearly shows the discontinuity of its derivative, due to the change in the effective mass at the well-barrier interface. The success of the FDM calculation with non-uniform grid is now clear from the excellent agreement of both the eigenvalue and the eigenfunction. The deficiencies of the FDM calculation with uniform grid (of 1 Å) are also apparent. The uniform grid has failed to provide an accurate solution even in the simpler one dimensional calculation of Tan *et al.* [66].

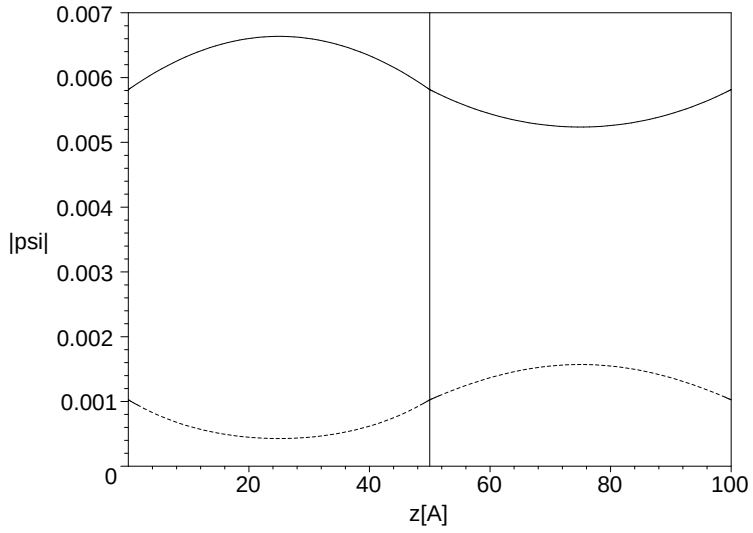

Figure 10.10: Ground state for the NWSL calculated with the FDM with non-uniform grid for a radius of 18 Å (solid curve) compared to a radius of 100 Å (dashed curve). The left layer is AlGaAs, the right layer is GaAs.

10.7.1 Physical Applications: Inversion

In Ref. [39], the authors predicted the existence of a critical radius for NWSL's, below which the role of well and barrier layers are reversed. This result followed directly from the exact one-dimensional Kronig-Penney equation of motion. However, the latter approach does not allow for an *ab initio* verification from the localization of the wave function. The latter would require a full two-dimensional solution without assuming the existence of the critical radius. We have carried this out using our FDM algorithm. Thus, the eigenvalue problem was solved for a small radius. From the Kronig-Penney model, the critical radius is expected to be around 20 Å. We, therefore, did a calculation for a radius of 18 Å, though we expect some correction of the quantitative data to be necessary at this small radius due to the approximations of the physical model of a parabolic band [75, 76, 77].

The resulting ground state wavefunction is given in Fig. 10.10 (a cross-section at $\rho = 0.5$ Å). The localization of the wavefunction in the $Al_{0.3}Ga_{0.7}As$ layer (to the left) is clear (solid curve). This is compared to the localization of the wavefunction in the GaAs layer for the much

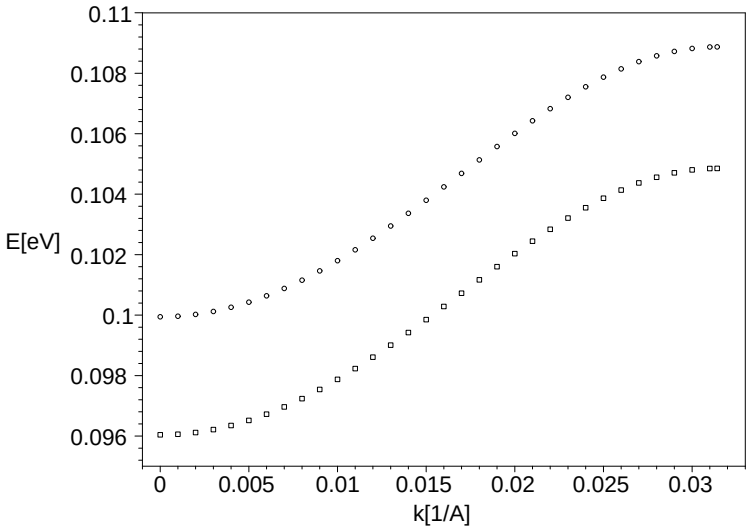

Figure 10.11: Lowest energy band in the first Brillouin zone for a finite outside barrier $V = 1.878$ eV (squares, lower curve) compared to an infinite barrier one (circles, upper curve). The structure is the same in both cases (radius of 100 Å).

larger radius (dashed curve). Thus, the numerical method is able to reproduce the correct wave function localization, a much more sensitive test than just getting the right energies. The difference in the vertical scale of the two functions is due to the much larger localization of the electron along the wire axis for the small radius. This is also a result not obtained within the one-dimensional exact model.

10.7.2 Physical Applications: Embedded nanowire

As a final example of a possible application of the new technique, we now consider a nanowire embedded in another semiconductor material. We can simulate this with AlAs outside the wire. Note that embedded NWSL have not yet been grown. However, embedded quantum wires had been actively grown in the past [85]. This problem is of interest because, for this physical system, there are no analytical solutions. Hence, the use of a numerical technique such as the FDM is necessary.

In the current calculation, we set the outside barrier height to be 1.878 eV and the effective

mass to be 0.1 m_o (pure AlAs). The grid in the z direction is the same as before for the infinite barrier problem. In the radial direction, we now have a dimension of 100 Å for the NWSL (i.e. same radius of 100 Å as before), and a width of 310 Å for the AlAs layer. The grid in the radial direction is 10 Å at 1 Å grid step, 100 Å at 2 Å, and 200 Å at 4 Å. Note that it is not necessary to have too many points in the outside barrier since the wavefunction decays exponentially there. In Fig. 10.11, we give the resulting energy band (lower curve) compared to the infinite barrier result obtained earlier (upper curve). As expected, it is lower than with an infinite barrier outside due to the reduced quantum confinement. For this particular structure, the band is more or less uniformly lower by about 4 %. We are, therefore, in a position to calculate the energies and wavefunctions of any NWSL, free standing or embedded, within the one-band model.

10.8 Conclusions

The theory of the finite difference method in cylindrical polar coordinates and with periodic boundary conditions (together with a non-uniform grid and a position-dependent mass) is given in detail. In particular, the implementation of the boundary condition on the cylinder axis is clarified. Applications to finite-length and infinite-length structures show that, for a finite NWSL with barrier layers at both ends, only about six unit cells are necessary in approximating the energy bands of a periodic system. However, the use of the Bloch theorem speeds up the solution of the latter problem and reduces the memory requirements. Verification of our two-dimensional computational model was achieved by comparing with one-dimensional exact results. We then used the model to obtain a numerical proof of the possible existence of inverted states without any *a priori* assumptions. New results were also obtained for the case of an embedded nanowire for which there are no exact solutions.

Chapter 11

Eight-Band $\mathbf{k} \cdot \mathbf{p}$ Calculations - ZB Quantum Well

11.1 Introduction

The simplest heterostructure to which we can apply the 8-band Hamiltonian is the quantum well (QW). The calculation of intervalence subband optical transitions in quantum wells goes back to a paper by Chang and James (CJ) in 1989 [40]. It established that these transitions can have both TE and TM polarizations. The calculations were done using the four-band Luttinger-Kohn (LK) Hamiltonian with infinite-barrier quantum-well states. Szmulowicz [29] generalized the CJ equation to allow for position-dependent $k \cdot p$ parameters.

In this chapter we present an envelope-function-representation derivation and calculations of the band structure and the momentum matrix elements between valence subbands in [001] quantum wells using the Luttinger-Kohn-Kane and the Burt-Foreman Hamiltonians. We show how to apply the finite difference method to solve the multi-band $\mathbf{k} \cdot \mathbf{p}$ equation for GaAs/$Al_{0.3}Ga_{0.7}$As and GaAs/AlAs quantum wells. Then we use the eigenfunctions to calculate momentum matrix elements, as described in Chapter 5. Both the Burt-Foreman and the Luttinger-Kohn Hamiltonians are used, and differences between the two methods are pointed out.

11.2 The Hamiltonian

The Hamiltonian H of the Burt theory, with no spin-orbit interaction, is shown in Table 11.2.

The momentum matrix element P, although supposed constant in Burt's derivation, in general depends on the semiconductor. Foreman [12], following an analysis of the spurious states, concluded that the right ordering of terms with $P(z)$ is the one shown in Table 11.2.

E_{CB} $+\frac{\hbar^2(\hat{k_x}^2+\hat{k_y}^2+\hat{k_z}^2)}{2m_o}$ $+\hat{k_x}A'\hat{k_x}$ $+\hat{k_y}A'\hat{k_y}$ $+\hat{k_z}A'\hat{k_z}$	$\frac{i\hbar P}{m_o}\hat{k_x}$ $+\hat{k_y}\frac{B}{2}\hat{k_z}$ $+\hat{k_z}\frac{B}{2}\hat{k_y}$	$\frac{i\hbar P}{m_o}\hat{k_y}$ $+\hat{k_z}\frac{B}{2}\hat{k_x}$ $+\hat{k_x}\frac{B}{2}\hat{k_z}$	$\frac{i\hbar P}{m_o}\hat{k_z}$ $+\hat{k_x}\frac{B}{2}\hat{k_y}$ $+\hat{k_y}\frac{B}{2}\hat{k_x}$
$-\frac{i\hbar P}{m_o}\hat{k_x}$ $+\hat{k_y}\frac{B}{2}\hat{k_z}$ $+\hat{k_z}\frac{B}{2}\hat{k_y}$	E_{VB} $+\frac{\hbar^2(\hat{k_x}^2+\hat{k_y}^2+\hat{k_z}^2)}{2m_o}$ $+\hat{k_x}(F'+2G)\hat{k_x}$ $+\hat{k_y}(H_1+H_2)\hat{k_y}$ $+\hat{k_z}(H_1+H_2)\hat{k_z}$	$\hat{k_x}(F'-G)\hat{k_y}$ $+\hat{k_y}(H_1-H_2)\hat{k_x}$	$\hat{k_x}(F'-G)\hat{k_z}$ $+\hat{k_z}(H_1-H_2)\hat{k_x}$
$-\frac{i\hbar P}{m_o}\hat{k_y}$ $+\hat{k_z}\frac{B}{2}\hat{k_x}$ $+\hat{k_x}\frac{B}{2}\hat{k_z}$	$\hat{k_y}(F'-G)\hat{k_x}$ $+\hat{k_x}(H_1-H_2)\hat{k_y}$	E_{VB} $+\frac{\hbar^2(\hat{k_x}^2+\hat{k_y}^2+\hat{k_z}^2)}{2m_o}$ $+\hat{k_y}(F'+2G)\hat{k_y}$ $+\hat{k_x}(H_1+H_2)\hat{k_x}$ $+\hat{k_z}(H_1+H_2)\hat{k_z}$	$\hat{k_y}(F'-G)\hat{k_z}$ $+\hat{k_z}(H_1-H_2)\hat{k_y}$
$-\frac{i\hbar P}{m_o}\hat{k_z}$ $+\hat{k_x}\frac{B}{2}\hat{k_y}$ $+\hat{k_y}\frac{B}{2}\hat{k_x}$	$\hat{k_z}(F'-G)\hat{k_x}$ $+\hat{k_x}(H_1-H_2)\hat{k_z}$	$\hat{k_z}(F'-G)\hat{k_y}$ $+\hat{k_y}(H_1-H_2)\hat{k_z}$	E_{VB} $+\frac{\hbar^2(\hat{k_x}^2+\hat{k_y}^2+\hat{k_z}^2)}{2m_o}$ $+\hat{k_z}(F'+2G)\hat{k_z}$ $+\hat{k_x}(H_1+H_2)\hat{k_x}$ $+\hat{k_y}(H_1+H_2)\hat{k_y}$

Table 11.2 Burt Hamiltonian, 4 bands and no spin.

When spin is included the total Hamiltonian H has the form

$$\begin{pmatrix} H_{1,1} & H_{1,2} & H_{1,3} & H_{1,4} & 0 & 0 & 0 & 0 \\ H_{2,1} & H_{2,2} & H_{2,3}-i\frac{\Delta}{3} & H_{2,4} & 0 & 0 & 0 & \frac{\Delta}{3} \\ H_{3,1} & H_{3,2}+i\frac{\Delta}{3} & H_{3,3} & H_{3,4} & 0 & 0 & 0 & -i\frac{\Delta}{3} \\ H_{4,1} & H_{4,2} & H_{4,3} & H_{4,4} & 0 & -\frac{\Delta}{3} & i\frac{\Delta}{3} & 0 \\ 0 & 0 & 0 & 0 & H_{1,1} & H_{1,2} & H_{1,3} & H_{1,4} \\ 0 & 0 & 0 & -\frac{\Delta}{3} & H_{2,1} & H_{2,2} & H_{2,3}+i\frac{\Delta}{3} & H_{2,4} \\ 0 & 0 & 0 & -i\frac{\Delta}{3} & H_{3,1} & H_{3,2}-i\frac{\Delta}{3} & H_{3,3} & H_{3,4} \\ 0 & \frac{\Delta}{3} & i\frac{\Delta}{3} & 0 & H_{4,1} & H_{4,2} & H_{4,3} & H_{4,4} \end{pmatrix}. \tag{11.1}$$

At each point z the eigenvalue problem is written as

$$(H)\begin{pmatrix} F_1(z) \\ F_2(z) \\ F_3(z) \\ F_4(z) \\ F_5(z) \\ F_6(z) \\ F_7(z) \\ F_8(z) \end{pmatrix} = E\begin{pmatrix} F_1(z) \\ F_2(z) \\ F_3(z) \\ F_4(z) \\ F_5(z) \\ F_6(z) \\ F_7(z) \\ F_8(z) \end{pmatrix}. \tag{11.2}$$

This will result in 8 equations for every grid point.

The simplest quantum well is grown in the [001] direction, that is the interface planes are orthogonal to the z axis. In two directions, x and y, the periodicity of the lattice is preserved. Therefore $\hat{k_x} \to k_x$ and $\hat{k_y} \to k_y$. The operator $\hat{k_z} \equiv -i\partial/\partial z$ will generate four kinds of terms: (a) terms with no derivative operators $H^{(a)}_{i,j}$, (b) terms with the derivative operator on the right $H^{(b)}_{i,j}$, (c) terms with the derivative operator on the left $H^{(c)}_{i,j}$, and (d) terms sandwiched between derivative operators $H^{(d)}_{i,j}$.

We now introduce the notation

$$H^{(a)}_{i,j} \equiv h^{(a)}_{i,j}, \tag{11.3}$$

$$H^{(b)}_{i,j} \equiv h^{(b)}_{i,j}\frac{\partial}{\partial z}, \tag{11.4}$$

$$H_{i,j}^{(c)} \equiv \frac{\partial}{\partial z} h_{i,j}^{(c)}, \tag{11.5}$$

$$H_{i,j}^{(d)} \equiv \frac{\partial}{\partial z} h_{i,j}^{(d)} \frac{\partial}{\partial z}. \tag{11.6}$$

The Hamiltonian elements of type (a) are

$$h_{1,1}^{(a)} = E_{CB} + \frac{\hbar^2(k_x^2+k_y^2)}{2m_o} + A'(k_x^2+k_y^2), \tag{11.7}$$

$$h_{1,2}^{(a)} = \frac{i\hbar P}{m_o} k_x, \tag{11.8}$$

$$h_{1,3}^{(a)} = \frac{i\hbar P}{m_o} k_y, \tag{11.9}$$

$$h_{1,4}^{(a)} = B k_x k_y, \tag{11.10}$$

$$h_{2,1}^{(a)} = -\frac{i\hbar P}{m_o} k_x, \tag{11.11}$$

$$h_{2,2}^{(a)} = E_{VB} + \frac{\hbar^2(k_x^2+k_y^2)}{2m_o} + (F'+2G)k_x^2 + (H_1+H_2)k_y^2, \tag{11.12}$$

$$h_{2,3}^{(a)} = (F'-G)k_x k_y + (H_1-H_2)k_x k_y, \tag{11.13}$$

$$h_{3,1}^{(a)} = -\frac{i\hbar P}{m_o} k_y, \tag{11.14}$$

$$h_{3,2}^{(a)} = (F'-G)k_x k_y + (H_1-H_2)k_x k_y, \tag{11.15}$$

$$h_{3,3}^{(a)} = E_{VB} + \frac{\hbar^2(k_x^2+k_y^2)}{2m_o} + (F'+2G)k_y^2 + (H_1+H_2)k_x^2, \tag{11.16}$$

$$h_{4,1}^{(a)} = B k_x k_y, \tag{11.17}$$

$$h_{4,4}^{(a)} = E_{VB} + \frac{\hbar^2(k_x^2+k_y^2)}{2m_o} + (H_1+H_2)k_x^2 + (H_1+H_2)k_y^2. \tag{11.18}$$

The Hamiltonian elements of type (b) are

$$h_{1,2}^{(b)} = -ik_y \frac{B}{2}, \tag{11.19}$$

$$h_{1,3}^{(b)} = -ik_x \frac{B}{2}, \tag{11.20}$$

$$h_{1,4}^{(b)} = \frac{\hbar P}{m_o}, \tag{11.21}$$

$$h_{2,1}^{(b)} = -ik_y \frac{B}{2}, \tag{11.22}$$

$$h_{2,4}^{(b)} = -ik_x(F'-G), \tag{11.23}$$

$$h_{3,1}^{(b)} = -ik_x \frac{B}{2}, \tag{11.24}$$

$$h_{3,4}^{(b)} = -ik_y(F'-G), \tag{11.25}$$

$$h_{4,1}^{(b)} = -\frac{\hbar P}{m_o}, \tag{11.26}$$

$$h_{4,2}^{(b)} = -ik_x(H_1 - H_2), \tag{11.27}$$

$$h_{4,3}^{(b)} = -ik_y(H_1 - H_2). \tag{11.28}$$

The Hamiltonian elements of type (c) are

$$h_{1,2}^{(c)} = -i\frac{B}{2}k_y, \tag{11.29}$$

$$h_{1,3}^{(c)} = -i\frac{B}{2}k_x, \tag{11.30}$$

$$h_{2,1}^{(c)} = -i\frac{B}{2}k_y, \tag{11.31}$$

$$h_{2,4}^{(c)} = -i(H_1 - H_2)k_x, \tag{11.32}$$

$$h_{3,1}^{(c)} = -i\frac{B}{2}k_x, \tag{11.33}$$

$$h_{3,4}^{(c)} = -i(H_1 - H_2)k_y, \tag{11.34}$$

$$h_{4,2}^{(c)} = -i(F' - G)k_x, \tag{11.35}$$

$$h_{4,3}^{(c)} = -i(F' - G)k_y. \tag{11.36}$$

The Hamiltonian elements of type (d) are

$$h_{1,1}^{(d)} = -(\frac{\hbar^2}{2m_o} + A'), \tag{11.37}$$

$$h_{2,2}^{(d)} = -(\frac{\hbar^2}{2m_o} + H_1 + H_2), \tag{11.38}$$

$$h_{3,3}^{(d)} = -(\frac{\hbar^2}{2m_o} + H_1 + H_2), \tag{11.39}$$

$$h_{4,4}^{(d)} = -(\frac{\hbar^2}{2m_o} + F' + 2G). \tag{11.40}$$

11.3 The Finite Difference Method

Let n label grid points along the z direction. With the notation $F_{j,n} \equiv F_j(z_n)$, $h_{i,j,n} \equiv h_{i,j}(z_n)$, the derivatives are calculated with a central difference scheme on the non-uniform grid as

$$\frac{\partial F_{j,n}}{\partial z} = F_{j,n-1}A_n + F_{j,n}B_n + F_{j,n+1}C_n, \tag{11.41}$$

where

$$A_n \equiv \frac{-\Delta z_n}{\Delta z_{n-1}(\Delta z_{n-1}+\Delta z_n)}, \tag{11.42}$$

$$B_n \equiv \frac{\Delta z_n - \Delta z_{n-1}}{\Delta z_{n-1}\Delta z_n}, \tag{11.43}$$

$$C_n \equiv \frac{\Delta z_{n-1}}{\Delta z_n(\Delta z_{n-1}+\Delta z_n)}, \tag{11.44}$$

and $\Delta z_n \equiv z_{n+1} - z_n$.

The terms sandwiched between derivatives are expanded as

$$\begin{aligned}
&\frac{\partial}{\partial z}\left(h^{(d)}_{i,j,n}\frac{\partial F_{j,n}}{\partial z}\right)\\
&= h^{(d)}_{i,j,n-1/2}\frac{\partial F_{j,n-1/2}}{\partial z}2A_n + h^{(d)}_{i,j,n}\frac{\partial F_{j,n}}{\partial z}2B_n + h^{(d)}_{i,j,n+1/2}\frac{\partial F_{j,n+1/2}}{\partial z}2C_n\\
&= \frac{h^{(d)}_{i,j,n-1}+h^{(d)}_{i,j,n}}{2}\frac{F_{j,n}-F_{j,n-1}}{\Delta z_{n-1}}2A_n + h^{(d)}_{i,j,n}\frac{F_{j,n+1}-F_{j,n-1}}{\Delta z_{n-1}+\Delta z_n}2B_n\\
&+\frac{h^{(d)}_{i,j,n+1}+h^{(d)}_{i,j,n}}{2}\frac{F_{j,n+1}-F_{j,n}}{\Delta z_n}2C_n.
\end{aligned} \tag{11.45}$$

In conclusion, four contributions appear in the eigenvalue problem:

$$h^{(a)}_{i,j,n}F_{j,n} = h^{(a)}_{i,j,n}F_{j,n}, \tag{11.46}$$

$$h^{(b)}_{i,j,n}\frac{\partial}{\partial z}F_{j,n} = F_{j,n-1}A_n h^{(b)}_{i,j,n} + F_{j,n}B_n h^{(b)}_{i,j,n} + F_{j,n+1}C_n h^{(b)}_{i,j,n}, \tag{11.47}$$

$$\frac{\partial}{\partial z}h^{(c)}_{i,j,n}F_{j,n} = F_{j,n-1}h^{(c)}_{i,j,n-1}A_n + F_{j,n}h^{(c)}_{i,j,n}B_n + F_{j,n+1}h^{(c)}_{i,j,n+1}C_n, \tag{11.48}$$

$$\begin{aligned}
&\frac{\partial}{\partial z}h^{(d)}_{i,j,n}\frac{\partial}{\partial z}F_{j,n} = F_{j,n-1}\left(-\frac{h^{(d)}_{i,j,n-1}+h^{(d)}_{i,j,n}}{\Delta z_{n-1}}A_n - \frac{h^{(d)}_{i,j,n}}{\Delta z_{n-1}+\Delta z_n}2B_n\right)\\
&+F_{j,n}\left(\frac{h^{(d)}_{i,j,n-1}+h^{(d)}_{i,j,n}}{\Delta z_{n-1}}A_n - \frac{h^{(d)}_{i,j,n+1}+h^{(d)}_{i,j,n}}{\Delta z_n}C_n\right)\\
&+F_{j,n+1}\left(\frac{h^{(d)}_{i,j,n}}{\Delta z_{n-1}+\Delta z_n}2B_n + \frac{h^{(d)}_{i,j,n+1}+h^{(d)}_{i,j,n}}{\Delta z_n}C_n\right).
\end{aligned} \tag{11.49}$$

When spin is included we have additional terms $h_{i+4,j+4,n} = h_{i,j,n}$. The spin-orbit Hamiltonian will give an extra contribution of type (a).

11.4 The Structure of Non-Zero Elements

The discretization of the 8 equations (11.2) obtained for every grid point will produce a matrix of dimension $8N_z$, where N_z is the number of grid points. The indexes of the matrix elements are obtained as $I = i+8(n-1)$, $J = j+8(n-1)$ where n is the index of the grid point, and i and j are indexes for the 8 bands. The first step in writing the sparse matrix is the identification of the non-zero elements. The structure of the non-zero 8×8 blocks is

1	2	0	0	0	...	0	0
3	4	5	0	0	...	0	0
0	6	7	8	0	...	0	0
0	0	9	10	11	...	0	0
0	0	0	12	13	...	0	0
...	...	...	...	...	...	...	...
0	0	0	0	0	...	K-3	K-2
0	0	0	0	0	...	K-1	K

, (11.50)

and the number of non-zero blocks is $K = 4 + 3(N_z - 2)$. The non-zero elements in the non-diagonal blocks are

1	2	3	4	0	0	0	0
5	6	7	8	0	0	0	0
9	10	11	12	0	0	0	0
13	14	15	16	0	0	0	0
0	0	0	0	17	18	19	20
0	0	0	0	21	22	23	24
0	0	0	0	25	26	27	28
0	0	0	0	29	30	31	32

. (11.51)

The non-zero elements in the diagonal blocks are

1	2	3	4	0	0	0	0
5	6	7	8	0	0	0	33
9	10	11	12	0	0	0	34
13	14	15	16	0	35	36	0
0	0	0	0	17	18	19	20
0	0	0	37	21	22	23	24
0	0	0	38	25	26	27	28
0	39	40	0	29	30	31	32

. (11.52)

Eight extra non-zero elements appear due to the spin-orbit interaction.

Once the non-zero elements have been identified, they have to be numbered, for the easy handling of the sparse matrix. The elements are numbered by running the sequence of non-zero blocks, in the order shown. In each block the non-zero elements are numbered in the order shown. The total number of non-zero elements is $144 + 104(N_z - 2)$.

11.5 Generation of the Sparse Matrix

The sparse matrix is generated by writing down the 8 equations (11.2) that correspond to every grid point. The non-zero blocks are filled in with the coefficients from (11.46)-(11.49). Then the contribution of the spin-orbit interaction is added to the diagonal block.

At the boundaries of the domain, for grid points with index $n = 1$ and $n = N_z$, Neumann boundary conditions are applied: $\partial F_j(z)/\partial z = 0$. This means that $F_{j,0} = F_{j,2}$ and $F_{j,N_z+1} = F_{j,N_z-1}$.

11.6 Electronic Structure and MME for a Quantum Well

A GaAs/$Al_{0.3}Ga_{0.7}$As and a GaAs/AlAs quantum well have been investigated. The quantum wells are 70 Å wide. The Kane parameters used are listed in Table 11.6 and Table 11.6. These Kane parameters result from the Luttinger parameters listed in [30]. The multiband

quantum-well Schrödinger equation was solved using a non-uniform grid finite-difference technique. Diagonalization was performed using the Lanczos algorithm of the ARPACK library [74]. Both 8-band and 6-band calculations have been performed, with both the Burt-Foreman Hamiltonian (red lines) and the Luttinger-Kohn (symmetrized) Hamiltonian (blue lines). The differences between the two models are very small, both in terms of energy bands (shown in Figures 11.1, 11.2, 11.3) and of momentum matrix elements (shown in Figures 11.4, 11.5, 11.6, 11.7, 11.8, 11.9). The difference between the two models is smaller for 8-band calculations than for 6-band calculations, in agreement with Ref. [24].

parameters	GaAs (well)	$Al_{0.3}Ga_{0.7}As$ (barrier)	AlAs (barrier)
E_{CB} [eV]	1.519	1.74346	2.2672
E_{VB} [eV]	-0.114333333	-0.257773333	-0.592466667
Δ [eV]	0.343	0.3244	0.281
A' [eV Å^2]	-10.5081159	-13.5189727	-13.0507385
B [eV Å^2]	0.0	0.0	0.0
F' [eV Å^2]	21.7239273	14.3009371	11.9969319
G [eV Å^2]	-4.2443222	-4.3692897	-4.66088055
H_1 [eV Å^2]	-15.0189573	-13.1764490	-8.87726296
H_2 [eV Å^2]	0.0	0.0	0.0
$\frac{\hbar P}{m_o}$ [eV Å]	10.4750915	10.4750915	10.4750915

Table 11.6 8-band Kane parameters for GaAs, $Al_{0.3}Ga_{0.7}As$, and AlAs.

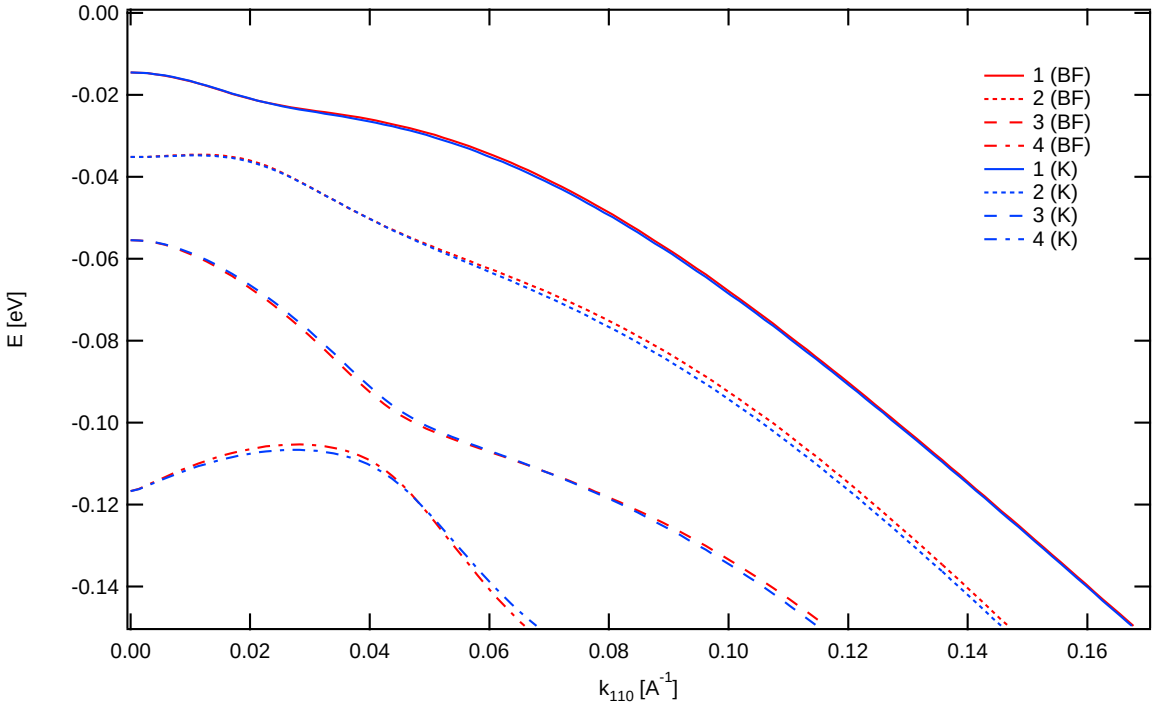

Figure 11.1: AlGaAs QW band structure. (eight-band calculation)

parameters	GaAs (well)	$Al_{0.3}Ga_{0.7}As$ (barrier)	AlAs (barrier)
E_{VB} [eV]	-0.114333333	-0.257773333	-0.592466667
Δ [eV]	0.343	0.3244	0.281
F [eV Å^2]	-50.5127693	-43.6608938	-27.6731845
G [eV Å^2]	-4.2443222	-4.3692897	-4.66088055
H_1 [eV Å^2]	-15.0189573	-13.1764490	-8.87726296
H_2 [eV Å^2]	0.0	0.0	0.0

Table 11.6 6-band Kane parameters for GaAs, $Al_{0.3}Ga_{0.7}As$, and AlAs.

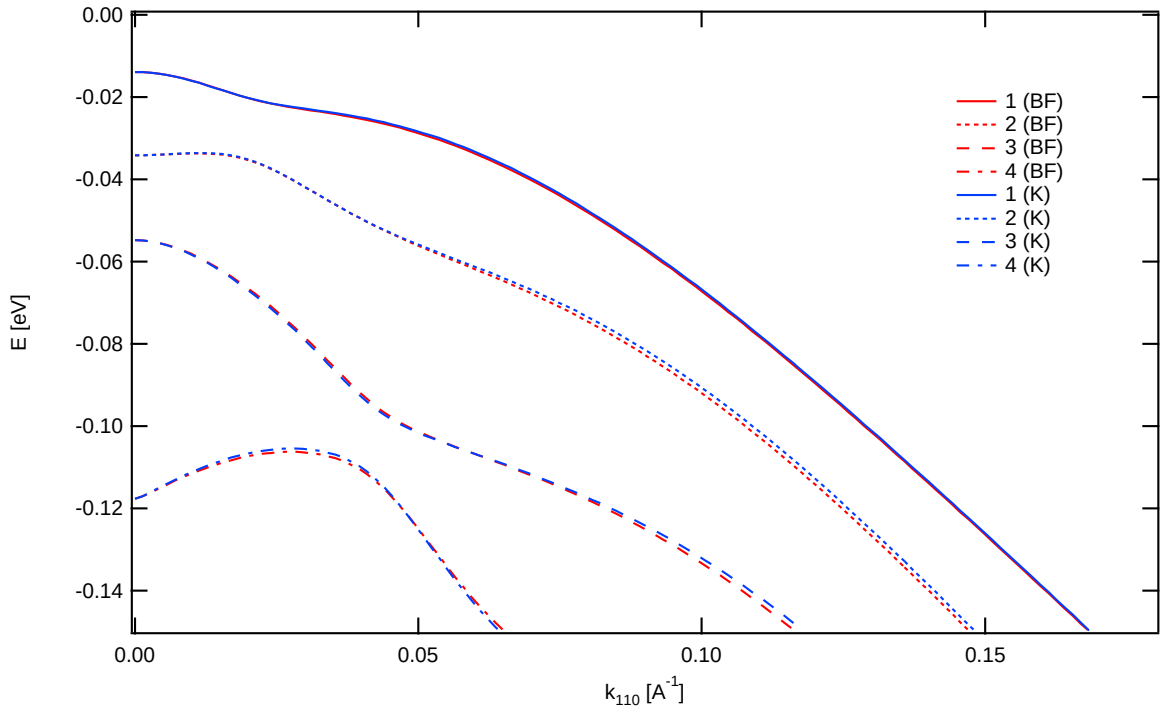

Figure 11.2: AlGaAs QW band structure. (six-band calculation)

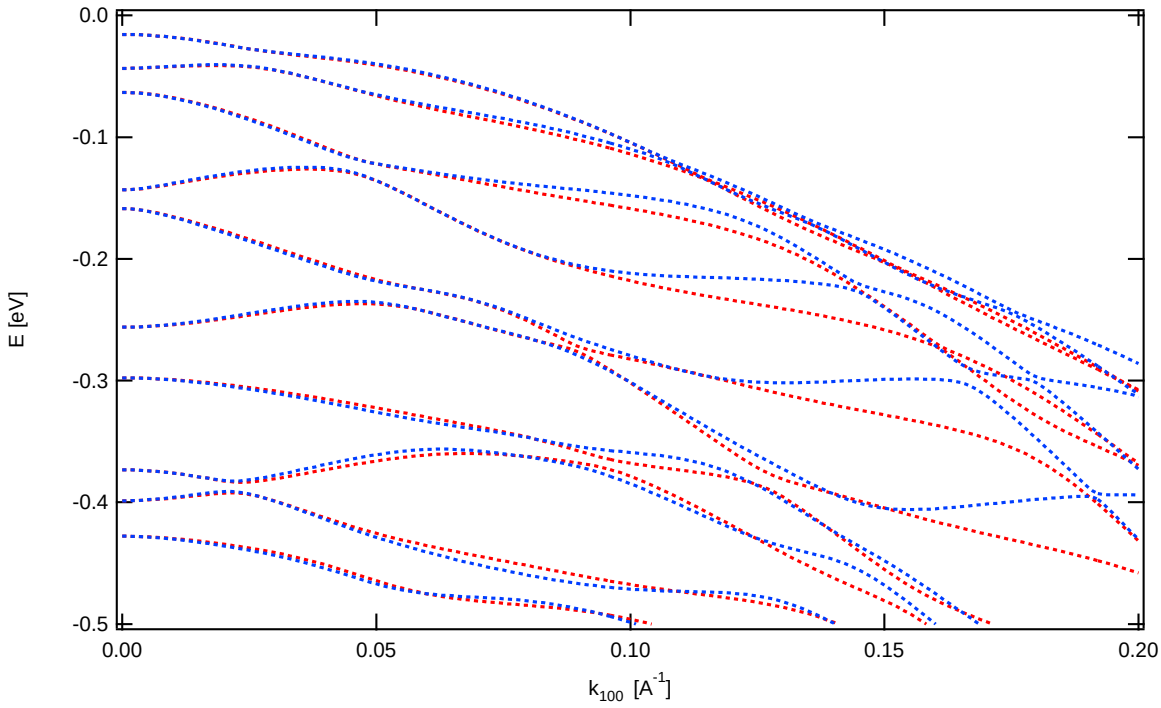

Figure 11.3: AlAs QW band structure. (six-band calculation)

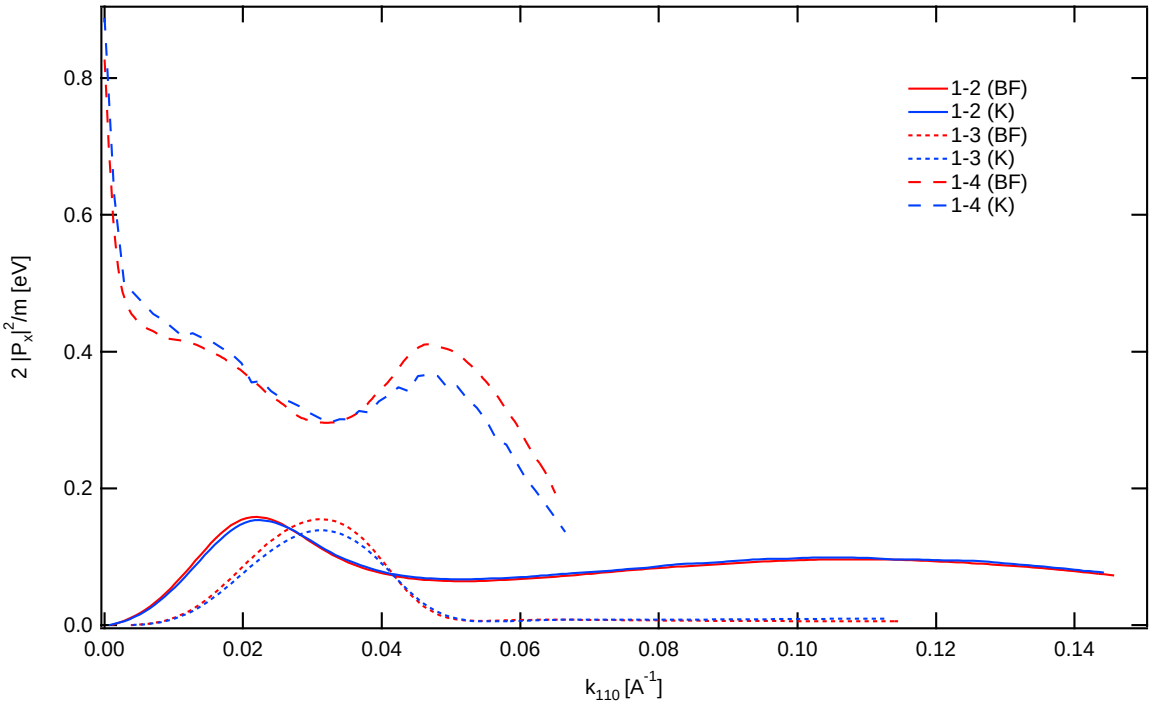

Figure 11.4: AlGaAs momentum matrix elements: x polarization. (eight-band calculation)

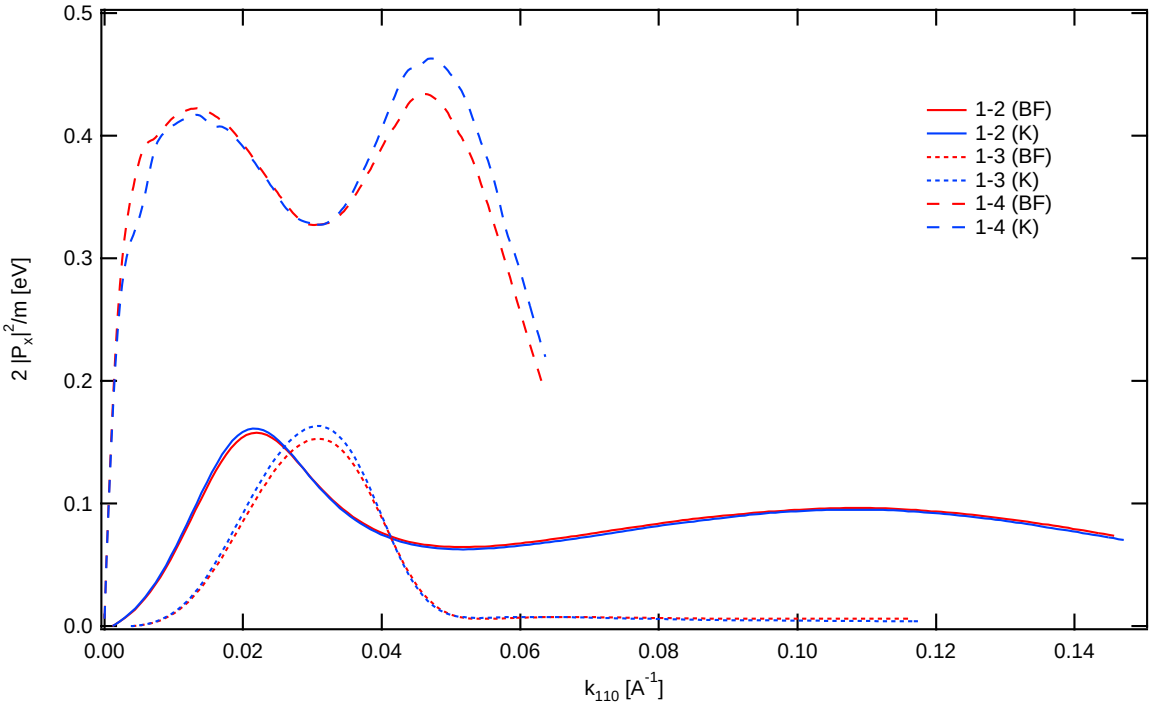

Figure 11.5: AlGaAs momentum matrix elements: x polarization. (six-band calculation)

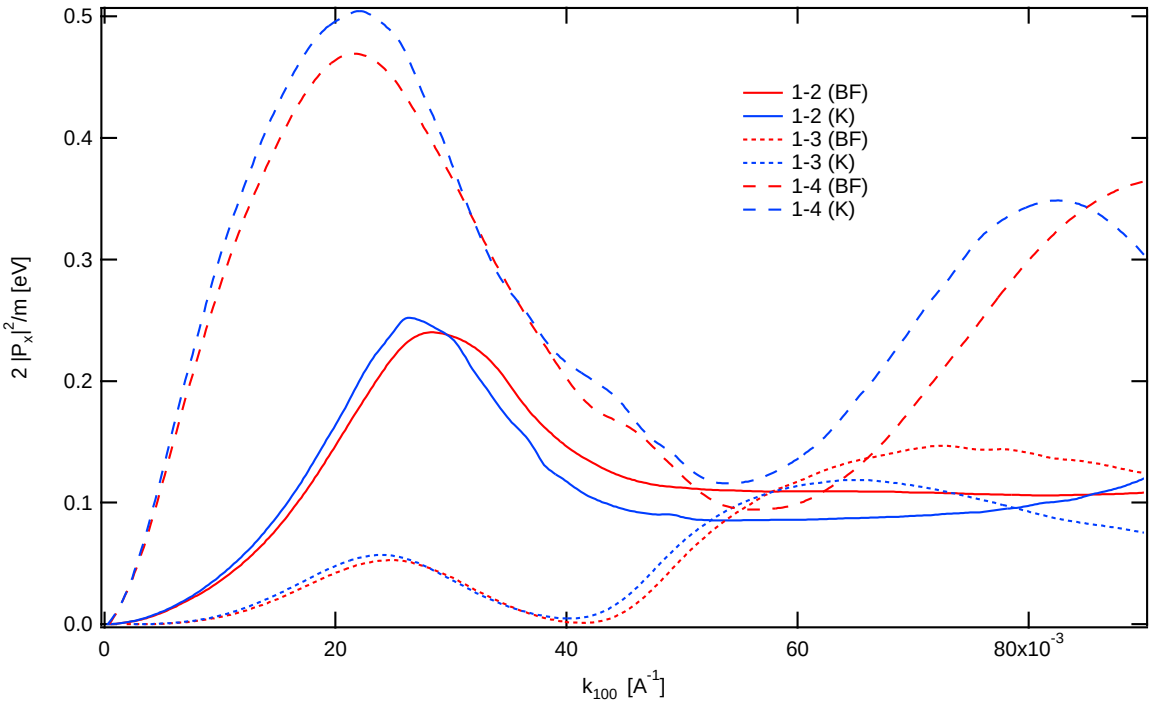

Figure 11.6: AlAs momentum matrix elements: x polarization. (six-band calculation)

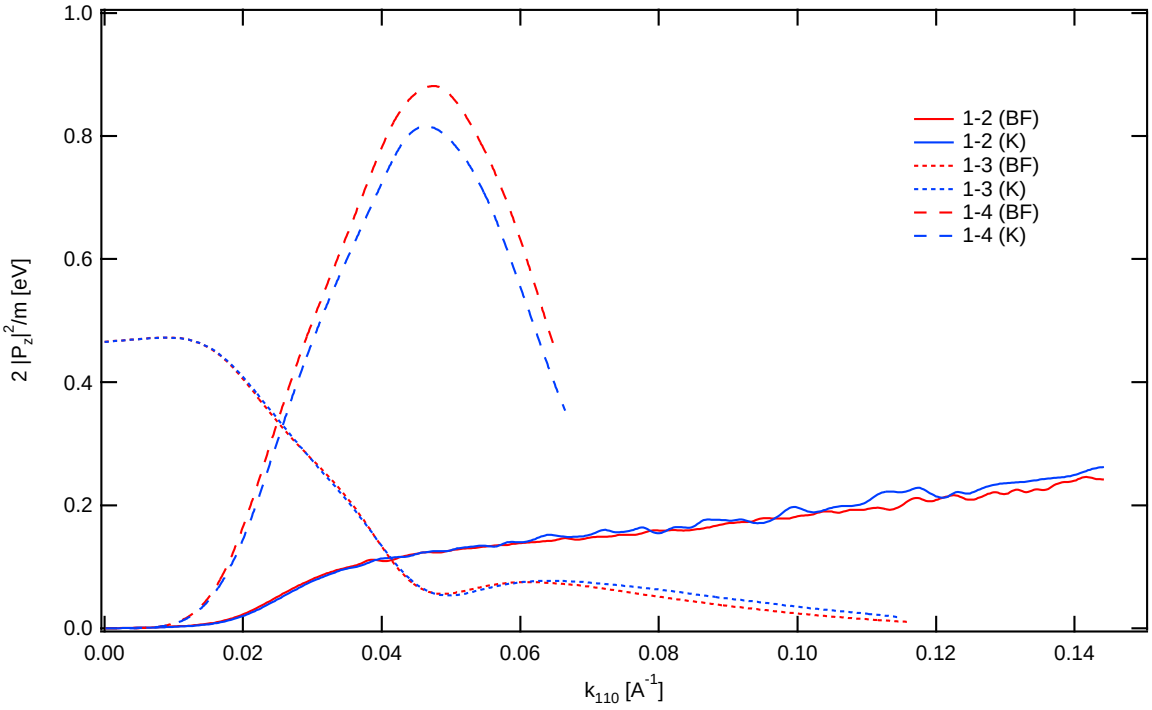

Figure 11.7: AlGaAs momentum matrix elements: z polarization. (eight-band calculation)

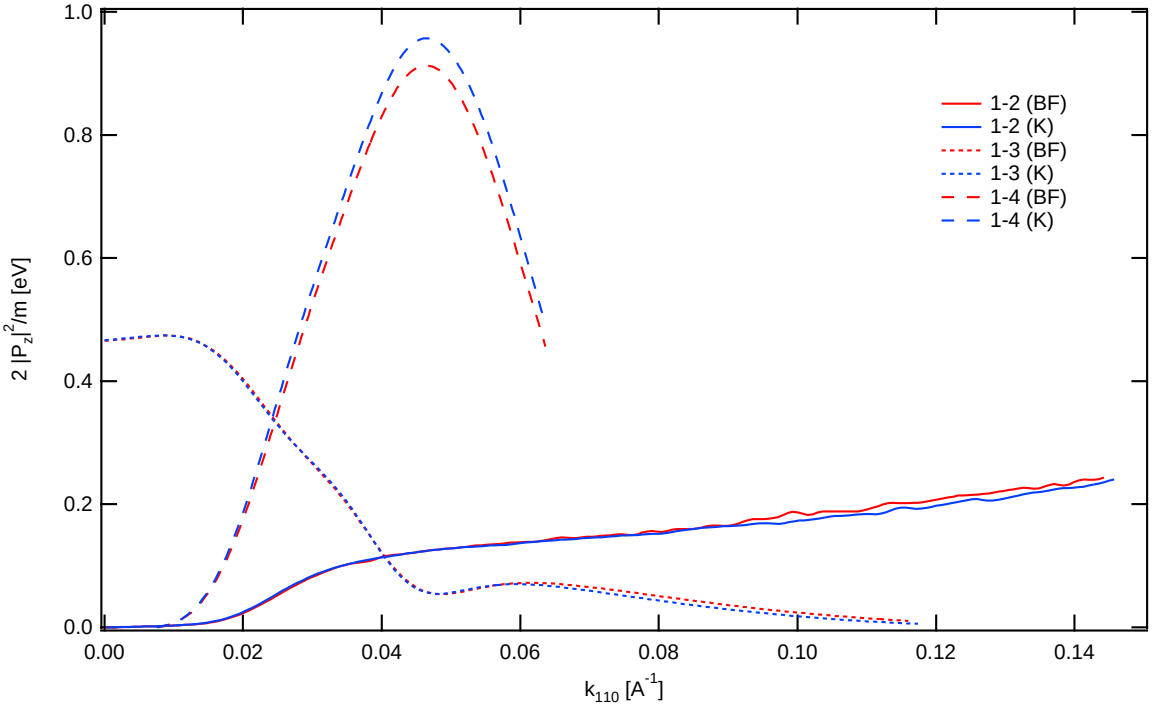

Figure 11.8: AlGaAs momentum matrix elements: z polarization. (six-band calculation)

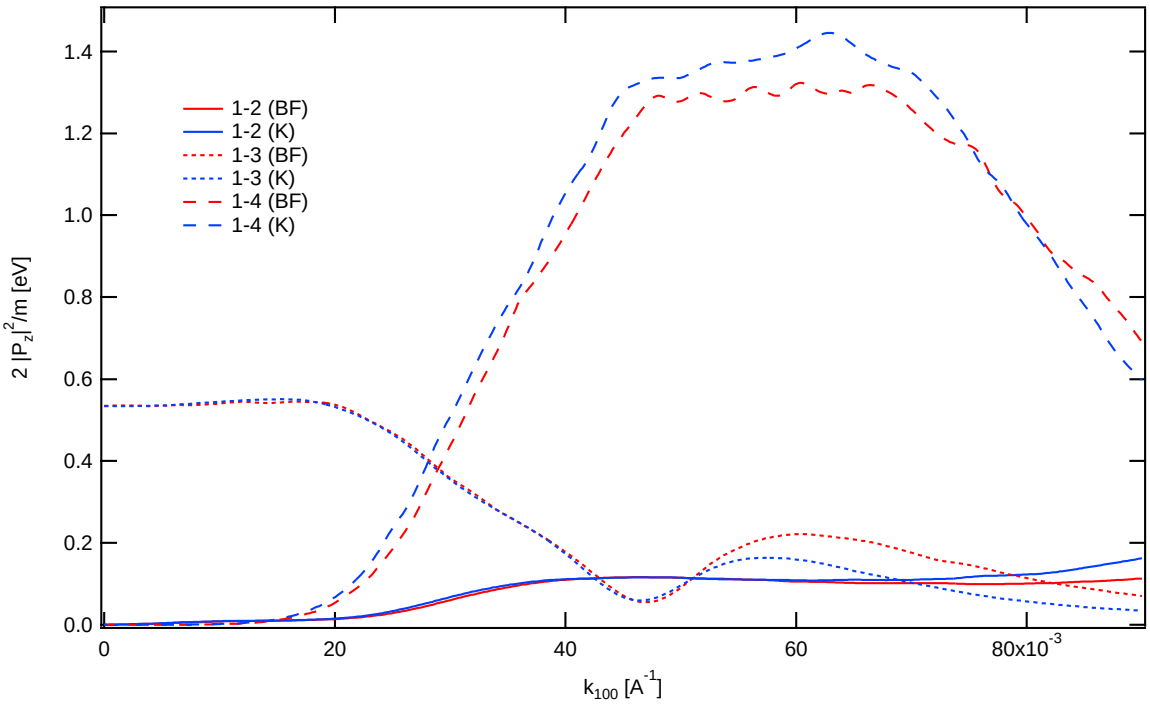

Figure 11.9: AlAs momentum matrix elements: z polarization. (six-band calculation)

Chapter 12

Six-Band $\mathbf{k} \cdot \mathbf{p}$ Calculations - WZ Cylindrical Dot

12.1 Introduction

The III-V nitride semiconductors, with wurtzite (WZ) crystal structure, have received a great deal of attention in recent years. In the 1950's there were numerous optical studies of bulk WZ semiconductors (see Ref. [41] for a recent review). However, the detailed band structure of these materials was not studied until the discovery (in 1993) of blue light emission of WZ GaN on sapphire [3]. Currently the interest in WZ materials has shifted to nanostructures such as CdSe quantum rods [86, 87, 88], ZnS nanowires [89], ZnO nanorods [90] and nanowires [91], AlN nanorods [92], and GaN nanowires [93]. On the theory side, the $\mathbf{k} \cdot \mathbf{p}$ theory of WZ bulk materials was developed by Rashba and Pikus [94, 33] and later applied to heterostructures by a number of authors [95, 31]. Mireles and Ulloa [25] have applied the theory to heterostructures using the envelope function formalism of Burt [10] and Foreman [12]. As far as we are aware, the model has only been applied to quantum wells [71] and pyramidal quantum dots [96]. In 1990, Sercel and Vahala (SV) presented a new formulation of the multiband envelope function theory and applied it to spherical quantum dots and cylindrical quantum wires of zincblende (ZB) materials [42, 43]. For ZB, the SV formulation was only possible provided the axial approximation ($\gamma_2 = \gamma_3$) was made in the Hamiltonian. The theory, within the Luttinger-

Kohn (LK) framework, has subsequently been applied to model quantum rods [88], quantum rings [97], and quantum dots [98].

The current interest in WZ nanowires [99] motivates the need for a model similar to the one introduced by Sercel and Vahala for ZB, for increasing the physical understanding of the $\mathbf{k}\cdot\mathbf{p}$ theory and for improving the efficiency of numerical computations for device applications. We propose a new formulation of the Rashba-Sheka-Pikus Hamiltonian with cylindrical symmetry. We have reformulated the $\mathbf{k}\cdot\mathbf{p}$ Hamiltonian in terms of the Sercel-Vahala (SV) representation for problems with axial symmetry. The SV representation is useful because it reduces the 3D problem to a 2D one when cylindrical polar coordinates are used. Contrary to the work of Sercel and Vahala, where the axial approximation had to be introduced for ZB materials, we show that the formulation is exact for WZ materials, i.e., *no axial approximation* was needed. In addition to the fundamental interest in the SV representation of the WZ Hamiltonian, the latter also helps make for more efficient computation for problems with axial symmetry. This includes free-standing and embedded cylindrical nanowires, modulated nanowires, quantum rods, spheroidal and spherical quantum dots.

12.2 Hamiltonian

The six-band Hamiltonian for a WZ semiconductor heterostructure, in the $|X\uparrow\rangle, |Y\uparrow\rangle, |Z\uparrow\rangle, |X\downarrow\rangle, |Y\downarrow\rangle, |Z\downarrow\rangle$ basis states of the Kane model is [31, 33, 25, 100]

$$\widehat{H} = \frac{\hbar^2}{2m_0}\begin{pmatrix} H_k & 0 \\ 0 & H_k \end{pmatrix} + H_\Delta, \tag{12.1}$$

where

$$H_k = \begin{pmatrix} \widehat{k}_x L_1 \widehat{k}_x + \widehat{k}_y M_1 \widehat{k}_y + \widehat{k}_z M_2 \widehat{k}_z & \widehat{k}_x N_1 \widehat{k}_y + \widehat{k}_y N_1' \widehat{k}_x & \widehat{k}_x N_2 \widehat{k}_z + \widehat{k}_z N_2' \widehat{k}_x \\ \widehat{k}_y N_1 \widehat{k}_x + \widehat{k}_x N_1' \widehat{k}_y & \widehat{k}_x M_1 \widehat{k}_x + \widehat{k}_y L_1 \widehat{k}_y + \widehat{k}_z M_2 \widehat{k}_z & \widehat{k}_y N_2 \widehat{k}_z + \widehat{k}_z N_2' \widehat{k}_y \\ \widehat{k}_z N_2 \widehat{k}_x + \widehat{k}_x N_2' \widehat{k}_z & \widehat{k}_z N_2 \widehat{k}_y + \widehat{k}_y N_2' \widehat{k}_z & \widehat{k}_x M_3 \widehat{k}_x + \widehat{k}_y M_3 \widehat{k}_y + \widehat{k}_z L_2 \widehat{k}_z \end{pmatrix}, \tag{12.2}$$

$$H_\Delta = \begin{array}{c} \begin{array}{cccccc} |X\uparrow\rangle & |Y\uparrow\rangle & |Z\uparrow\rangle & |X\downarrow\rangle & |Y\downarrow\rangle & |Z\downarrow\rangle \end{array} \\ \begin{pmatrix} \Delta_1 & -i\Delta_2 & 0 & 0 & 0 & \Delta_3 \\ i\Delta_2 & \Delta_1 & 0 & 0 & 0 & -i\Delta_3 \\ 0 & 0 & 0 & -\Delta_3 & i\Delta_3 & 0 \\ 0 & 0 & -\Delta_3 & \Delta_1 & i\Delta_2 & 0 \\ 0 & 0 & -i\Delta_3 & -i\Delta_2 & \Delta_1 & 0 \\ \Delta_3 & i\Delta_3 & 0 & 0 & 0 & 0 \end{pmatrix} \end{array}. \tag{12.3}$$

Next, one can use the $|u_1\rangle, |u_2\rangle, |u_3\rangle, |u_4\rangle, |u_5\rangle, |u_6\rangle$ basis states defined in Table 12.1. The advantage of using this basis is that now the zone-center Bloch functions are described by an angular momentum J. The envelope part of the total wave function behaves like the spherical harmonics, with an angular momentum L. The periodic Bloch space and the slowly varying envelope space are coupled by the $\mathbf{k}\cdot\mathbf{p}$ interaction. For problems with cylindrical symmetry, the projection of the total angular momentum $F_z = L_z + J_z$ is a good quantum number.

Next, we express the $\mathbf{k}\cdot\mathbf{p}$ Hamiltonian in terms of cylindrical polar coordinates ρ, ϕ, z. The total wave function is then written as

$$\begin{aligned} \psi(\mathbf{r}) &= \sum_i f_i(\mathbf{r})|u_i\rangle = \sum_i g_i(\rho,z)e^{iL_{zi}\phi}|u_i\rangle \\ &= \sum_i g_i(\rho,z)e^{i(F_z-J_{zi})\phi}|u_i\rangle = \sum_i g_i(\rho,z)|u_i'\rangle. \end{aligned} \tag{12.4}$$

There is a double degeneracy with respect to the sign of F_z due to inversion and time-reversal symmetry. The new matrix elements are given by

$$\begin{aligned} &\langle f_i(\mathbf{r})|\widehat{H}|f_j(\mathbf{r})\rangle \\ &= \langle g_i(\rho,z)|e^{-i(F_z-J_{zi})\phi}\widehat{H}e^{i(F_z'-J_{zj})\phi}|g_j(\rho,z)\rangle \\ &= \langle g_i(\rho,z)|\widehat{H'}|g_j(\rho,z)\rangle. \end{aligned} \tag{12.5}$$

These matrix elements are zero unless $F_z = F_z'$.

For the sake of clarity we will explicitly derive one Hamiltonian matrix element in the cylindrical formulation. In the $|X\uparrow\rangle, |Y\uparrow\rangle, |Z\uparrow\rangle, |X\downarrow\rangle, |Y\downarrow\rangle, |Z\downarrow\rangle$ basis we have:

$$H_{11} = \frac{\hbar^2}{2m_0}\Big\{\widehat{k}_x L_1 \widehat{k}_x + \widehat{k}_y M_1 \widehat{k}_y + \widehat{k}_z M_2 \widehat{k}_z\Big\} + \Delta_1. \tag{12.6}$$

n	$\|u_n\rangle$	J_{zn}
1	$\|u_1\rangle = -\frac{1}{\sqrt{2}}\|(X+iY)\uparrow\rangle$	$\frac{3}{2}$
2	$\|u_2\rangle = \frac{1}{\sqrt{2}}\|(X-iY)\uparrow\rangle$	$-\frac{1}{2}$
3	$\|u_3\rangle = \|Z\uparrow\rangle$	$\frac{1}{2}$
4	$\|u_4\rangle = \frac{1}{\sqrt{2}}\|(X-iY)\downarrow\rangle$	$-\frac{3}{2}$
5	$\|u_5\rangle = -\frac{1}{\sqrt{2}}\|(X+iY)\downarrow\rangle$	$\frac{1}{2}$
6	$\|u_6\rangle = \|Z\downarrow\rangle$	$-\frac{1}{2}$

Table 12.1: Basis states for the valence bands of wurtzite [31].

In the $|u_1\rangle, |u_2\rangle, |u_3\rangle, |u_4\rangle, |u_5\rangle, |u_6\rangle$ basis we have:

$$\begin{aligned}\widetilde{H}_{11} &= \frac{\hbar^2}{2m_0}\frac{1}{2}\Big\{\widehat{k}_x(L_1+M_1)\widehat{k}_x + \widehat{k}_y(L_1+M_1)\widehat{k}_y + 2\widehat{k}_z M_2\widehat{k}_z \\ &+ i[\widehat{k}_x(N_1-N_1')\widehat{k}_y - \widehat{k}_y(N_1-N_1')\widehat{k}_x]\Big\} + \Delta_1 + \Delta_2. \end{aligned} \tag{12.7}$$

In cylindrical coordinates we have:

$$H_{11}' = e^{-i(F_z-J_1)\phi}\widetilde{H}_{11}e^{i(F_z-J_1)\phi}. \tag{12.8}$$

Since

$$\widehat{k}_x = -i\frac{\partial}{\partial x} = -i\left[\cos(\phi)\frac{\partial}{\partial\rho} - \frac{\sin(\phi)}{\rho}\frac{\partial}{\partial\phi}\right], \tag{12.9}$$

$$\widehat{k}_y = -i\frac{\partial}{\partial y} = -i\left[\sin(\phi)\frac{\partial}{\partial\rho} + \frac{\cos(\phi)}{\rho}\frac{\partial}{\partial\phi}\right], \tag{12.10}$$

and using the cylindrical symmetry of the Kane parameters, $L_1 = L_1(\rho, z)$ and $M_1 = M_1(\rho, z)$, we have

$$\begin{aligned}\widehat{k}_x(L_1+M_1)\widehat{k}_x &= -\cos^2(\phi)\frac{\partial}{\partial\rho}\left[(L_1+M_1)\frac{\partial}{\partial\rho}\right] - \frac{\sin(\phi)}{\rho^2}(L_1+M_1)\frac{\partial}{\partial\phi}\left[\sin(\phi)\frac{\partial}{\partial\phi}\right] \\ &+ \sin(\phi)\cos(\phi)\frac{\partial}{\partial\rho}\left[\frac{L_1+M_1}{\rho}\frac{\partial}{\partial\phi}\right] + \frac{\sin(\phi)}{\rho}(L_1+M_1)\frac{\partial}{\partial\phi}\left[\cos(\phi)\frac{\partial}{\partial\rho}\right], \end{aligned} \tag{12.11}$$

$$\begin{aligned}\widehat{k}_y(L_1+M_1)\widehat{k}_y &= -\sin^2(\phi)\frac{\partial}{\partial\rho}\left[(L_1+M_1)\frac{\partial}{\partial\rho}\right] - \frac{\cos(\phi)}{\rho^2}(L_1+M_1)\frac{\partial}{\partial\phi}\left[\cos(\phi)\frac{\partial}{\partial\phi}\right] \\ &- \sin(\phi)\cos(\phi)\frac{\partial}{\partial\rho}\left[\frac{L_1+M_1}{\rho}\frac{\partial}{\partial\phi}\right] - \frac{\cos(\phi)}{\rho}(L_1+M_1)\frac{\partial}{\partial\phi}\left[\sin(\phi)\frac{\partial}{\partial\rho}\right]. \end{aligned} \tag{12.12}$$

As a result

$$\begin{aligned}&\widehat{k}_x(L_1+M_1)\widehat{k}_x+\widehat{k}_y(L_1+M_1)\widehat{k}_y\\&=-\frac{\partial}{\partial\rho}\left[(L_1+M_1)\frac{\partial}{\partial\rho}\right]-\frac{L_1+M_1}{\rho^2}\frac{\partial^2}{\partial\phi^2}-\frac{L_1+M_1}{\rho}\frac{\partial}{\partial\rho}.\end{aligned}\tag{12.13}$$

Finally

$$\begin{aligned}&e^{-i(F_z-J_1)\phi}\frac{\hbar^2}{2m_0}\frac{1}{2}\Big\{\widehat{k}_x(L_1+M_1)\widehat{k}_x+\widehat{k}_y(L_1+M_1)\widehat{k}_y\Big\}e^{i(F_z-J_1)\phi}\\&=-\frac{\hbar^2}{2m_0}\frac{1}{2}\Big\{\frac{\partial}{\partial\rho}\left[(L_1+M_1)\frac{\partial}{\partial\rho}\right]-\frac{L_1+M_1}{\rho^2}(F_z-J_1)^2+\frac{L_1+M_1}{\rho}\frac{\partial}{\partial\rho}\Big\}.\end{aligned}\tag{12.14}$$

The remaining terms in H'_{11} are found in the same way.

It is found that all ϕ dependence goes away following the SV transformation, without making an axial approximation as for ZB. The validity of this result is due to the axial symmetry already found to be true for the bulk dispersion relation [31]. This can also be seen from a group theoretic point of view by noting that the group of the wave vector is the same for all wave vectors in the plane perpendicular to the c axis. Finally, the WZ Hamiltonian in cylindrical coordinates is

$$\widehat{H'}=\begin{array}{c}\begin{array}{cccccc}|u'_1\rangle&|u'_2\rangle&|u'_3\rangle&|u'_4\rangle&|u'_5\rangle&|u'_6\rangle\end{array}\\\begin{pmatrix}S_{11}\\{\scriptstyle+\Delta_1+\Delta_2}&S_{12}&S_{13}&0&0&0\\S_{21}&S_{22}\\{\scriptstyle+\Delta_1-\Delta_2}&S_{23}&0&0&\sqrt{2}\Delta_3\\S_{31}&S_{32}&S_{33}&0&\sqrt{2}\Delta_3&0\\0&0&0&S_{44}\\{\scriptstyle+\Delta_1+\Delta_2}&S_{45}&S_{46}\\0&0&\sqrt{2}\Delta_3&S_{54}&S_{55}\\{\scriptstyle+\Delta_1-\Delta_2}&S_{56}\\0&\sqrt{2}\Delta_3&0&S_{64}&S_{65}&S_{66}\end{pmatrix}\end{array},\tag{12.15}$$

where

$$S_{11}\;=\;-\frac{\hbar^2}{2m_0}\frac{1}{2}\left\{\frac{\partial}{\partial\rho}\left((L_1+M_1)\frac{\partial}{\partial\rho}\right)+\frac{(L_1+M_1)}{\rho}\frac{\partial}{\partial\rho}\right.$$

$$
\begin{aligned}
&+ \quad 2\frac{\partial}{\partial z}M_2\frac{\partial}{\partial z} - \frac{(F_z-J_1)}{\rho}\frac{\partial(N_1-N_1')}{\partial\rho} \\
&- \quad \frac{(F_z-J_1)^2}{\rho^2}(L_1+M_1)\Bigg\}, \qquad (12.16)\\
S_{22} &= -\frac{\hbar^2}{2m_0}\frac{1}{2}\Bigg\{\frac{\partial}{\partial\rho}\left((L_1+M_1)\frac{\partial}{\partial\rho}\right) + \frac{(L_1+M_1)}{\rho}\frac{\partial}{\partial\rho} \\
&+ \quad 2\frac{\partial}{\partial z}M_2\frac{\partial}{\partial z} + \frac{(F_z-J_2)}{\rho}\frac{\partial(N_1-N_1')}{\partial\rho} \\
&- \quad \frac{(F_z-J_2)^2}{\rho^2}(L_1+M_1)\Bigg\}, \qquad (12.17)\\
S_{33} &= -\frac{\hbar^2}{2m_0}\Bigg\{\frac{\partial}{\partial\rho}\left(M_3\frac{\partial}{\partial\rho}\right) + \frac{M_3}{\rho}\frac{\partial}{\partial\rho} \\
&+ \quad \frac{\partial}{\partial z}L_2\frac{\partial}{\partial z} - \frac{(F_z-J_3)^2}{\rho^2}M_3\Bigg\}, \qquad (12.18)\\
S_{12} &= \frac{\hbar^2}{2m_0}\frac{1}{2}\Bigg\{\frac{\partial}{\partial\rho}\left((L_1-M_1)\frac{\partial}{\partial\rho}\right) \\
&+ \quad (F_z-J_2)\frac{\partial}{\partial\rho}\left(\frac{(L_1-M_1)}{\rho}\cdot\right) \\
&+ \quad (F_z-J_2-1)\frac{(L_1-M_1)}{\rho}\frac{\partial}{\partial\rho} \\
&+ \quad \frac{(F_z-J_2)(F_z-J_2-1)}{\rho^2}(L_1-M_1)\Bigg\}, \qquad (12.19)\\
S_{21} &= \frac{\hbar^2}{2m_0}\frac{1}{2}\Bigg\{\frac{\partial}{\partial\rho}\left((L_1-M_1)\frac{\partial}{\partial\rho}\right) \\
&- \quad (F_z-J_1)\frac{\partial}{\partial\rho}\left(\frac{(L_1-M_1)}{\rho}\cdot\right) \\
&- \quad (F_z-J_1+1)\frac{(L_1-M_1)}{\rho}\frac{\partial}{\partial\rho} \\
&+ \quad \frac{(F_z-J_1)(F_z-J_1+1)}{\rho^2}(L_1-M_1)\Bigg\}, \qquad (12.20)\\
S_{13} &= \frac{\hbar^2}{2m_0}\frac{1}{\sqrt{2}}\Bigg\{\frac{\partial}{\partial\rho}\left(N_2\frac{\partial}{\partial z}\right) + \frac{\partial}{\partial z}\left(N_2'\frac{\partial}{\partial\rho}\right) \\
&+ \quad (F_z-J_3)\left[\frac{\partial}{\partial z}\left(\frac{N_2'}{\rho}\cdot\right) + \frac{N_2}{\rho}\frac{\partial}{\partial z}\right]\Bigg\}, \qquad (12.21)\\
S_{31} &= \frac{\hbar^2}{2m_0}\frac{1}{\sqrt{2}}\Bigg\{\frac{\partial}{\partial\rho}\left(N_2'\frac{\partial}{\partial z}\right) + \frac{\partial}{\partial z}\left(N_2\frac{\partial}{\partial\rho}\right)
\end{aligned}
$$

$$
\begin{aligned}
&- (F_z - J_1)\left[\frac{\partial}{\partial z}\left(\frac{N_2}{\rho}\cdot\right) + \frac{N_2'}{\rho}\frac{\partial}{\partial z}\right]\Bigg\}, && (12.22)\\
S_{23} &= -\frac{\hbar^2}{2m_0}\frac{1}{\sqrt{2}}\Bigg\{\frac{\partial}{\partial\rho}\left(N_2\frac{\partial}{\partial z}\right) + \frac{\partial}{\partial z}\left(N_2'\frac{\partial}{\partial\rho}\right)\\
&- (F_z - J_3)\left[\frac{\partial}{\partial z}\left(\frac{N_2'}{\rho}\cdot\right) + \frac{N_2}{\rho}\frac{\partial}{\partial z}\right]\Bigg\}, && (12.23)\\
S_{32} &= -\frac{\hbar^2}{2m_0}\frac{1}{\sqrt{2}}\Bigg\{\frac{\partial}{\partial\rho}\left(N_2'\frac{\partial}{\partial z}\right) + \frac{\partial}{\partial z}\left(N_2\frac{\partial}{\partial\rho}\right)\\
&+ (F_z - J_2)\left[\frac{\partial}{\partial z}\left(\frac{N_2}{\rho}\cdot\right) + \frac{N_2'}{\rho}\frac{\partial}{\partial z}\right]\Bigg\}, && (12.24)\\
S_{44} &= -\frac{\hbar^2}{2m_0}\frac{1}{2}\Bigg\{\frac{\partial}{\partial\rho}\left((L_1 + M_1)\frac{\partial}{\partial\rho}\right) + \frac{(L_1 + M_1)}{\rho}\frac{\partial}{\partial\rho}\\
&+ 2\frac{\partial}{\partial z}M_2\frac{\partial}{\partial z} + \frac{(F_z - J_4)}{\rho}\frac{\partial(N_1 - N_1')}{\partial\rho}\\
&- \frac{(F_z - J_4)^2}{\rho^2}(L_1 + M_1)\Bigg\}, && (12.25)\\
S_{55} &= -\frac{\hbar^2}{2m_0}\frac{1}{2}\Bigg\{\frac{\partial}{\partial\rho}\left((L_1 + M_1)\frac{\partial}{\partial\rho}\right) + \frac{(L_1 + M_1)}{\rho}\frac{\partial}{\partial\rho}\\
&+ 2\frac{\partial}{\partial z}M_2\frac{\partial}{\partial z} - \frac{(F_z - J_5)}{\rho}\frac{\partial(N_1 - N_1')}{\partial\rho}\\
&- \frac{(F_z - J_5)^2}{\rho^2}(L_1 + M_1)\Bigg\}, && (12.26)\\
S_{66} &= -\frac{\hbar^2}{2m_0}\Bigg\{\frac{\partial}{\partial\rho}\left(M_3\frac{\partial}{\partial\rho}\right) + \frac{M_3}{\rho}\frac{\partial}{\partial\rho}\\
&+ \frac{\partial}{\partial z}L_2\frac{\partial}{\partial z} - \frac{(F_z - J_6)^2}{\rho^2}M_3\Bigg\}, && (12.27)\\
S_{45} &= \frac{\hbar^2}{2m_0}\frac{1}{2}\Bigg\{\frac{\partial}{\partial\rho}\left((L_1 - M_1)\frac{\partial}{\partial\rho}\right)\\
&- (F_z - J_5)\frac{\partial}{\partial\rho}\left(\frac{(L_1 - M_1)}{\rho}\cdot\right)\\
&- (F_z - J_5 + 1)\frac{(L_1 - M_1)}{\rho}\frac{\partial}{\partial\rho}\\
&+ \frac{(F_z - J_5)(F_z - J_5 + 1)}{\rho^2}(L_1 - M_1)\Bigg\}, && (12.28)\\
S_{54} &= \frac{\hbar^2}{2m_0}\frac{1}{2}\Bigg\{\frac{\partial}{\partial\rho}\left((L_1 - M_1)\frac{\partial}{\partial\rho}\right)
\end{aligned}
$$

$$
\begin{aligned}
&+ (F_z - J_4)\frac{\partial}{\partial\rho}\left(\frac{(L_1 - M_1)}{\rho}\cdot\right) \\
&+ (F_z - J_4 - 1)\frac{(L_1 - M_1)}{\rho}\frac{\partial}{\partial\rho} \\
&+ \frac{(F_z - J_4)(F_z - J_4 - 1)}{\rho^2}(L_1 - M_1)\Big\}, \qquad (12.29)
\end{aligned}
$$

$$
\begin{aligned}
S_{46} &= -\frac{\hbar^2}{2m_0}\frac{1}{\sqrt{2}}\Big\{\frac{\partial}{\partial\rho}\left(N_2\frac{\partial}{\partial z}\right) + \frac{\partial}{\partial z}\left(N_2'\frac{\partial}{\partial\rho}\right) \\
&- (F_z - J_6)\left[\frac{\partial}{\partial z}\left(\frac{N_2'\cdot}{\rho}\right) + \frac{N_2}{\rho}\frac{\partial}{\partial z}\right]\Big\}, \qquad (12.30)
\end{aligned}
$$

$$
\begin{aligned}
S_{56} &= \frac{\hbar^2}{2m_0}\frac{1}{\sqrt{2}}\Big\{\frac{\partial}{\partial\rho}\left(N_2\frac{\partial}{\partial z}\right) + \frac{\partial}{\partial z}\left(N_2'\frac{\partial}{\partial\rho}\right) \\
&+ (F_z - J_6)\left[\frac{\partial}{\partial z}\left(\frac{N_2'\cdot}{\rho}\right) + \frac{N_2}{\rho}\frac{\partial}{\partial z}\right]\Big\}, \qquad (12.31)
\end{aligned}
$$

$$
\begin{aligned}
S_{64} &= -\frac{\hbar^2}{2m_0}\frac{1}{\sqrt{2}}\Big\{\frac{\partial}{\partial\rho}\left(N_2'\frac{\partial}{\partial z}\right) + \frac{\partial}{\partial z}\left(N_2\frac{\partial}{\partial\rho}\right) \\
&+ (F_z - J_4)\left[\frac{\partial}{\partial z}\left(\frac{N_2\cdot}{\rho}\right) + \frac{N_2'}{\rho}\frac{\partial}{\partial z}\right]\Big\}, \qquad (12.32)
\end{aligned}
$$

$$
\begin{aligned}
S_{65} &= \frac{\hbar^2}{2m_0}\frac{1}{\sqrt{2}}\Big\{\frac{\partial}{\partial\rho}\left(N_2'\frac{\partial}{\partial z}\right) + \frac{\partial}{\partial z}\left(N_2\frac{\partial}{\partial\rho}\right) \\
&- (F_z - J_5)\left[\frac{\partial}{\partial z}\left(\frac{N_2\cdot}{\rho}\right) + \frac{N_2'}{\rho}\frac{\partial}{\partial z}\right]\Big\}, \qquad (12.33)
\end{aligned}
$$

where $J_n \equiv J_{zn}$. Note that in general $S_{ij} \neq S_{ji}^{\dagger}$.

Xia *et al.* [101, 102, 103] have added to the Hamiltonian (12.2) a term linear in k.

$$
H_k^{(linear)} = \frac{\hbar^2}{2m_0}\begin{pmatrix} 0 & 0 & A\widehat{k}_x \\ 0 & 0 & A\widehat{k}_y \\ A\widehat{k}_x & A\widehat{k}_y & 0 \end{pmatrix}. \qquad (12.34)
$$

In cylindrical coordinates this linear contribution is

$$
\begin{aligned}
S_{31}^{(linear)} &= \frac{\hbar^2}{2m_0}\Big\{-\frac{A}{\sqrt{2}}\frac{\partial}{\partial\rho} + \frac{A}{\sqrt{2}}\frac{F_z - J_1}{\rho}\Big\}, \qquad (12.35) \\
S_{13}^{(linear)} &= \frac{\hbar^2}{2m_0}\Big\{-\frac{A}{\sqrt{2}}\frac{\partial}{\partial\rho} - \frac{A}{\sqrt{2}}\frac{F_z - J_3}{\rho}\Big\}, \qquad (12.36) \\
S_{23}^{(linear)} &= \frac{\hbar^2}{2m_0}\Big\{\frac{A}{\sqrt{2}}\frac{\partial}{\partial\rho} - \frac{A}{\sqrt{2}}\frac{F_z - J_3}{\rho}\Big\}, \qquad (12.37)
\end{aligned}
$$

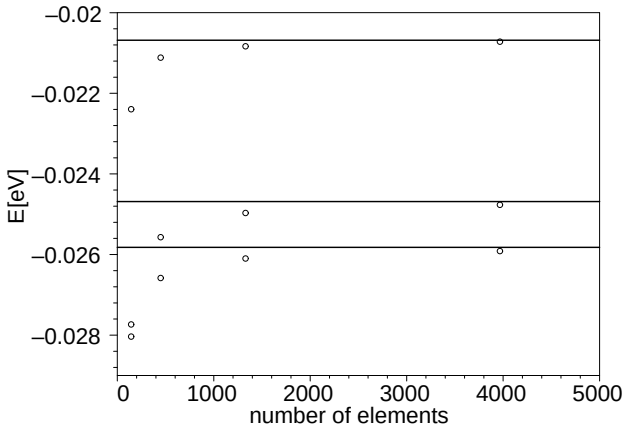

Figure 12.1: The energies of the top three valence sublevels of a WZ GaN cylindrical quantum dot, calculated with the 3D program (circles). The solid lines are the converged values obtained with the 2D program.

$$S_{32}^{(linear)} = \frac{\hbar^2}{2m_0}\Big\{\frac{A}{\sqrt{2}}\frac{\partial}{\partial\rho}+\frac{A}{\sqrt{2}}\frac{F_z-J_2}{\rho}\Big\}, \tag{12.38}$$

$$S_{64}^{(linear)} = \frac{\hbar^2}{2m_0}\Big\{\frac{A}{\sqrt{2}}\frac{\partial}{\partial\rho}+\frac{A}{\sqrt{2}}\frac{F_z-J_4}{\rho}\Big\}, \tag{12.39}$$

$$S_{46}^{(linear)} = \frac{\hbar^2}{2m_0}\Big\{\frac{A}{\sqrt{2}}\frac{\partial}{\partial\rho}-\frac{A}{\sqrt{2}}\frac{F_z-J_6}{\rho}\Big\}, \tag{12.40}$$

$$S_{56}^{(linear)} = \frac{\hbar^2}{2m_0}\Big\{-\frac{A}{\sqrt{2}}\frac{\partial}{\partial\rho}-\frac{A}{\sqrt{2}}\frac{F_z-J_6}{\rho}\Big\}, \tag{12.41}$$

$$S_{65}^{(linear)} = \frac{\hbar^2}{2m_0}\Big\{-\frac{A}{\sqrt{2}}\frac{\partial}{\partial\rho}+\frac{A}{\sqrt{2}}\frac{F_z-J_5}{\rho}\Big\}. \tag{12.42}$$

12.3 Numerical Results and Discussion

A free standing WZ GaN cylindrical quantum dot, with a radius of 50 Å and a height of 100 Å, with the axis along the crystallographic c-axis, has been studied using both the 3D and 2D methods. The parameters for GaN have been taken from the literature [100]. The 3D Hamiltonian (12.1) and the 2D Hamiltonian (12.15) have been implemented using FEMLAB; this is a software using the finite element method. Different meshes have been generated, and the convergence of the eigenvalues has been studied. Due to the reduced dimensionality, the

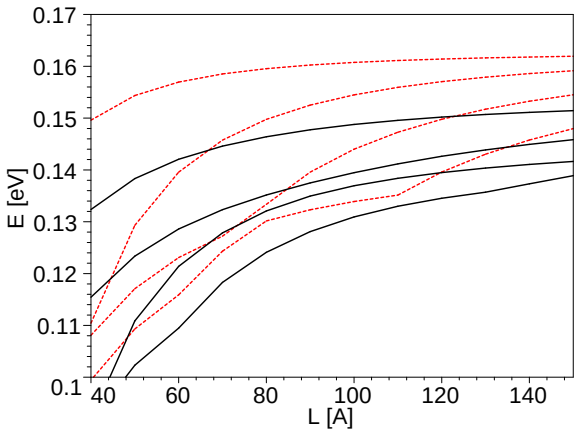

Figure 12.2: The energies of the lowest states as a function of the CdSe quantum dot aspect ratio. The linear term is not included in the Hamiltonian. Shown are the first four states with $F_z = 1/2$ (solid black lines) and with $F_z = 3/2$ (dotted red lines).

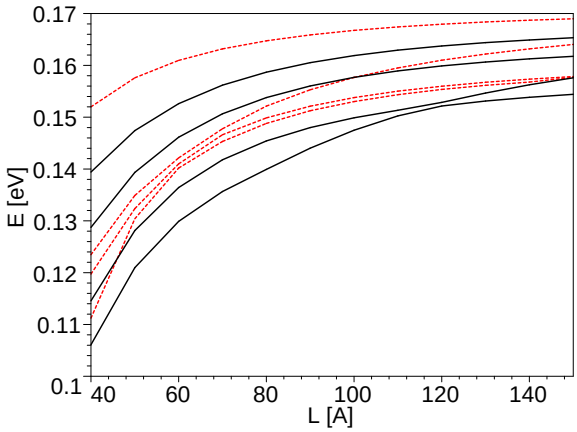

Figure 12.3: The energies of the lowest states as a function of the CdSe quantum dot aspect ratio. The linear term is included in the Hamiltonian. Shown are the first four states with $F_z = 1/2$ (solid black lines) and with $F_z = 3/2$ (dotted red lines).

eigenvalue problem in 2D can be solved much faster, in minutes instead of hours, and with less memory requirements than the eigenvalue problem in 3D. After only one mesh refinement (2040 elements) the 2D eigenvalues have converged. However, even after three mesh refinements (3967 elements) the 3D eigenvalues are not fully converged, as seen from Fig. 12.1.

A free standing WZ CdSe cylindrical quantum dot, with a radius of 50 Å and a height of 40–150 Å, has also been investigated. The parameters for CdSe have been taken from the literature [95, 103]. By varying the height we can study shape effects on semiconductor nanocrystals. From Figures 12.2-12.3 we notice that there are crossings between states with $F_z = 1/2$ (solid lines) and $F_z = 3/2$ (dotted lines). The inclusion of the linear term in the Hamiltonian dramatically changes the energy band structure, and results in anticrossings between energy bands [101].

parameters	GaN	CdSe
A_1	-6.56	-5.06
A_2	-0.91	-0.43
A_3	5.65	4.5
A_4	-2.83	-1.29
A_5	-3.13	1.29
A_6	-4.86	0.46669
Δ_1 [eV]	0.019	0.039
Δ_2 [eV]	0.004666	0.138666
Δ_3 [eV]	0.004666	0.138666
$\frac{\hbar^2}{2m_o}A$ [eV Å]	0	-0.555 i

Table 12.3 6-band parameters for WZ GaN and $CdSe$.

The parameters used in these calculations are listed in Table 12.3. The Kane parameters are given by [100]

$$L_1 = A_2 + A_4 + A_5, \tag{12.43}$$

$$L_2 = A_1, \tag{12.44}$$

$$M_1 = A_2 + A_4 - A_5, \tag{12.45}$$

$$M_2 = A_1 + A_3, \tag{12.46}$$

$$M_3 = A_2, \tag{12.47}$$

$$N_1 = 1 + 3A_5 - A_2 - A_4, \tag{12.48}$$

$$N_1' = -1 + A_2 + A_4 - A_5, \tag{12.49}$$

$$N_2 = 1 - A_1 - A_3 + \sqrt{2}A_6, \tag{12.50}$$

$$N_2' = -1 + A_1 + A_3. \tag{12.51}$$

In CdSe nanocrystals with a radius of 15 Å and a gelcap shape a crossing between the lowest two valence sublevels appears at an aspect ratio of 1.25 [86]. There are also some experimental studies of the transition from 3D to 2D confinement in CdSe quantum rods [86, 104]. Theoretical work on the electronic properties of the transition reported so far include empirical pseudopotential calculations on a rather artificial shape [86], and $\mathbf{k}\cdot\mathbf{p}$ calculations for cylindrical ZB structures [88, 105] and for spheroidal WZ structures [103]. We hope that our new formulation for studying the electronic structure of wurzite quantum dots with cylindrical symmetry will be a very useful tool in this important research area.

12.4 Conclusions

We have extended the Sercel-Vahala technique to WZ heterostructures with cylindrical symmetry and shown this to be an exact result. This is crucial for applications in enabling greatly decreased computational resources. We have studied GaN and CdSe cylindrical quantum dots, calculating the effect of the aspect ratio on energy levels and wavefunctions.

Chapter 13

Summary

A multiband Burt-Foreman formulation of the $\mathbf{k} \cdot \mathbf{p}$ theory was successfully carried out for arbitrary nanostructures. This went beyond previous work in the computation of optical matrix elements for ZB quantum wells, in the investigation of shape effects in quantum dots, and in a new formulation for WZ cylindrical nanostructures along the [0001] direction. We have shown that the one-band $\mathbf{k} \cdot \mathbf{p}$ equation for an elliptical quantum dot embedded in a finite barrier material is not separable. We have demonstrated a possible electron localization in a nanowire superlattice in a barrier material, using a full numerical solution to the one band $\mathbf{k} \cdot \mathbf{p}$ equation. The difference between bandstructures and momentum matrix elements calculated with both the Burt-Foreman and the Luttinger-Kohn Hamiltonians has been shown to be small, especially when using an 8-band model. We have found that the axial approximation was not required when the 6-band Burt-Foreman theory was extended to cylindrical coordinates using the Sercel-Vahala transformation for WZ semiconductors. This is different from the results of others on corresponding ZB nanostructures.

Future work may include the effect of strain on bandstructures and optical properties. From a computational point of view we need newer and improved algorithms to solve the secular equation for a very large and sparse matrix.

Bibliography

[1] P. S. Zory jr. *Quantum Well Lasers*. Academic, Boston, 1993.

[2] P. Harrison. *Quantum Wells, Wires and Dots*. Wiley, New York, 1999.

[3] S. Nakamura, S. Pearton, and G. Fasol. *The Blue Laser Diode*. Springer, New York, 2000.

[4] J. M. Luttinger and W. Kohn. Motion of electrons and holes in perturbed periodic fields. *Phys. Rev.*, 97(4):869–883, Feb 1955.

[5] M. G. Burt. An exact formulation of the envelope function method for the determination of electronic states in semiconductor microstructures. *Semicond. Science and Technology*, 2:460–462, 1987.

[6] M. G. Burt. An exact formulation of the envelope function method for the determination of electronic states in semiconductor microstructures (erratum). *Semicond. Science and Technology*, 2:701, 1987.

[7] M. G. Burt. An exact formulation of the envelope function method for the determination of electronic states in semiconductor microstructures. *Semicond. Science and Technology*, 3:739–753, 1988.

[8] M. G. Burt. A new effective-mass equation for microstructures. *Semicond. Science and Technology*, 3:1224–1226, 1988.

[9] M. G. Burt. Exact envelope function equations for microstructures and the particle in a box model. In A. Abram and M. Jaros, editors, *Bandstructure Engineering in Semicon-*

ductor Microstructures, NATO ASI Series B, vol. 189, pages 99–109. Plenum, New York, 1989.

[10] M. G. Burt. The justification for applying the effective-mass approximation to microstructures. *J. Phys.: Condens. Matter*, 4:6651–6690, 1992.

[11] B. A. Foreman. Effective-mass hamiltonian and boundary conditions for the valence bands of semiconductor microstructures. *Phys. Rev. B*, 48(7):4964–4967, Aug 1993.

[12] B. A. Foreman. Elimination of spurious solutions from eight-band $\mathbf{k} \cdot \mathbf{p}$ theory. *Phys. Rev. B*, 56(20):R12748–R12751, Nov 1997.

[13] W. E. Buhro and V. L. Colvin. Shape matters. *Nature Mat.*, 2:138–139, 2003.

[14] P.Y. Yu and M. Cardona. *Fundamentals of Semiconductors*. Springer, 1999.

[15] P.T. Landsberg. *Solid State Theory*. Wiley, 1969, p. 252.

[16] G. Dresselhaus, A. F. Kip, and C. Kittel. Cyclotron resonance of electrons and holes in silicon and germanium crystals. *Phys. Rev.*, 98(2):368–384, Apr 1955.

[17] E. O. Kane. Energy band structure in p-type germanium and silicon. *J. Phys. Chem. Sol.*, 1:82–99, 1956.

[18] E. O. Kane. Band structure of indium antimonide. *J. Phys. Chem. Sol.*, 1:249–261, 1957.

[19] E. O. Kane. The semi-empirical approach to band structure. In H. Brooks, editor, *Advances in Semiconductor Science*, pages 38–44. Pergamon, New York, 1959.

[20] E. O. Kane. The $\mathbf{k} \cdot \mathbf{p}$ method. In R. K. Willardson and A. C. Beer, editors, *Physics of III-V Compounds*, volume 1 of *Semiconductors and Semimetals*, chapter 3, pages 75–100. Academic, New York, 1966.

[21] E. O. Kane. Band structure of narrow gap semiconductors. In W. Zawadzki, editor, *Narrow Gap Semiconductors*, pages 13–31. Springer-Verlag, Berlin, 1980.

[22] E. O. Kane. Energy band theory. In T. S. Moss, editor, *Handbook on Semiconductors*, pages 193–217. North-Holland, Amsterdam, 1982.

[23] P.-O. Löwdin. A note on quantum-mechanical perturbation theory. *J. Chem. Phys.*, 19(11):1396–1401, Nov 1951.

[24] A. T. Meney, B. Gonul, and E. P. O'Reilly. Evaluation of various approximations used in the envelope-function method. *Phys. Rev. B*, 50(15):10893–10904, Oct 1994.

[25] F. Mireles and S. E. Ulloa. Ordered Hamiltonian and matching conditions for heterojunctions with wurtzite symmetry: GaN/Al_xGa_{1-x}N quantum wells. *Phys. Rev. B*, 60(19):13659–13667, 1999.

[26] F. Mireles and S. E. Ulloa. Strain and crystallographic orientation effects on the valence subbands of wurtzite quantum wells. *Phys. Rev. B*, 62(4):2562–2572, 2000.

[27] B. Lassen, L.C. Lew Yan Voon, M. Willatzen, and R. Melnik. Exact envelope-function theory versus symmetrized hamiltonian for quantum wires: a comparison. *Solid State Com.*, 132(3-4):141–149, Oct 2004.

[28] E. P. Pokatilov, V. A. Fonoberov, V. M. Fomin, and J. T. Devreese. Development of an eight-band theory for quantum dot heterostructures. *Phys. Rev. B*, 64(24):245328–1–245328–16, 2001.

[29] F. Szmulowicz. Derivation of a general expression for the momentum matrix elements within the envelope-function approximation. *Phys. Rev. B*, 51(3):1613, Jan 1995.

[30] F. Szmulowicz and G. J. Brown. Calculation and photoresponse measurement of the bound-to-continuum infrared absorption in *p*-type GaAs/Al_xGa_{1-x}As quantum wells. *Phys. Rev. B*, 51(19):13203–13220, May 1995.

[31] S. L. Chuang and C. S. Chang. $k \cdot p$ method for strained wurtzite semiconductors. *Phys. Rev. B*, 54(4):2491–2504, Jul 1996.

[32] M. Grundmann, O. Stier, and D. Bimberg. InAs/GaAs pyramidal quantum dots: Strain distribution, optical phonons, and electronic structure. *Phys. Rev. B*, 52:11969–11980, 1995.

[33] G. L. Bir and G. E. Pikus. *Symmetry and Strain-Induced Effects in Semiconductors.* Wiley, New York, 1975.

[34] L. C. Lew Yan Voon, C. Galeriu, and M. Willatzen. Comment on: "Confined states in two-dimensional flat elliptic quantum dots and elliptic quantum wires". *Physica E*, 18:547–549, 2003.

[35] M. van den Broek and F. M. Peeters. Confined states in two-dimensional flat elliptic quantum dots and elliptic quantum wires. *Physica E*, 11:345–355, 2001.

[36] C. Galeriu, L. C. Lew Yan Voon, R. N. Melnik, and M. Willatzen. Modeling a nanowire superlattice using the finite difference method in cylindrical polar coordinates. *Comp. Phys. Commun.*, 157:147–159, 2004.

[37] M. S. Gudiksen, L. J. Lauhon, J. Wang, D. C. Smith, and C. M. Lieber. Growth of nanowire superlattice structures for nanoscale photonics and electronics. *Nature*, 415:617–620, Feb 2002.

[38] R. Solanki, J. Huo, J. L. Freeouf, and B. Miner. Atomic layer deposition of ZnSe/CdSe superlattice nanowires. *App. Phys. Lett.*, 81(20):3864–3866, Nov 2002.

[39] L. C. Lew Yan Voon and M. Willatzen. Electron states in modulated nanowires. *J. App. Phys.*, 93:9997–10000, 2003.

[40] Y.-C. Chang and R. B. James. Saturation of intersubband transitions in p-type semiconductor quantum wells. *Phys. Rev. B*, 39(17):12672–12681, Jun 1989.

[41] L. C. Lew Yan Voon, M. Willatzen, M. Cardona, and N. E. Christensen. Terms linear in k in the band structure of wurtzite-type semiconductors. *Phys. Rev. B*, 53(16):10703–10714, 1996.

[42] K. J. Vahala and P. C. Sercel. Application of a total-angular-momentum basis to quantum-dot band structure. *Phys. Rev. Lett.*, 65(2):239–242, Jul 1990.

[43] P. C. Sercel and K. J. Vahala. Analytical technique for determining quantum-wire and quantum-dot band structure in the multiband envelope-function representation. *Phys. Rev. B*, 42(6):3690–3711, Aug 1990.

[44] L. Landau and E. Lifchitz. *Mécanique Quantique*. Mir, Moscow, 1966, p. 415.

[45] J.J. Sakurai. *Modern Quantum Mechanics*. Addison-Wesley, 1994, p. 239.

[46] G.F. Koster, J.O. Dimmock, R.G. Wheeler, and H. Statz. *Properties of the thirty-two point groups*. MIT Press, 1963.

[47] L. C. Lew Yan Voon. *Electronic and Optical Properties of Semiconductors: A Study Based on the Empirical Tight Binding Model*. Dissertations.com, 1997, p. 176.

[48] J.J. Sakurai. *Modern Quantum Mechanics*. Addison-Wesley, 1994, p. 164.

[49] G. Dresselhaus. Spin-orbit coupling effects in zinc blende structures. *Phys. Rev.*, 100(2):580–586, 1955.

[50] G. Bastard. *Wave Mechanics Applied to Semiconductor Heterostructures*. Halsted Press, 1988.

[51] D.G. Seiler, B.D. Bajaj, and A.E. Stephens. Inversion-asymmetry splitting of the conduction band in InSb. *Phys. Rev. B*, 16(6):2822–2833, Sep 1977.

[52] L. Landau and E. Lifchitz. *Mécanique Quantique*. Mir, Moscow, 1966, p. 162.

[53] R. Eppenga, M.F.H. Schuurmans, and S. Colak. New $\mathbf{k} \cdot \mathbf{p}$ theory for GaAs/$Ga_{1-x}Al_xAs$ - type quantum wells. *Phys. Rev. B*, 36(3):1554–1564, Jul 1987.

[54] D. Gershoni, C. H. Henry, and G.A. Baraff. Calculating the optical properties of multidimensional heterostructures: Application to the modeling of quaternary quantum well lasers. *IEEE J. Quantum Elec.*, 29(9):2433–2450, Sep 1993.

[55] S. A. Stoklitsky, Q. X. Zhao, P. O. Holtz, B. Monemar, and T. Lundström. Optical intervalence-subband transitions in strained p-type $In_{1-x}Ga_xAs/InP$ quantum wells. *J. App. Phys.*, 77(10):5256–5262, 1995.

[56] O. Stier and D. Bimberg. Modeling of strained quantum wires using eight-band $\mathbf{k} \cdot \mathbf{p}$ theory. *Phys. Rev. B*, 55(12):7726–7732, Mar 1997.

[57] O. Stier, M. Grundmann, and D. Bimberg. Electronic and optical properties of strained quantum dots modeled by 8-band $\mathbf{k} \cdot \mathbf{p}$ theory. *Phys. Rev. B*, 59(8):5688–5701, Feb 1999.

[58] G. Shechter and L. D. Shvartsman. Theory of bound-to-continuum infrared absorption in p-type quantum wells based on a mapping of the continuum spectrum. *Phys. Rev. B*, 58(7):3941–3953, 1998.

[59] P. Enders, A. Brwolff, M. Woerner, and D. Suisky. $\mathbf{k} \cdot \mathbf{p}$ theory of energy bands, wave functions, and optical selection rules in strained tetrahedral semiconductors. *Phys. Rev. B*, 51(23):16695–16704, Jun 1995.

[60] K.I. Kolokolov, S.D. Beneslavski, N.Y. Minina, and A.M. Savin. Far-infrared intersubband absorption in p-type $GaAs/Al_xGa_{1-x}As$ single heterojunctions under uniaxial compression. *Phys. Rev. B*, 63(19):195308–1–195308–6, May 2001.

[61] L. Landau and E. Lifchitz. *Théorie de L' Élasticité.* Mir, Moscow, 1967.

[62] Herbert Reismann and Peter S. Pawlik. *Elasticity, Theory and Applications.* John Wiley, New York, 1980.

[63] A. S. Saada. *Elasticity Theory and Applications.* Krieger, Malabar, 1993.

[64] A. K. Ghatak, K. Thyagarajan, and M. R. Shenoy. A novel numerical technique for solving the one-dimensional Schrödinger equation using matrix approach — application to quantum well structures. *IEEE J. Quantum Elec.*, 24(8):1524–1531, Aug 1988.

[65] K. Nakamura, A. Shimizu, M. Koshiba, and K. Hayata. Finite-element analysis of quantum wells of arbitrary semiconductors with arbitrary potential profiles. *IEEE J. Quantum Elec.*, 25(5):889–895, May 1989.

[66] I.-H. Tan, G. L. Snider, L. D. Chang, and E. L. Hu. A self-consistent solution of Schrödinger-Poisson equations using a nonuniform mesh. *J. App. Phys.*, 68(8):4071–7, Oct 1990.

[67] M. Tsetseri and G. P. Triberis. A study of the ground state of quantum wires using the finite difference method. *Superlattices and Microstructures*, 32(1):79–90, July 2002.

[68] D. El-Moghraby, R. G. Johnson, and P. Harrison. Calculating modes of quantum wire and dot systems using a finite differencing technique. *Comput. Phys. Comm.*, 150(3):235–246, Feb 2003.

[69] D. L. Mathine, S. K. Myjak, and G. N. Maracas. A computational Fourier series solution of the BenDaniel-Duke Hamiltonian for arbitrary shaped quantum wells. *IEEE J. Quantum Elec.*, 31(7):1216, Jul 1995.

[70] G. Lamouche and Y. Lépine. Ground state of a quantum disk by the effective-index method. *Phys. Rev. B*, 51(3):1950–1953, Jan 1995.

[71] S. L. Chuang and C. S. Chang. A band-structure model of strained quantum-well wurtzite semiconductors. *Semicond. Sci. Technol.*, 12:252–263, 1997.

[72] L. C. Lew Yan Voon and M. Willatzen. Angular confinement, non-integral quantum numbers, and controllable degeneracies. *Europhys. Lett.*, 62:299–305, 2003.

[73] P.M. Morse and H. Feshbach. *Methods of Theoretical Physics*. McGraw-Hill, New York, 1953.

[74] R. Lehoucq, D.C. Sorensen, and C. Yang. *Arpack User's Guide*. SIAM, 1998.

[75] Y. Li, J.-L. Liu, O. Voskoboynikov, C. P. Lee, and S. M. Sze. Electron energy level calculations for cylindrical narrow gap semiconductor quantum dot. *Comput. Phys. Comm.*, 140(3):399–404, Nov 2001.

[76] Y. Li, O. Voskoboynikov, C. P. Lee, and S. M. Sze. Computer simulation of electron energy levels for different shape InAs/GaAs semiconductor quantum dots. *Comput. Phys. Comm.*, 141(1):66–72, Nov 2001.

[77] Y. Li, O. Voskoboynikov, C. P. Lee, and S. M. Sze. Energy and coordinate dependent effective mass and confined electron states in quantum dots. *Solid State Comm.*, 120(2-3):79–83, Sep 2001.

[78] Y. Wu, R. Fan, and P. Yang. Block-by-block growth of single-crystalline Si/SiGe superlattice nanowires. *Nano Lett.*, 2:83–86, 2002.

[79] M. T. Björk, B. J. Ohlsson, T. Sass, A. I. Persson, C. Thelander, M. H. Magnusson, K. Deppert, L. R. Wallenberg, and L. Samuelson. One-dimensional steeplechase for electrons realized. *Nano Lett.*, 2:87–89, 2002.

[80] M. Kawamura, N. Paul, V. Cherepanov, and B. Voigtlander. Nanowires and nanorings at the atomic level. *Phys. Rev. Lett.*, 91(9):096102–1–096102–4, 2003.

[81] R. M. Kolbas and N. Holonyak Jr. Man-made quantum wells: A new perspective on the finite square-well problem. *Am. J. Phys*, 52(5):431–437, May 1984.

[82] R. Verzicco and P. Orlandi. A finite-difference scheme for three-dimensional incompressible flows in cylindrical coordinates. *J. Comput. Phys.*, 123(2):402–414, Feb 1996.

[83] H.-S. Cho and P. R. Prucnal. New formalism of the kronig-penney model with application to superlattices. *Phys. Rev. B*, 36(6):3237–3242, Aug 1987.

[84] L. C. Lew Yan Voon. Discontinuities in the effective-mass equation. *Superlattices and Microstructures*, 31(6):269–276, 2002.

[85] E. Kapon, D. M. Hwang, and R. Bhat. Stimulated emission in semiconductor quantum wire heterostructures. *Phys. Rev. Lett.*, 63(4):430–433, 1989.

[86] J. Hu, L. Li, W. Yang, L. Manna, L. Wang, and A. P. Alivisatos. Linearly polarized emission from colloidal semiconductor quantum rods. *Science*, 292:2060–2063, Jun 2001.

[87] L. Li, J. Hu, W. Yang, and A. P. Alivisatos. Band gap variation of size- and shape-controlled colloidal CdSe quantum rods. *Nano Lett.*, 1(7):349–351, 2001.

[88] D. Katz, T. Wizansky, O. Millo, E. Rothenberg, T. Mokari, and U. Banin. Size-dependent tunneling and optical spectroscopy of CdSe quantum rods. *Phys. Rev. Lett.*, 89(8):086801–1–086801–4, 2002.

[89] Y. Wang, L. Zhang, C. Liang, G. Wang, and X. Peng. Catalitic growth and photoluminescence properties of semiconductor single-crystal ZnS nanowires. *Chem. Phys. Lett.*, 357:314–318, May 2002.

[90] Z. R. Tian, J. A. Voigt, J. Liu, B. McKenzie, M. J. McDermott, M. A. Rodriguez, H. Konishi, and H. Xu. Complex and oriented ZnO nanostructures. *Nature Materials*, 2:821–826, Dec 2003.

[91] M. H. Huang, S. Mao, H. Feick, H. Yan, Y. Wu, H. Kind, E. Weber, R. Russo, and P. Yang. Room-temperature ultraviolet nanowire nanolasers. *Science*, 292:1897–1899, Jun 2001.

[92] Q. L. Liu, T. Tanaka, J. Q. Hu, F. F. Xu, and T. Sekiguchi. Green emission from *c*-axis oriented AlN nanorods doped with Tb. *Appl. Phys. Lett.*, 83(24):4939–4941, Dec 2003.

[93] J. C. Johnson, H. Choi, K. P. Knutsen, R. D. Schaller, P. Yang, and R. J. Saykally. Single gallium nitride nanowires lasers. *Nature Materials*, 1:106–110, Oct 2002.

[94] E. I. Rashba. Symmetry of energy bands in crystals of wurtzite type. *Sov. Phys. Solid State*, 1:368–380, 1959.

[95] J.-B. Jeon, Y. M. Sirenko, K. W. Kim, M. A. Littlejohn, and M. A. Stroscio. Valence band parameters of wurtzite materials. *Solid State Comm.*, 99(6):423–426, 1996.

[96] A. D. Andreev and E. P. OReilly. Theory of the electronic structure of GaN/AlN hexagonal quantum dots. *Phys. Rev. B*, 62(23):15851–15870, Dec 2000.

[97] J. Planelles, W. Jaskólski, and J. I. Aliaga. Energy structure of quantum rings in a magnetic field. *Phys. Rev. B*, 65(3):033306–1–033306–4, 2002.

[98] F. B. Pedersen and Y.-C. Chang. Energy levels of one and two holes in parabolic quantum dots. *Phys. Rev. B*, 53(3):1507–1516, Jan 1996.

[99] X. Duan and C. M. Lieber. General synthesis of compound semiconductor nanowires. *Adv. Mat.*, 12(4):298–301, 2000.

[100] V. A. Fonoberov and A. A. Balandin. Excitonic properties of strained wurtzite and zinc-blende GaN/$Al_xGa_{1-x}N$ quantum dots. *J. Appl. Phys.*, 94(11):7178–7186, Nov 2003.

[101] J.-B. Xia, K. W. Cheah, X.-L. Wang, D.-Z. Sun, and M.-Y. Kong. Energy bands and acceptor binding energies of GaN. *Phys. Rev. B*, 59(15):10119–10124, Apr 1999.

[102] J.-B. Xia and J. Li. Electronic structure of quantum spheres with wurtzite structure. *Phys. Rev. B*, 60(16):11540–11544, Oct 1999.

[103] X.-Z. Li and J.-B. Xia. Electronic structure and optical properties of quantum rods with wurtzite structure. *Phys. Rev. B*, 66(11):115316–1–115316–6, Sep 2002.

[104] H. Yu, J. Li, R. A. Loomis, P. C. Gibbons, L.-W. Wang, and W. E. Buhro. Cadmium selenide quantum wires and the transition from 3D to 2D confinement. *J. Am. Chem. Soc.*, 125:16168–16169, 2003.

[105] L. C. Lew Yan Voon, R. Melnik, B. Lassen, and M. Willatzen. Influence of aspect ratio on the lowest states of quantum rods. *Nano Lett.*, 4(2):289–292, 2004.